MODELING THE EFFECTS OF VARIABLE COAL PROPERTIES
ON METHANE PRODUCTION DURING
ENHANCED COALBED METHANE RECOVERY

A THESIS SUBMITTED TO
THE GRADUATE SCHOOL OF NATURAL AND APPLIED SCIENCES
OF
MIDDLE EAST TECHNICAL UNIVERSITY

BY

HÜSEYİN ONUR BALAN

IN PARTIAL FULFILLMENT OF THE REQUIREMENTS
FOR
THE DEGREE OF MASTER OF SCIENCE
IN
PETROLEUM AND NATURAL GAS ENGINEERING

JUNE 2008

Approval of the thesis:

MODELING THE EFFECTS OF VARIABLE COAL PROPERTIES ON METHANE PRODUCTION DURING ENHANCED COALBED METHANE RECOVERY

submitted by **HÜSEYİN ONUR BALAN** in partial fulfillment of the requirements for the degree of **Master of Science** in **Petroleum and Natural Gas Engineering Department, Middle East Technical University** by,

Prof. Dr. Canan Özgen   _____
Dean, Graduate School of **Natural and Applied Sciences**

Prof. Dr. Mahmut Parlaktuna   _____
Head of Department, **Petroleum and Natural Gas Engineering**

Prof. Dr. Fevzi Gümrah   _____
Supervisor, **Petroleum and Natural Gas Engineering Dept., METU**

Examining Committee Members:

Prof. Dr. Ender Okandan   _____
Petroleum and Natural Gas Engineering Dept., METU

Prof. Dr. Fevzi Gümrah   _____
Petroleum and Natural Gas Engineering Dept., METU

Prof. Dr. Mahmut Parlaktuna   _____
Petroleum and Natural Gas Engineering Dept., METU

Prof. Dr. Nurkan Karahanoğlu   _____
Geological Engineering Dept., METU

Assist. Prof. Dr. Evren Özbayoğlu   _____
Petroleum and Natural Gas Engineering Dept., METU

                                                    Date: _____

I hereby declare that all information in this document has been obtained and presented in accordance with academic rules and ethical conduct. I also declare that, as required by these rules and conduct, I have fully cited and referenced all materials and results that are not original to this work.

Name, Surname: Hüseyin Onur BALAN

Signature:

ABSTRACT

MODELING THE EFFECTS OF VARIABLE COAL PROPERTIES
ON METHANE PRODUCTION DURING
ENHANCED COALBED METHANE RECOVERY

Balan, Hüseyin Onur

M.Sc., Department of Petroleum and Natural Gas Engineering

Supervisor: Prof. Dr. Fevzi Gümrah

June 2008, 144 pages

Most of the coal properties depend on carbon content and vitrinite reflectance, which are rank dependent parameters. In this study, a new approach was followed by constructing a simulation input database with rank-dependent coal properties published in the literature which are namely cleat spacing, coal porosity, density, and parameters related to strength of coal, shrinkage, swelling, and sorption.

Simulations related to enhanced coalbed methane (ECBM) recovery, which is the displacement of adsorbed CH_4 in coal matrix with CO_2 or CO_2/N_2 gas injection, were run with respect to different coal properties, operational parameters, shrinkage and swelling effects by using a compositional reservoir simulator of CMG (Computer Modeling Group) /GEM module. Sorption-controlled behavior of coalbeds and interaction of coal media with injected gas mixture, which is called shrinkage and swelling, alter the coal properties controlling gas flow with respect to

injection time. Multicomponent shrinkage and swelling effects were modeled with extended Palmer and Mansoori equation.

In conclusion, medium-volatile bituminous coal rank, dry coal reservoir type, inverted 5-spot pattern, 100 acre drainage area, cleat permeability from 10 to 25 md, CO_2/N_2 molar composition between 50/50 % and 75/25 %, and drilling horizontal wells rather than vertical ones are better selections for ECBM recovery. In addition, low-rank coals and dry coal reservoirs are affected more negatively by shrinkage and swelling. Mixing CO_2 with N_2 prior to its injection leads to a reduction in swelling effect. It has been understood that elastic modulus is the most important parameter controlling shrinkage and swelling with a sensitivity analysis.

Keywords: Rank of Coal, Coalbed Methane, Enhanced Coalbed Methane Recovery, Shrinkage, Swelling, CO_2 Sequestration.

ÖZ

GELİŞTİRİLMİŞ KÖMÜR YATAĞI METAN GAZI KURTARIMINDA DEĞİŞKEN KÖMÜR ÖZELLİKLERİNİN METAN ÜRETİMİNE OLAN ETKİSİNİN MODELLENMESİ

Balan, Hüseyin Onur

Yüksek Lisans, Petrol ve Doğal Gaz Mühendisliği Bölümü

Tez Yöneticisi: Prof. Dr. Fevzi Gümrah

Kömüre ait birçok fiziksel özellik kömürleşme (rank) derecesine bağlı olarak karbon içeriği ve vitrinit yansımasına göre değişmektedir. Bu çalışmada kömürün rank derecesi ve fiziksel özellikleri arasında literatür de var olan ilişkiler kullanılarak bir veri bankası oluşturulmuş ve bu bilgiler simülasyon çalışmasına girdi olarak kullanılmıştır. Bu parametreler arasında çatlak aralığı, kömür gözenekliliği, kömürün yoğunluğu, mukavemeti, büzülme, şişme ve soğurma parametreleri yer almaktadır.

Kömür yüzeyine tutunan metanın, CO_2 ya da CO_2/N_2 gaz karışımı enjeksiyonu ile ötelenmesi olarak tanımlanan "geliştirilmiş kömür yatağı metan gazı kurtarımı" (ECBM) tekniği çeşitli kömür özellikleri, farklı üretim teknikleri, büzülme ve şişme etkileri çerçevesinde CMG (Computer Modeling Group) firmasının GEM kompozisyonal rezervuar simülatörü kullanılarak incelenmiştir. Metanın üretilmesi ve gaz karışımlarının enjeksiyonu kömürün büzülüp ve şişmesine neden olmakta ve gaz

akışını etkileyen kömür özelliklerini zamana bağlı değiştirmektedir. Birden çok gaz bileşeni içeren sistemlerde şişme ve büzülme etkisinin modellenmesi için genişletilmiş Palmer ve Mansoori geçirgenlik denklemi kullanılmıştır.

Sonuç olarak, orta derecede uçucu madde içeren bitümlü kuru kömürlerin, 5 noktalı kuyu şablonunun, 100 acre drenaj alanın, 10 – 25 md çatlak geçirgenliği aralığının ve % (50/50) - % (75/25) arasındaki CO_2/N_2 molar kompozisyonun ECBM için daha uygun olduğu anlaşılmıştır. Kuyu çeşitleri ile yapılan simülasyon çalışmasında ise yatay kuyuların dikey kuyulara göre ECBM için daha iyi performans sağladığı anlaşılmıştır. Ayrıca düşük rank derecesine sahip kuru kömürlerin büzülme ve şişme olayından daha olumsuz etkilendiği görülmüştür. N_2'nin enjekte edilen CO_2 ile karıştırılması şişme etkisini azalttığı ortaya çıkmıştır. Son olarak yapılan hassasiyet analizine göre elastik sabitin büzülme ve şişmeyi kontrol eden en önemli parametre olduğu sonucuna varılmıştır.

Anahtar Kelimeler: Kömürleşme Derecesi, Kömür Yatağı Gazı, Geliştirilmiş Kömür Yatağı Gazı Kurtarımı, Büzülme, Şişme, Karbon dioksitin tecridi

To My Family

ACKNOWLEDGMENTS

TABLE OF CONTENTS

LIST OF TABLES

LIST OF FIGURES

xvi

NOMENCLATURE

a	Ash content, weight fraction
B_{gi}	Gas formation volume factor at initial reservoir conditions, rcf/Mscf
c_f	Fracture compressibility, 1/psia
C_{gi}	Initial sorbed gas concentration, scf/ton
D	Diffusion coefficient, cm^2/s
Da	Drainage area, acre
D_e	Effective diffusivity, 1/s
Dp	Depth, ft
E	Elastic modulus, psia
G_i	Gas in place at initial reservoir conditions, Mscf
G_S	Gas storage capacity, scf/ton
G_{Si}	Multicomponent gas storage capacity of component i, (in situ basis, scf/ton)
h	Net coal thickness, ft
k	Cleat (fracture) permeability, md
k_f	Absolute cleat (fracture) permeability, md
k_{fi}	Initial fracture permeability, md
k_{rw}	Water relative permeability, dimensionless
k_{rg}	Gas relative permeability, dimensionless
K	Bulk modulus, psia
m	Moisture content, weight fraction
M	Constraint axial modulus, psia
n	Number of diffusing species
nc	Total number of gas components
P	Total pressure of free gas phase, psia
P_i	Initial pressure, psia
P_{inf}	Infinite pressure, psia
P_L	Langmuir pressure, psia

$P_{L\,i,j}$	Pure component Langmuir pressure i or j, psia
r_p	Diffusion path length, cm
$\overline{Rr}$, R_{or}	Vitrinite reflectance, %
Rt	Coal reservoir type
S_{wi}	Initial water saturation in cleats, fraction
S_w	Water saturation in cleats, fraction
t	Time, s
T	Temperature, °F
V_{inf}	Total adsorbed or desorbed volume, cm^3
V_L	Dry and ash-free Langmuir volume, scf/ton
V_{Li}	Pure component Langmuir volume of component i, (dry and ash-free basis, scf/ton)
$V_{measured}$	Actual gas content in coal matrix at reservoir conditions, scf/ton
V_T	Total gas desorbed at time t, cm^3
w	Fracture aperture, cm
w_C	Moisture content, weight fraction
$y_{i,j}$	Molar fraction of component i or j (free gas state), fraction
z	Fracture spacing, cm

Greek Letters

ε_{inf}	Infinite strain, dimensionless
ϱ_c	Coal pure density, g/cm^3
σ_h	Effective stress on fracture surfaces, psia
φ_f	Fracture porosity, fraction
φ_{fi}	Initial fracture porosity, fraction
ε_V	Volumetric strain at a given pressure, dimensionless
v	Poisson's ratio, dimensionless

Subscripts

i	Initial condition
i, j, k	Each gas component

ABBREVIATIONS

An	Anisotropy
C	Component Name
CBM	Coalbed methane
Cr	Coal Rank
DLD	Direct line drive well-pattern
ECBM	Enhanced coalbed methane
F	Fracture
Hvb	High-volatile bituminous coal rank
IPCC	Intergovernmental Panel on Climate Change
Inv.Hex.7	Inverted Hexagonal 7-spot well-pattern
Inv.5	Inverted 5-spot well-pattern
Inv.9	Inverted 9-spot well-pattern
Ma	Matrix
Mo	Molar composition of injected fluid
Mvb	Medium-volatile bituminous coal rank
N.Hex.7	Normal Hexagonal 7-spot well-pattern
N.9	Normal 9-spot well-pattern
Rt	Coal reservoir type
S	Methane saturated coal
Sb	Sub-bituminous coal rank
SLD	Staggered line drive well-pattern
SS	Shrinkage and swelling
TMRB	Total methane recovery at CO_2 breakthrough, %
US	Methane undersaturated coal
Wp	Well-pattern

CHAPTER 1

INTRODUCTION

The concentration of carbon dioxide in the atmosphere has been increasing since industrialization in the 19th century, and consensus is forming that mankind is having a visible impact on the world's climate. It is generally acknowledged that the most important environmental impact of fossil fuel burning is an increased global warming from the buildup of greenhouse gases in the atmosphere. This warming occurs when the added greenhouse gases trap more of the earth's outgoing heat radiation. The greatest contributor to global warming over the past century has been carbon dioxide. The foremost contributor to increased atmospheric CO_2 is fossil fuel combustion for power generation, transport, industry, and domestic use (Sengul, 2006).

Estimates of economic growth, energy use associated with economic activity, and CO_2 emissions associated with energy suggest that the concentration of CO_2 in the atmosphere will continue to grow during this century unless significant steps are taken to reduce releases of CO_2 to the atmosphere (Franklin, 2004). Therefore, the global warming issue has recently become one of the main concerns of Europe and other developed societies. By agreeing on Kyoto Protocol in 1997, developed countries decided to reduce their CO_2 emissions by 5.2% below 1990 levels. Since the world will continue to rely on energy from fossil fuels for several decades, there is growing recognition that the energy industry can be part of the solution to global warming by capturing CO_2 emissions and securely storing it underground (Sengul, 2006).

Geological sequestration is a potential mean to reduce large amount of CO_2 that otherwise be released into the atmosphere from petroleum developments as well as

other stationary sources including fossil-fired power plants (Nguyen, 2003). Carbon dioxide sequestration begins with the capture of CO_2 from large stationary sources, continues with its transportation to an appropriate injection site where it is pumped into underground geological formations. Geological storage sites include depleted natural gas and oil fields, deep saline aquifers, and coal seams (Kheshgi et al., 2006).

An attractive option for disposal of CO_2 is sequestration in deep, unmineable coal seams. Not only these formations have high potential for adsorbing CO_2, but the injected CO_2 can displace adsorbed CH_4 in the coal matrix, thus producing a valuable by-product and decreasing the overall cost of CO_2 sequestration. Because it has a large internal surface area, coal can store several times more CO_2 than the equivalent volume of a conventional gas reservoir (Klara et al., 2003). The global estimates of coalbed methane (CBM) resources are of the order of $2980 - 9260*10^{12}$ scf. Converting these to CO_2 storage capacity, assuming two molecules of CO_2 displacing one molecule of CH_4, yields a potential of 82 - 263 Gt CO_2 (Gunter et al., 1998).

In reservoir engineering terms, coalbeds are naturally fractured, low-pressure, water-saturated reservoirs, where most of the gas is retained in the micropore structure of the coal by physical adsorption. A reservoir is that portion of the coal seam that contains gas and water as a connected system. Thus, coal serves as a reservoir and a source rock, containing relatively pure methane. Compared to conventional gas reservoirs, coal reservoirs have low effective porosity and high compressibility and are dominated by gas adsorption. Gas stored by sorption in the coal matrix accounts for 95% or 98% of the gas in the coal seam. The remaining gas is stored in the natural fractures, or cleats, either free or dissolved in water (White et al., 2005).

CBM recovery technology has relied on depressurizing the coal reservoir so far. This is achieved by pumping off formation water to elicit methane desorption and production. Depressurization typically recovers 20% to 60% of original gas in place. This process is called primary recovery of CBM. However, more efficient recovery, theoretically up to 100% of original gas in place, may be obtained by injecting CO_2, N_2, or other inert gases into the coal reservoir. These injected gases can improve recovery by directly displacing the methane from the coal or by lowering the effective partial

pressure of the methane. Injected CO_2 remains sequestered on the coal unless it is mined or substantially depressurized (Gale and Freund, 2001). This recovery technique is named as enhanced coalbed methane (ECBM) recovery in the literature.

Flow in coalbeds occurs primarily in the fracture network (cleats in coal). Injected CO_2 flows through the cleats, diffusing into matrix blocks and replacing adsorbed CH_4. Thus, CO_2 can be used to enhance CH_4 recovery. There is evidence that coal permeability changes with the amount of adsorbed gas. Typically, as CH_4 is removed from coal, permeability increases, and as CO_2 adsorbs, permeability decreases. This phenomenon is called as shrinkage and swelling effect. Thus, displacement processes in coalbeds will involve a complex interplay of flow in the cleat system, changes in permeability, diffusion, and adsorption (Franklin, 2004).

Coalbeds are the least well understood option for CO_2 sequestration than others such as petroleum and natural gas reservoirs. Field experience with CO_2 injection into coalbeds is limited, although field tests are planned or are being conducted in the U.S., Canada, Poland, Australia, and Japan. The complex physical mechanisms and flows will offer challenges as well as opportunities. The combination of physical mechanisms and the potential for offsetting costs of CO_2 storage by CH_4 recovery suggest that more investigation of this approach is warranted (Franklin, 2004).

The subject of this study is modeling the effects of variable coal properties on methane production during enhanced coalbed methane recovery. In the literature, there are many parametric simulation studies (Smith et al., 2003; Davis et al., 2004; Maricic et al., 2005; Sinayuç, 2007) investigating the effects of physical coal properties on primary and enhanced coalbed methane recovery. However, simulation studies for ECBM recovery are limited. The trend is generally to change a model parameter in its given range and to observe its impact on total methane recovery. In this study, however, a new approach was followed during preparation of input data for a commercial compositional reservoir simulator, CMG (Computer Modeling Group) /GEM module. Instead of using a real field or a hypothetical data set, rank-dependent coal properties in the literature were gathered to construct a database. After modeling coalbed reservoir with this database, ECBM recovery simulations

were run for different coal ranks, reservoir types, well-patterns, drainage areas, anisotropies, cleat permeabilities, molar compositions of injected fluid and well types to be able to understand the effects of both coal properties and operational parameters on total methane recovery and CO_2 sequestration. For all these cases, shrinkage and swelling, which is the dominant transient process controlling cleat permeability, was taken into account by making use of extended version of Palmer and Mansoori (P&M) (1998) permeability model, which was first introduced by Mavor and Gunter (2004). This version enables to define multicomponent shrinkage and swelling effects to the simulator. Furthermore, effects of shrinkage and swelling on ECBM recovery and CO_2 sequestration were also studied separately with rank-dependent coal properties. In addition to coal rank, different reservoir types, molar compositions of injected fluid, and parameters within the extended P&M permeability model were considered with a sensitivity analysis. Therefore, the effects of variable coal properties on the total methane recovery, displacement ratio, CO_2 breakthrough and CO_2 storage were investigated with various ECBM recovery simulation scenarios.

CHAPTER 2

LITERATURE SURVEY

2.1 Introduction

This chapter firstly gives information about global warming and CO_2 sequestration into geological formations. Secondly, literature survey on the coal properties affecting storage and transport of methane, carbon dioxide and nitrogen is provided. Finally, transient processes occurring in the coal reservoir during application of primary and enhanced coalbed methane recovery techniques are described in detail.

2.2 Global Warming

Global warming refers to the increase in the average temperature of the earth's near-surface air and oceans in recent decades and its projected continuation. Usage of fossil fuels as a main energy source is leading to the increase in concentrations of greenhouse gases in the atmosphere. Greenhouse gases alter radiative balances and tend to warm the atmosphere. The climate models project that the mean annual global surface temperature will have increased by 1 - 3.5°C by 2100. Global mean sea level will have risen by 15 - 95 cm as a result of that process. The average rate of warming probably would be greater than any seen in the past 10,000 years (IPCC, 1997). According to "Climate Change 2001" report of Intergovernmental Panel on Climate Change (IPCC), departures in world average temperature in °C from the 1961- 1990 average is like in Figure 2.1. The increasing trend in the average temperature of the world after industrial revolution is clearly seen.

The greatest contributor to global warming over the past century has been carbon dioxide, mostly from deforestation and fossil fuel burning. Methane and Nitrous

oxide follow it. The foremost contributor to increased atmospheric CO_2 is fossil fuel combustion for power generation, transport, industry, and domestic use (Sengul, 2006).

One of the biggest problems faced by the climatologists is that even a small increase in the average temperature of the earth is expected to cause the temperatures in the Polar Regions rise three to four times, the average temperature and therefore the impact of warming will be much greater than originally envisioned. In addition, the climatic variations due to global warming could be significant, resulting in flooding of the coastal areas worldwide due to sea level rise (Sinha, 2000). Therefore, the global warming issue has become one of the main concerns in Europe and other developed societies. Through the Kyoto Protocol, developed countries agreed to reduce their CO_2 emissions by 5.2 % below 1990 levels. Since the world will continue to rely on energy from fossil fuels for several decades, there is growing recognition that the energy industry can be part of the solution to global warming by capturing CO_2 emissions and securely storing the CO_2 underground (Sengul, 2006).
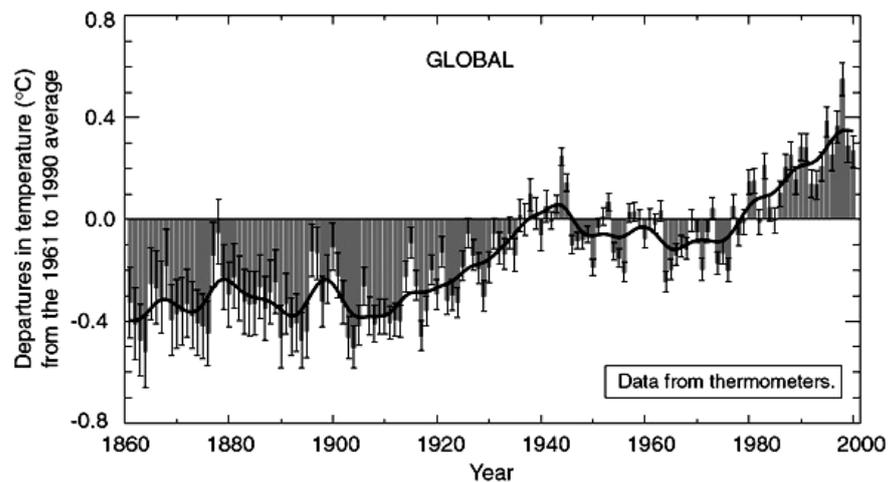
Figure 2.1 Departures in World Average Temperatures from the 1961- 1990 Average (IPCC, 2001).

2.2.1 Greenhouse Gases

Greenhouse gases include those listed in the Kyoto Protocol: Methane (CH_4), nitrous oxide (N_2O), hydro fluorocarbons (HFCs), per fluorocarbons (PFCs), sulphur hexafluoride (SF_6) and those listed under the Montreal Protocol and its amendments the chlorofluorocarbons (CFCs), the hydro chlorofluorocarbons (HCFCs).

United States is the largest emitter of all greenhouse gases (18.4 % of global emissions), followed by the former Soviet Union (13.5 %), China (9.1 %), Japan (4.7 %), India (4.1%), Brazil (3.9 %) and Germany (3.4 %). More than 50 % of the CO_2, the main gas contributing towards the greenhouse effect, is emitted by the industrialized countries of the world (Sinha, 2000). Composition of the emitted greenhouse gas in the United States of America is shown in Figure 2.2. It is seen that CO_2 emission from fossil fuel consumption forms 82 % of the total greenhouse emissions of the U.S.A.
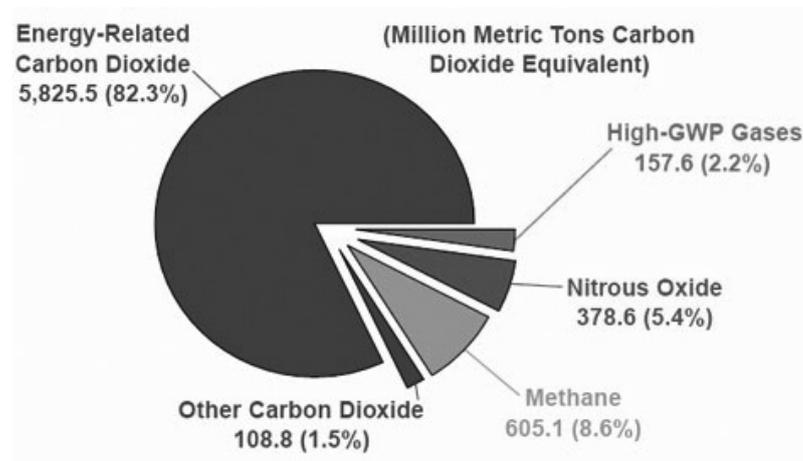
Figure 2.2 Greenhouse Gas Emissions in the U.S.A. in 2006 (EIA, 2008).

2.2.2 World Fossil Fuel Consumption

Oil, coal and gas are the dominant current sources of energy. Over the next 30 years, energy use is forecast to grow by more than 60 percent, fuelling economic and social

development, with 16 trillion dollars of investment in infrastructure related to production and use (Kheshgi et al., 2006).

In the period of 1970 - 2005, International Energy Agency data show that fossil fuel use increased by some 42% globally. However, over the next 25 years, development and industrialization, particularly in the Asian economies such as China and India, is forecast to drive a further increase in fossil fuel utilization of some 70%. All current indications suggest that fossil fuels will continue to drive the development of the global economy for several decades. This situation can also be seen in Figure 2.3 prepared by Energy Information Administration (EIA), U.S. Department of Energy (Espie, 2005). This high energy demand will also drive world to emit more greenhouse gases to atmosphere.
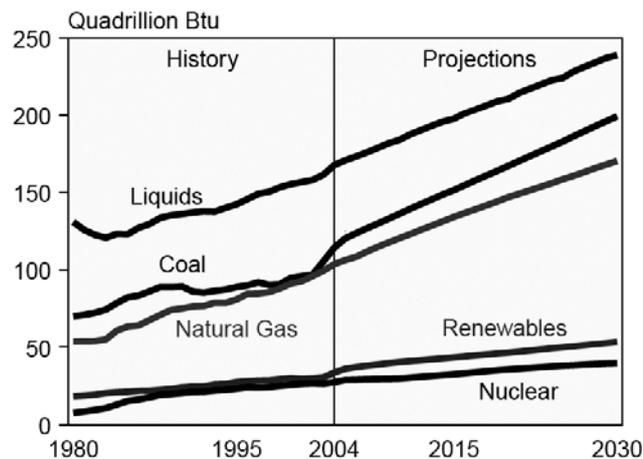
Figure 2.3 World Energy Usages by Fuel Type, 1980 - 2030 (EIA, 2007).

2.2.3 World CO$_2$ Emissions

In Figure 2.4, global emission scenarios of cumulative carbon dioxide are presented by IPCC (2000). Each case assumes a different direction for future world economic developments (IPCC, 2000). As it is realized in Figure 2.4, carbon dioxide concentration is increasing in all scenarios from 1990 to 2100. It means that global

carbon dioxide emission will continue to increase in all economic conditions of the world. Therefore, it seems that the main concern of the world will be to capture and store the emitted carbon dioxide with new technologies. One way is to sequester CO_2 into geological formations.
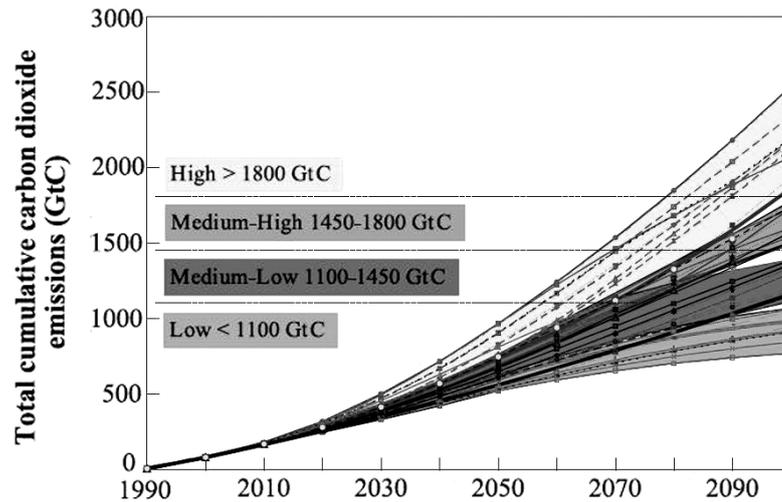
Figure 2.4 Cumulative Carbon Dioxide Emissions of the World (IPCC, 2000).

2.3 CO_2 Capture and Storage into Geologic Formations

Carbon dioxide sequestration begins with capturing of CO_2 from large stationary sources and its transportation to an appropriate injection site where it is pumped into underground geological formations. The capture of CO_2 can be realized by separating it from produced natural gas or from flue gases emitted from industrial facilities due to fossil fuel usage. Once captured, the CO_2 can be transported by high pressure pipelines or tankers to land-based or offshore geological sites. At the site CO_2 can then be injected for storage (Kheshgi et al., 2006). In Figure 2.5, deep underground formations into which CO_2 can be stored are represented as follows:

9

1. Depleted oil and gas reservoirs.

2. Usage of CO_2 in enhanced oil recovery.

3. Deep unused saline aquifers.

4. Deep unmineable coal seams.

5. Usage of CO_2 in enhanced coalbed methane recovery.

6. Other suggested storage options such as basalt, oil shales and cavities.
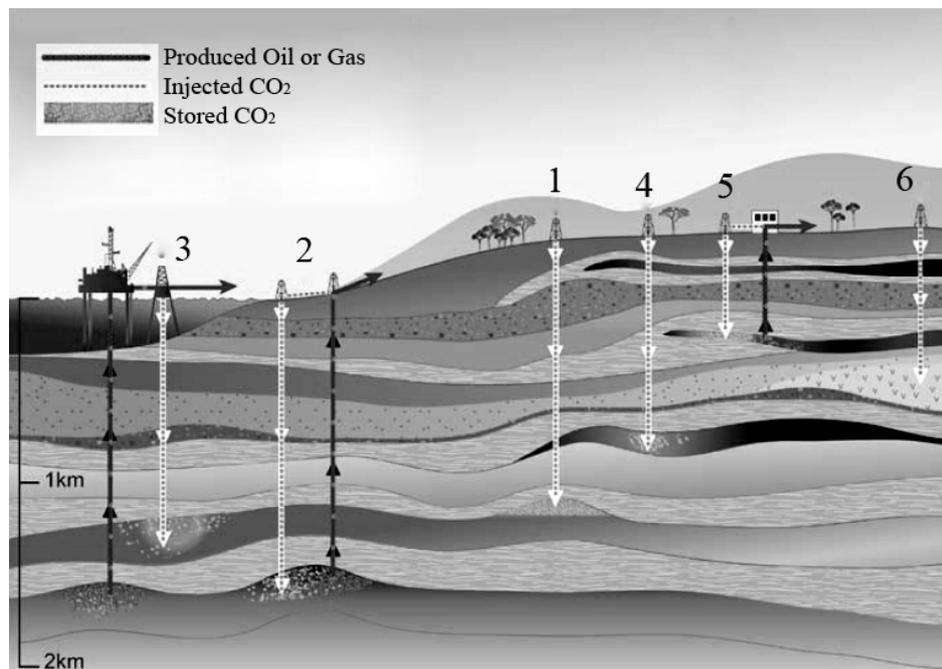
Figure 2.5 Deep Underground Formations for CO_2 Storage (IPCC, 2005).

In Table 2.1, estimated CO_2 storage capacities of deep geological formations are provided. Deep aquifers and depleted oil and gas reservoirs have the highest capacity and retention time, but usage of CO_2 for enhanced oil recovery and enhanced coalbed methane recovery is more attractive for energy companies. The reason is that sequestration of CO_2 and production of valuable products such as oil and methane are realized with the same process at low costs.

Table 2.1 Estimated CO$_2$ Storage Capacities of Geological Formations (Grimston et al., 2001).

Sink Name	CO$_2$ Capacity	Retention Time
-	Gt	Year
Enhanced Oil Recovery	20 - 65	Tens
Coalbeds	80 - 260	>100,000
Depleted Oil and Gas Reservoirs	130 - 500	>100,000
Deep Aquifers	30 - 650	>100,000

2.3.1 Oil Fields

Enhanced oil recovery is the most mature and commercially proven way to both sequester CO$_2$ and produce extra oil from heavy oil reservoirs. Under favorable reservoir conditions, an additional 5 to 20 % of the original oil in place may be recoverable. Most of the injected CO$_2$ fills the pore space of the reservoir. It is sequestered as long as the wells are in operation and reservoir pressure is maintained. Capping the production and injection wells will also maintain CO$_2$ sequestration (Stevens et al., 2001). In addition to enhanced oil recovery projects, CO$_2$ can be sequestered into depleted oil fields.

2.3.2 Gas Fields

The most obvious application is to convert depleted gas fields for long term CO$_2$ storage at the end of economic hydrocarbon production. The alterations required are generally small and it may even be possible to utilize the previous gas export line for CO$_2$ import. Although this option has the great advantage that initial capital costs are likely to be small, it suffers from the disadvantage that it generates no income stream in the absence of carbon trading credits or fiscal incentives. It will nevertheless offer a cheap disposal option when CO$_2$ transportation costs are low (Espie, 2005).

An alternative option that may offer the opportunity to generate an incremental income stream is Enhanced Gas Recovery. This is the injection of CO$_2$ back into the base of a producing gas reservoir. The properties of CO$_2$ are such that its density is greater than virtually all hydrocarbon gases under normal reservoir conditions

while its viscosity is less than that of hydrocarbon gas. This means that the potential exists for a gravity stable gas to gas displacement. Hence, CO_2 injection could not only maintain pressure and well performance but also increase ultimate gas recovery (Espie, 2005).

2.3.3 Deep Saline Aquifers

CO_2 storage into brine filled formations represents the largest potential worldwide. However, neither many of the formations have not been extensively explored nor appraised for CO_2 storage; they also have a large uncertainty. Storage in brine filled formations involves immiscible gravity dominated displacement by supercritical CO_2 with only of order of 10 % or less dissolving into the brine phase. However, over time, as CO_2 accumulates and spreads at the top of the formation, the surface area between the brine and the CO_2 increases, and increasing amounts of CO_2 will dissolve in the brine. The resulting CO_2 saturated brine will be slightly heavier than unsaturated brine and will tend to sink to the bottom of the formation. Once dissolved into the brine phase, the CO_2 is in a very secure state (Espie, 2005).

2.3.4 Enhanced Coalbed Methane (ECBM) Recovery

CH_4 and other gases are generated during the conversion of plant materials to coal in the bituminous stage of coalification. These gases are largely adsorbed onto the coal surface and small quantities are dispersed in the pore system of the coal. Coals have a dual porosity system, namely microporosity and macroporosity. The controlling factors for the amount of CH_4 stored in coals are the confining pressure and the surface contained within coal micropore system. Coal seams can easily contain up to five times the amount of gas contained in a conventional gas reservoir of comparable size. CH_4 in a coalbed is stored in three states: an adsorbed state, as free gas or dissolved in water in the fractures. A two-phase fluid system exists in the cleats, consisting of water and gas. As the water is removed from the cleat system, pressure in the coal is reduced until the water pressure equals to the gas pressure. It is termed as desorption pressure at which coalbed methane (CBM) is desorbed from the matrix to the cleats (Gentzis, 2000).

CBM recovery technology has relied on depressurizing the coal reservoir so far. This is achieved by pumping off formation water to elicit methane desorption and production. Depressurization typically recovers 20% to 60% of original gas in place. This process is called primary recovery of coalbed methane. However, more efficient recovery, theoretically up to 100% of original gas in place, may be obtained by injecting CO_2, N_2, or other inert gases into the coal reservoir. These injected gases can improve recovery by directly displacing the methane from the coal or by lowering the effective partial pressure of the methane. Injected CO_2 remains sequestered on the coal unless it is mined or substantially depressurized (Gale and Freund, 2001).

CO_2 fixation by adsorption onto the surface of coals is the main process for storage in coals. It involves a combination of physical and chemical processes that occurs very rapidly when CO_2 is injected, on a timescale of days. The nature of the fixation makes leakage processes different and since the CO_2 is bound to the coal, the presence of a top seal may not be necessary. The main release mechanism is by depressuring which could occur if water or coalbed methane extraction takes place, or if uplift occurs after CO_2 storage (Espie, 2005).

Up to date, only a few experimental ECBM recovery tests involving CO_2 injection have been conducted throughout the world. The sites for these tests show great potential for both CO_2 sequestration and ECBM recovery. Coalbed thickness is of great importance for ECBM recovery, because thicker coalbeds have greater CH_4 volumes and advanced production techniques are more applicable in thick coalbeds (Klara et al., 2003).

The Alberta Research Council in Canada is investigating an alternative approach using flue gas or combined N_2 - CO_2 injection. With N_2 injection, early N_2 breakthrough at the production well causes additional operational costs because the N_2 must be separated from the methane before sale. Combining CO_2 and N_2 injection will improve the economics because the breakthrough of N_2 will be retarded compared to N_2 injection alone, and the methane production rate will be increased by the addition of CO_2. To date, however, there is little experience of injecting flue gas into geological formations (Gale and Freund, 2001).

2.4 Physical and Chemical Properties of CO_2

CO_2 is mostly injected in supercritical state (31 °C and 73 atm) in order to avoid adverse effects from CO_2 separating into liquid and gas phases in the injection system. The supercritical fluid is the name given to a substance that is at a temperature and pressure above the critical point. Supercritical fluids have unique properties that lie between that of liquid and that of gas: polarity, viscosity, diffusivity, and density (Ebbing and Gammon, 1999).
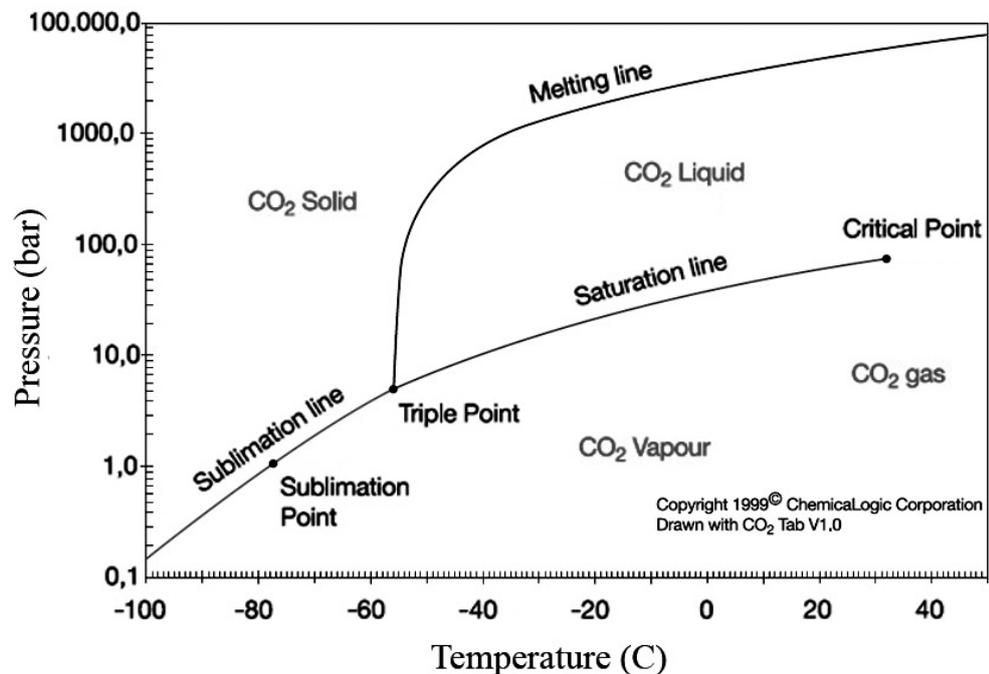
Figure 2.6 CO_2 Pressure vs. Temperature (IPCC, 2005).

At normal temperature and pressure, carbon dioxide is a gas. The physical state of CO_2 varies with temperature and pressure as shown in Figure 2.6. Above critical point, the density of CO_2 can be very large, approaching or even exceeding the density of liquid water (IPCC, 2005).

In aqueous solutions, CO_2 forms carbonic acid, which is too unstable to be easily isolated. The solubility of CO_2 in water decreases with increasing temperature and decreasing pressure. Moreover, the solubility of CO_2 in water also decreases with increasing water salinity by as much as one order of magnitude. Selected physical properties of CO_2 are given in Table 2.2 (IPCC, 2005).

Table 2.2 Physical Properties of CO_2 (IPCC, 2005).

Property	Units	Value
Molecular Weight	g/gmole	44.01
Critical Temperature	°C	31.1
Critical Pressure	bar	73.9
Critical Density	kg m^{-3}	467
Triple Point Temperature	°C	-56.5
Triple Point Pressure	bar	5.18
Boiling Point @ 1.013 bar	°C	-78.5
Gas Density @ STP [1]	kg/ m^3	1.976
Viscosity @ STP	μPa.s	13.72
Solubility in Water @ STP	vol vol^{-1}	1.716

[1] Standard Temperature and Pressure (60 F° & 14.7 psia)

2.5 Physical and Chemical Properties of Coal

Coal deposits function as self-sourced natural gas reservoirs wherein the three crucial petroleum system elements of source rock, reservoir and trap are located together in a single geologic unit (Nelson, 2000). For this reason, information about chemical and physical properties of coal are provided under the headings of "Coal as a Source Rock" and "Coal as a Reservoir Rock" in following sections.

2.5.1 Coal as a Source Rock

Coal is a fossil fuel. It is a combustible, sedimentary, organic rock, which is composed mainly of carbon, hydrogen and oxygen. It is a heterogeneous mixture of components. Mineral matter, water and methane are natural components of coal;

their relative proportions are important influences on the value of coal. Coal composition has evolved in response to temperature, pressure, and the chemical environment. Though solid in appearance, coal contains gas and oil-like substances, which are formed during coalification. Part of these substances is retained in the coal and part of them is expelled. Coal rank and the relative abundance of various components determine most of the physical and chemical properties of coal (GRI, 1996).

2.5.1.1 The Origin and Formation of Coal
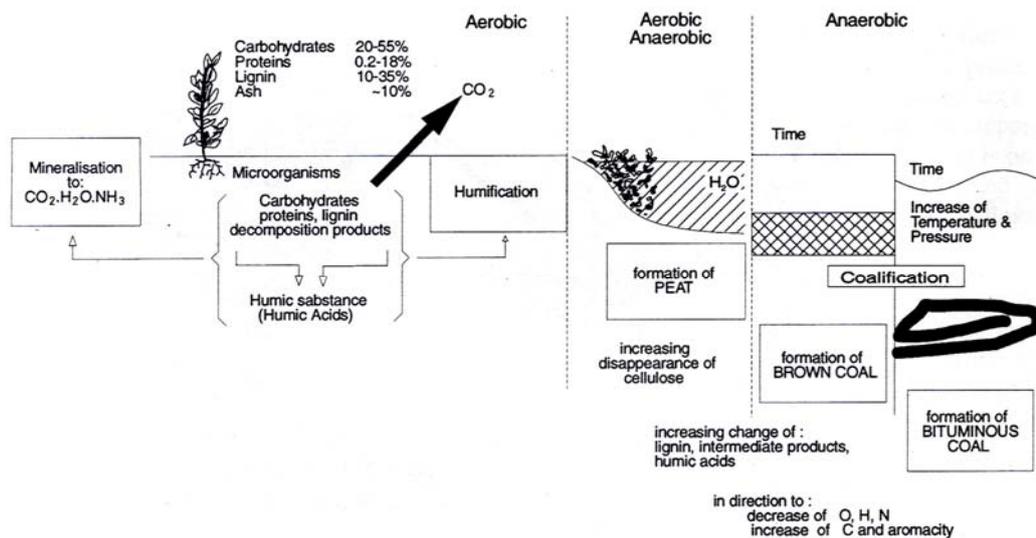
Figure 2.7 Formations of Peat, Brown Coal and Bituminous Coal (Kural, 1994).

Formation of coal began during the carboniferous period, which is known as the first coal age spanning from 360 million to 290 million years ago (WCI, 2007). As organic material is buried, compressed, and dewatered, peat is formed. Peat is a dark brown residuum produced by the partial decomposition and disintegration of plants that grow in marshes and swamps. As peat is buried more deeply, heat and pressure progressively drive off water and volatiles. Peat is then transformed into coal as the carbon content of the fossil organic material increases through devolatilization. In

this process called coalification, coals increase in rank from lignite, to sub-bituminous, bituminous, and anthracite. Coal rank is important because it directly influences the gas storage capacity of coal. Several factors influence the rank and type of coal formed: the type of organic material, depositional setting, pH, temperature, reducing potential, depth of burial, and time of burial (GRI, 1996). In Figure 2.7, processes taking place during formation of peat, brown coal and bituminous coal are represented.

The quality of each coal deposit is determined by temperature and pressure and by the length of time in formation, which is referred to as its 'organic maturity'. Low rank coals, such as lignite and sub-bituminous coals are typically softer, friable materials with a dull, earthy appearance. They are characterized by high moisture levels and low carbon content, and therefore low energy content. Higher rank coals are generally harder and stronger and often have a black, vitreous lustre. They contain more carbon, have lower moisture content, and produce more energy (WCI, 2007). In Figure 2.8, rank dependencies of carbon and moisture content of coal are shown with their percentages in world coal reserves.
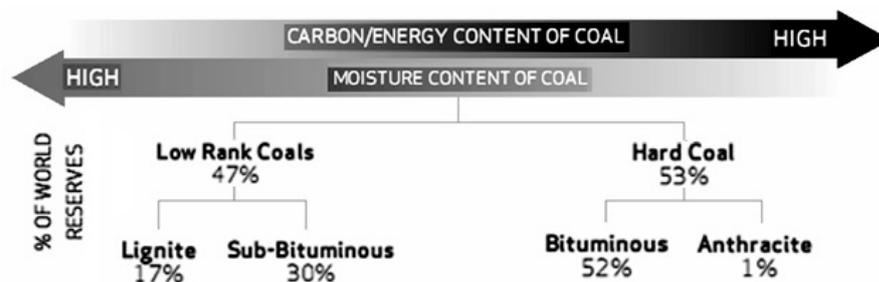
Figure 2.8 Rank Dependencies of Carbon and Moisture Content of Coal (WCI, 2007).

2.5.1.2 Maceral Composition of Coal

Maceral is defined as the organic material inside coal seam. The macerals are classified in three groups, namely, vitrinite, inertinite and exinite. Vitrinite group is

the most abundant and important maceral group in coal. The inertinite group of macerals has a variable abundance in coal. They have the highest reflectance properties, the highest carbon, lowest hydrogen contents and lowest volatile matter yield. Exinite group of macerals forms the minor part of coal (Kural, 1994).

2.5.1.3 Classification of Coal

Physical and chemical properties can vary significantly from seam to seam and over a short distance within a seam. Coal is usually classified by three fundamental characteristics:

Grade : The relative percentage of organic to mineral components.

Type : The various organic constituents.

Rank : The level of maturation reached, ranging from peat through anthracite.
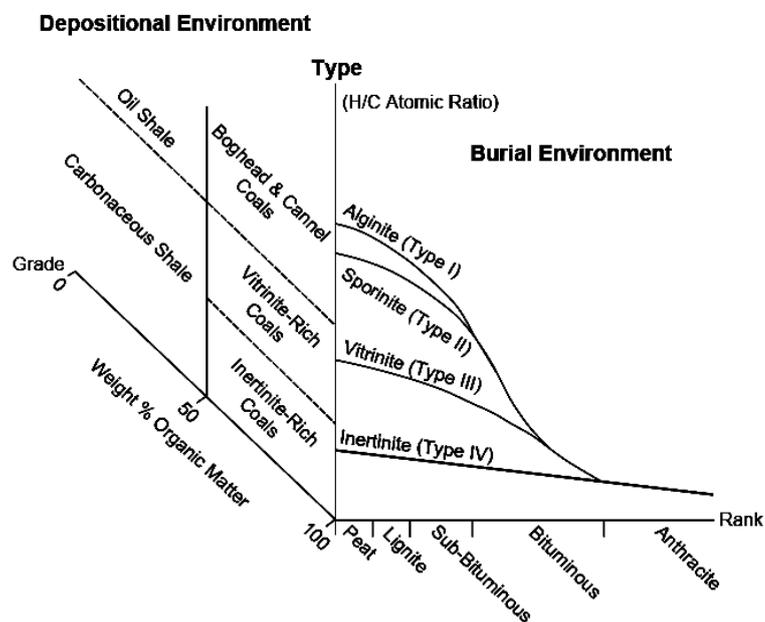
Figure 2.9 Coal Classifications by Grade, Type, and Rank (GRI, 1996).

18

These characteristics are used in classifying coal, as shown in Figure 2.9. The three-axis diagram is a petrographic classification of coal composition in which grade, type, and rank are depicted on three orthogonal axes.

The composition of coal often is described by proximate analysis and ultimate analysis. A proximate analysis provides the percentage of fixed carbon (FC), volatile matter (VM), moisture (H_2O), and ash content of the coal, as shown in Figure 2.10. An ultimate analysis provides the chemical makeup of the coal as percentages of carbon, oxygen, hydrogen, nitrogen, sulfur, and ash.
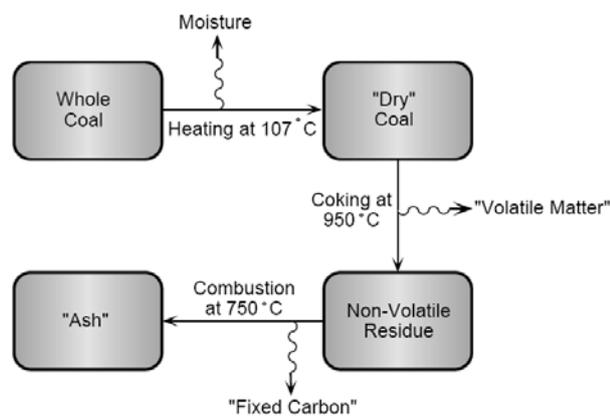
Figure 2.10 Proximate Analysis Process (GRI, 1996).

The relative amount of these components can be reported in several ways; the most common include:

- "As received" basis includes FC, VM, H_2O, and ash based on moisture in the coal as received for analysis.
- "Air dried" basis is the same as "as received" except the moisture content is equilibrated to the lab atmosphere.
- "Dry" basis includes only FC, VM, and ash, normalized to 100 percent.
- "Ash-free" basis includes only FC, VM, and H_2O normalized to 100 percent.

19

- "Dry, ash-free" basis includes only FC and VM, the organic components, normalized to 100 percent.

Rank		Refl. Rm$_{oil}$	Vol. M d.a.f. %	Carbon d.a.f. Vitrinite	Bed Moisture	Cal. Value Btu/lb (kcal/kg)	Applicability of Different Rank Parameters
German	USA						
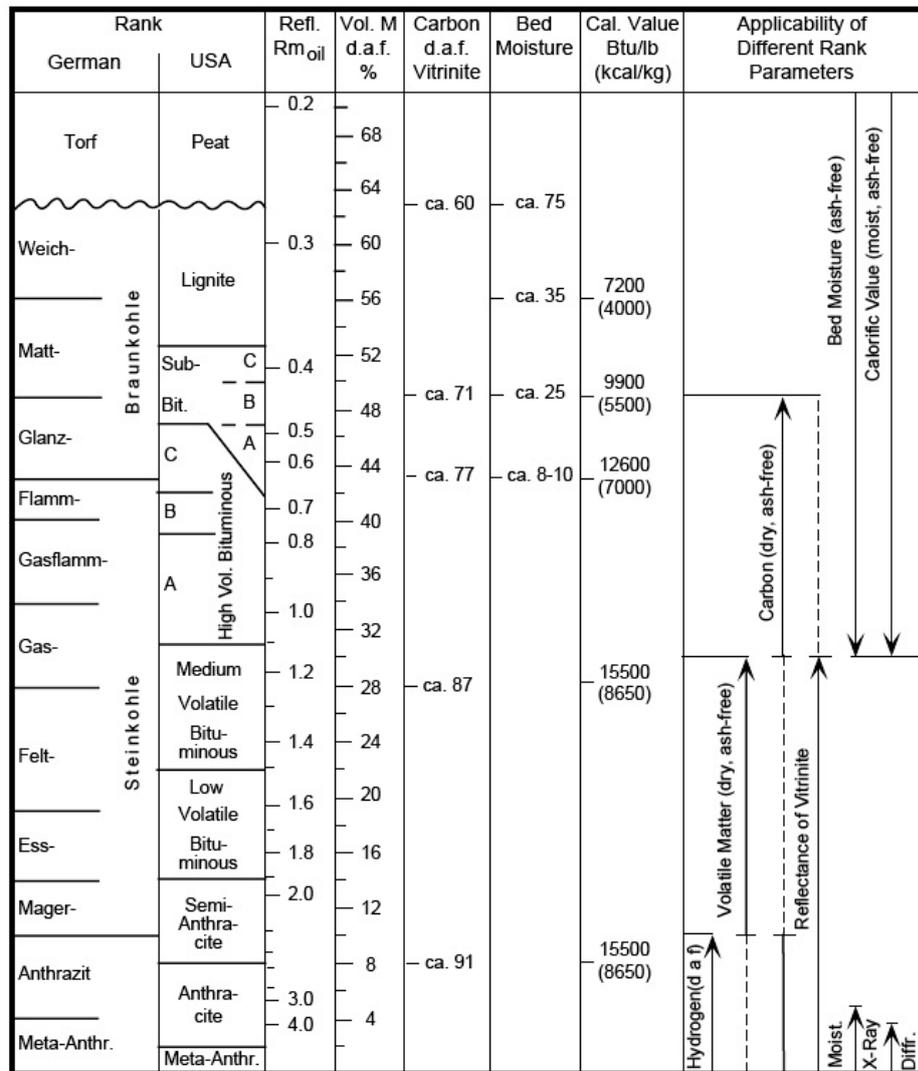
Figure 2.11 Classification of Coal by Rank (GRI, 1996).

With increasing coalification rank, the macerals change in their chemical and physical properties. There is a distinct relationship between the reflectance of vitrinite and its carbon or volatile matter yield. This means that the rank of a coal can be determined exactly by measuring its reflectance on a polished surface (Kural, 1994). The

classification standard in Figure 2.11 covers the classification of coals by rank, that is, according to their degree of metamorphism, or progressive alteration, in the natural series from lignite to anthracite. This classification is applicable to coals that are composed mainly of vitrinite. In addition to vitrinite reflectance of coal, carbon content, bed moisture and volatile matter in coal are provided with respect to rank of coal. Moreover, according to coal classification standard of American Society for Testing & Materials (ASTM), the relationship between vitrinite reflectance and rank of coal is also provided in Figure 2.12.
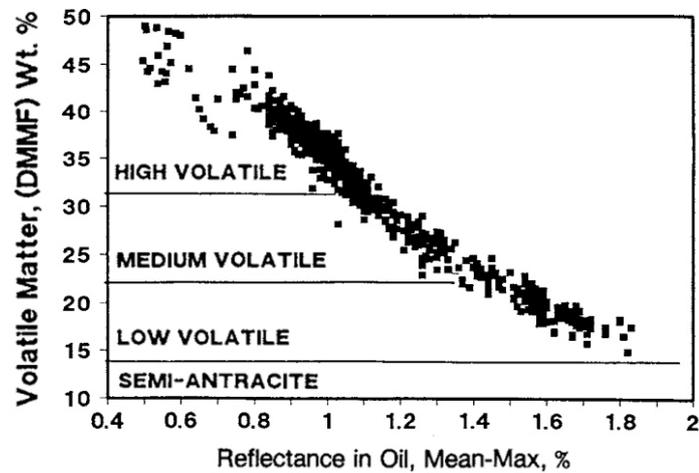
Figure 2.12 Ranks of U.S. Coal vs. Vitrinite Reflectance (ASTM, 2005).

2.5.2 Coal as a Reservoir Rock

Coal is also a reservoir rock, since CH_4 is directly produced from the coal seams. Coals are dual-porosity media composing of matrix blocks and fractures called cleats. Therefore, reservoir properties of coal seams are classified into two groups namely, matrix system and fracture (cleat) system.

2.5.2.1 Matrix System in Coal Seams

In this section, information about matrix porosity, matrix permeability, density, strength, gas storage capacity, and diffusion coefficient of coal are provided.

2.5.2.1.1 Matrix Porosity

Coal porosity is the volume fraction of coal occupied by empty spaces, which may be occupied by a particular fluid. In its natural state, in the seam, coal also contains inherent moisture, which occupies part of the pore structure. The volume fraction free to be occupied by gases in sorption processes corresponds to the so-called void volume (Rodrigues and Lemos de Sousa, 2002).
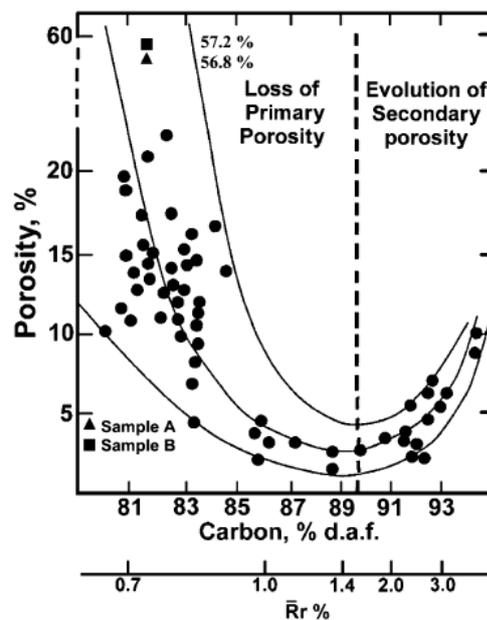
Figure 2.13 Total Coal Porosity vs. Carbon Content and Vitrinite Reflectance of Coal (Rodrigues and Lemos de Sousa, 2002).

Coal is characterized by a dual porosity, which consists of micropore and macropore systems. The micropore system is estimated to have pore diameters less than 2 nm,

22

which occur as part of the coal matrix. The macropore system is established by the fracture network that is designated by the cleat system. In Figure 2.13, total coal porosity, which includes both matrix and fracture porosities, vs. carbon content and vitrinite reflectance of coal is provided. Macropores (primary porosity) predominate in lower rank coals. Geophysical factors, such as compaction and water expulsion, progressively reduce primary porosity. At about low-volatile bituminous coal rank, the development of secondary porosity begins with the formation of meso and micropores. This implies an increase of porosity due to well-known progressive changes in the molecular structure through higher ranks. Therefore, as coal rank increases, macro (fracture) porosity decreases, but meso and micro (matrix) porosities increase (Rodrigues and Lemos de Sousa, 2002).

Porosity is also related to the maceral composition. Vitrinite predominantly contains microporous contents, whereas inertinite predominantly contains meso and macroporous contents (Rodrigues and Lemos de Sousa, 2002). More information on cleat porosity of coal can be found in "Fracture System in Coal Seams" Section.

2.5.2.1.2 Matrix Permeability

Over 95% of the gas in coal is stored in micropores that are estimated to have diameters ranging from 0.5 to 1 nm. These values are so small that the coal matrix may have no effective permeability (Laubach et al., 1998).

2.5.2.1.3 Density of Coal

Coal resources can be more accurately estimated if the coal density is known. Because of the porous nature of coal, it can be difficult to accurately determine its volume and thus its density. Usually, apparent density is measured rather than true density. The apparent density of coal reaches a minimum at about 85% carbon content as shown in Figure 2.14 (GRI, 1996).
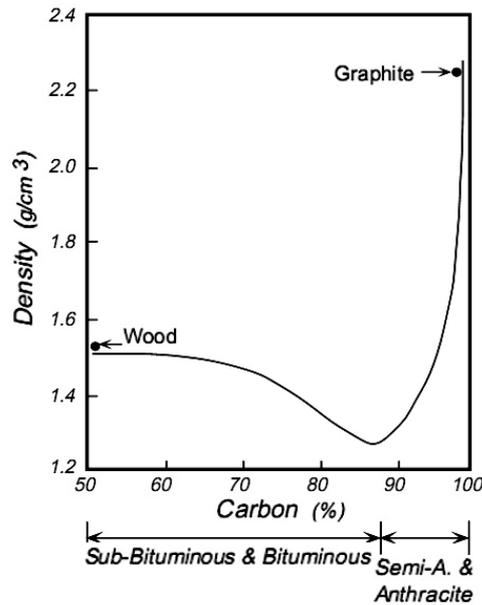
Figure 2.14 Apparent Density vs. Carbon Content of Coal (GRI, 1996).

2.5.2.1.4 Strength Parameters

As it is provided by Kural (1994) elastic modulus from different references are plotted with respect to carbon contents of coal in Figure 2.15. Carbon content of the coal is related to rank of coal. For all references in Figure 2.15 elastic modulus show an increasing trend between sub-bituminous (~70% carbon content) and medium-volatile bituminous (~%85). After medium-volatile bituminous coal rank, however, it has a decreasing trend.

According to published data in Berkowitz's (1979) book, there is no relation between Poisson's ratio and carbon content of coal. Its value is constant between sub-bituminous and medium-volatile bituminous coal ranks as in Figure 2.16.
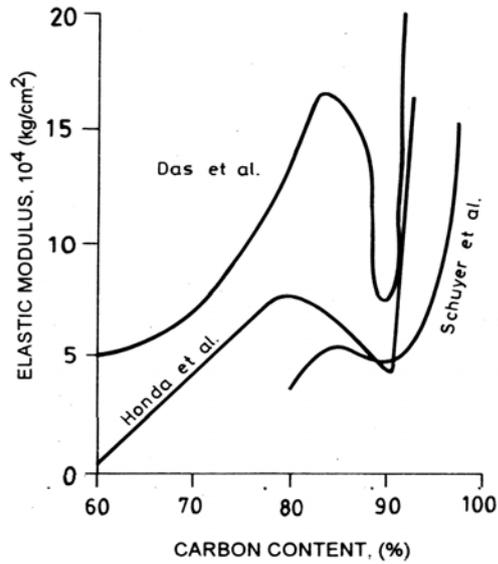
Figure 2.15 Elastic Modulus vs. Carbon Content of Coal (Kural, 1994).
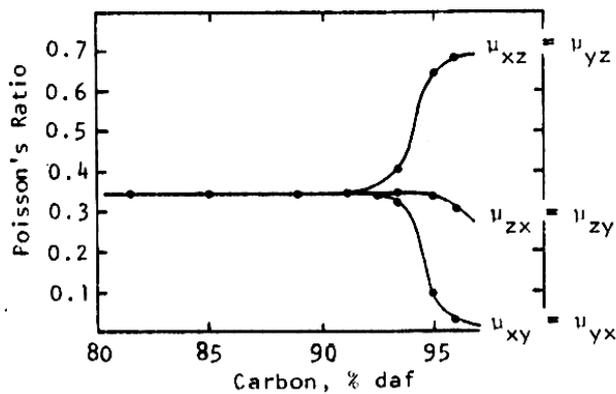
Figure 2.16 Poisson's ratio vs. Carbon Content of Coal (Dry, Ash Free) (Berkowitz, 1979)

2.5.2.1.5 Gas Storage Capacity

Methane adsorbed in coal matrix typically accounts for 98% of the gas within a coal seam, depending on the pressure at which the gas is adsorbed. In addition, gas is stored in the pore or cleat space either free or in solution (Gray, 1987). Gas adsorption on the coal surface is a physical phenomenon. During physical sorption, fluid molecules experience a net attraction to a solid surface. Because of the

25

attraction, the density of the fluids near the pore walls is increased. The increased density means that at low pressure, greater volumes of gas can be stored by sorption than by compression. The most common model in use for coal is the Langmuir isotherm, which relates the capacity of coal to store gas to the external pressure of the gas. As the name implies, an isotherm is evaluated at a constant temperature. A form of the Langmuir isotherm that can be used for pure component storage capacity is given below (GRI, 1996).

$$G_S = V_L \cdot [1 - (a + m)] \cdot \left[\frac{P}{P + P_L} \right] \tag{2.1}$$

, where G_S is gas storage capacity, (scf/ton); V_L is dry and ash-free Langmuir volume, (scf/ton); P_L is Langmuir pressure, (psia); P is pressure, (psia); a is ash content, (weight fraction); m is moisture content, (weight fraction).
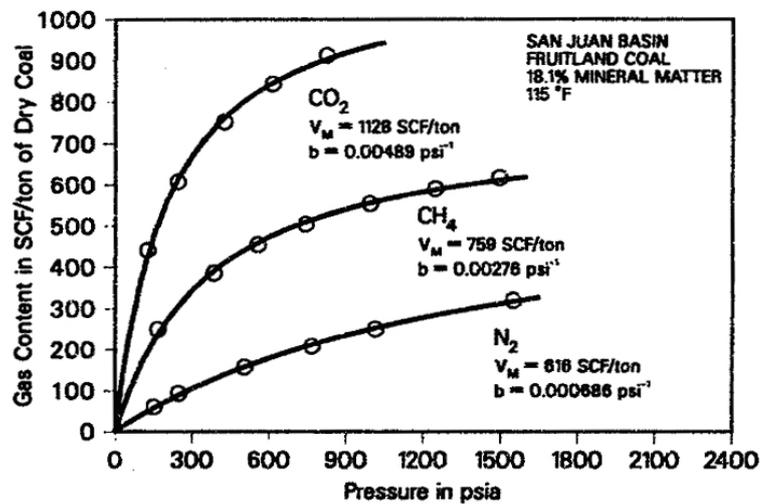
Figure 2.17 Pure Sorption Isotherms of CO$_2$, CH$_4$ and N$_2$ (Arri et al., 1992).

Pure sorption isotherms of CO$_2$, CH$_4$ and N$_2$ are provided by Arri et al. (1992) in Figure 2.17. In this experimental study, the amount of CO$_2$ stored is 1.5 times greater

than CH_4 and nearly 3 times greater than N_2. Theoretically, this phenomenon enables engineers to both displace CH_4 adsorbed in coal matrix and store injected CO_2 during application of ECBM recovery technique.

In a multicomponent gas system, however, adsorption of one gas component onto coal surface affects the others. Therefore, total amount of gas stored at a selected pressure is between the storage capacities of each pure gas forming the multicomponent system. This phenomenon is called as multicomponent effect on storage capacity and it is modeled by extended Langmuir isotherm. For instance, in Figure 2.18 total amount of gas stored at constant pressure is smaller than maximum storage capacity of pure CO_2 and greater than maximum storage capacity of CH_4 with respect to different mole fractions of CO_2 in CH_4/CO_2 mixture (GRI, 1996).
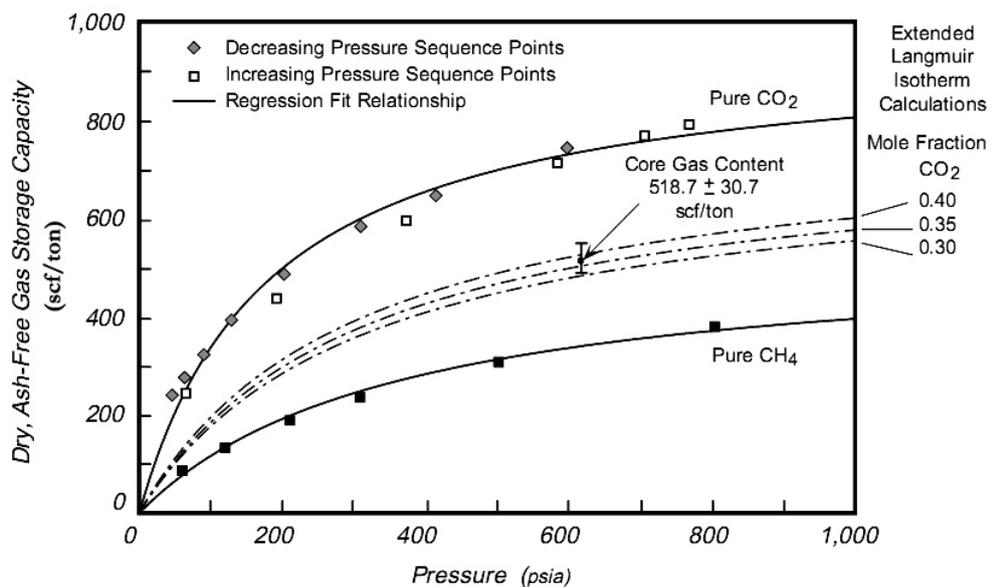
Figure 2.18 Multicomponent Effects on Total Gas Storage Capacity (GRI, 1996).

With the extended Langmuir isotherm, the gas content of each component can be directly calculated from its partial pressure. Only the Langmuir constants from pure gas sorption are used, and no binary sorption constants are needed (Arri et al., 1992).

27

$$G_{si} = V_{Li} \cdot [1 - (a + m)] \cdot \dfrac{(y_i \cdot P)\big/ P_{Li}}{1 + \sum\limits_{j=1}^{nc} (y_j \cdot P)\big/ P_{Lj}} \qquad (2.2)$$

, where G_{Si} is multicomponent gas storage capacity of component i , (in situ basis, scf/ton); V_{Li} is pure component Langmuir volume i, (dry and ash-free basis, scf/ton); P_{Li} or P_{Lj} is pure component Langmuir pressure i or j, (psi); P is total pressure of free gas phase, (psi); y_i or y_j is molar fraction of component i or j; a is ash content, (weight fraction); m is moisture content, (weight fraction); nc is the number of gas components.

Coal properties, such as rank of coal, mineral matter (ash), maceral content, in-situ moisture contents and reservoir conditions, such as pressure, temperature are important parameters affecting the sorption, desorption and, therefore, total gas storage capacity of coalbeds.

Rank of Coal: In addition to component-dependent gas storage capacity of coal, rank of coal has also an important effect on the amount of gas stored. In Figure 2.19 it is clearly seen that the amount of CH_4 stored at the same pressure increases as the rank of coal increases. Moreover, the same trend is also observed for CO_2 and N_2 by Reeves and Gonzales (2005).

Mineral Matter (Ash) Content: Mineral matter acts as inert diluents and does not contribute to any gas sorption. The mineral matter content decreases the gas sorption capacity because it takes the place of organic matter in coal on which sorption occurs (Katyal et al., 2007). In order to compare gas content measurements among various coal samples and to determine gas content trends within or among basins, it is important that the sorption isotherms and gas content measurements are corrected for ash contents (Scott, 2002).
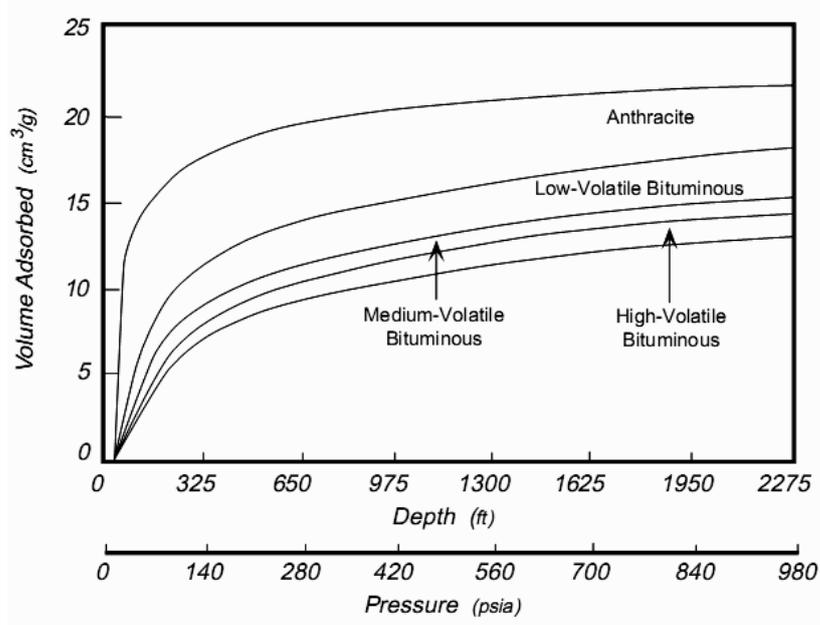
Figure 2.19 CH₄ Storage Capacities for Different Coal Ranks (GRI, 1996).

Maceral Content: Amount of gas adsorbed on coal matrix depends on not only the amount of macerals, but also the maceral types. As it is stated by Scott (2002), coals with the lowest methane sorption capacity are inertinite-rich, whereas vitrinite-rich coals have the highest sorption capacity. It is also indicated in Figure 2.20.
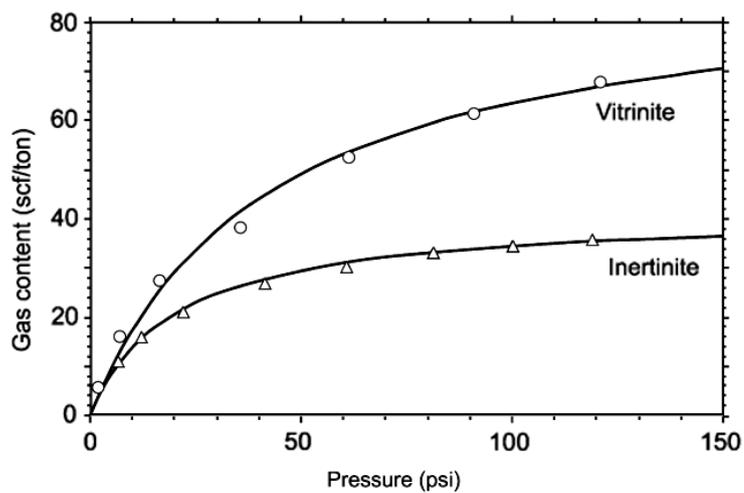
Figure 2.20 Effect of Maceral Type on Gas Sorption Capacity (Scott, 2002).

29

In-situ Moisture Content: Moisture content decreases with increasing coal rank and most of the water is lost before coal reaches the high volatile bituminous rank. Sorption capacity can decrease significantly with increasing moisture content and it should be corrected for moisture (Scott, 2002). Water shares the same sort of relationship with the coal matrix as carbon constituents such as methane and CO_2, with which it competes for accessibility in the coal structure. The adsorbed water molecules occupy a certain amount of surface area otherwise available for methane adsorption and may block access of gas to the microporosity (Katyal et al., 2007). Therefore, increasing moisture content leads to a decreasing sorption capacity.

Pressure and Temperature: Adsorption capacity of coal depends on both pressure and temperature. As the pressure increases, the amount of gas adsorbed on the coal surface increases. But this process occurs on the same Langmuir isotherm. Langmuir isotherm curve shifts up and down according to temperature change. As it is shown in Figure 2.21, coal sorption capacity decreases with increasing temperature at the same pressure indicating that the coal surface area available for sorption changes with temperature (Scott, 2002).
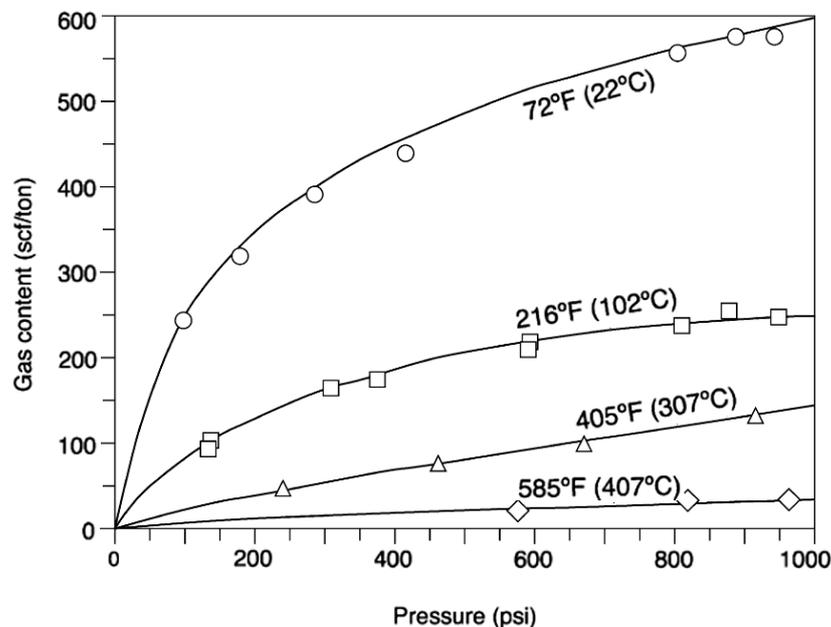
Figure 2.21 Temperature Effect on CH_4 Langmuir Isotherms (Scott, 2002).

2.5.2.1.6 Diffusion Coefficient

During gas production and injection, gases diffuse from the coal matrix to the cleat system or from cleats to coal matrix. Therefore, the gas diffusion plays an important role in gas flow through coal media.

With its relatively smaller kinetic diameter, CO_2 can permeate not only macropores but also ultra micropores, which likely block CH_4 and N_2 that have slightly larger kinetic diameters, resulting in one or two order of magnitude higher diffusivity of CO_2 than those of CH_4 and N_2 in the coal matrix as in Figure 2.22. Carbon dioxide can also be preferentially adsorbed into smaller pores because of the higher adsorption energies in those smaller pores and into pores of larger sizes due to its larger adsorption affinity. Hence, there is a strong selective diffusion of CO_2 over CH_4 (Cui et al., 2004). In addition, experimental study done by Busch et al. (2004) also reveals that CO_2 sorption rates are considerably higher by an order of 2 to 3 than CH_4.
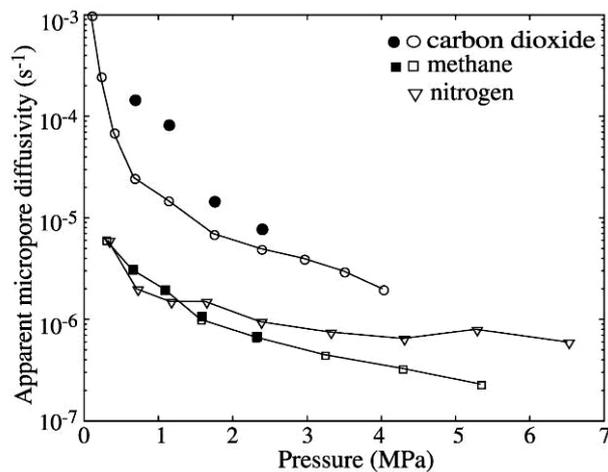
Open symbols : Micro diffusivities derived from experimental data.

Solid symbols : Best-fit model diffusivities when macropore diffusivities are constrained to theoretical predictions.

Figure 2.22 Apparent Micropore Diffusivity of CO_2, CH_4 and N_2 through Coal Media vs. Pressure (Cui et al., 2004).

Diffusivities of gases in the coal matrix decrease significantly with increasing gas pressure as in Figure 2.22, which can be attributed to both the intensive gas molecule–molecule collision and the strong adsorption swelling of coal matrix (Cui et al., 2004).
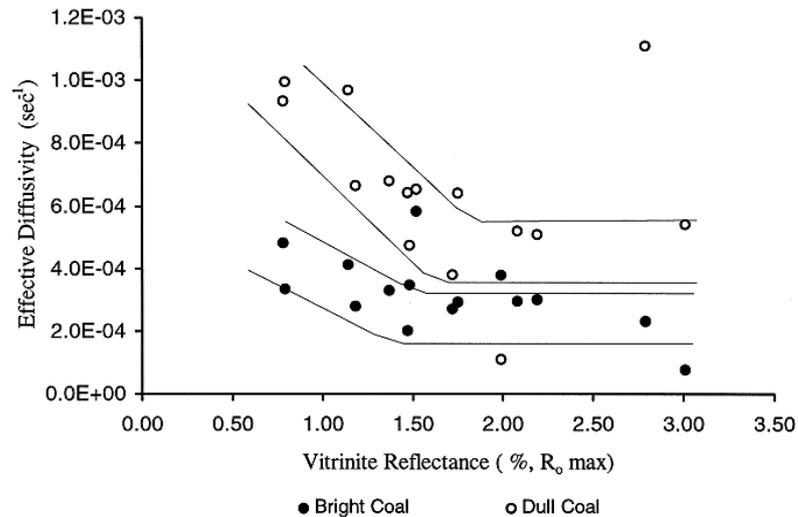
Figure 2.23 Effective Diffusivity of CH$_4$ vs. Vitrinite Reflectance (Laxminarayana and Crosdale, 1999).

According to study done by Laxminarayana and Crosdale (1999) in Figure 2.23, CH$_4$ desorption rate of crushed coals measured at 0.5 MPa indicates that coal type and coal rank have important influences and there is a general trend of decreasing desorption rate with increasing rank. Coals of lower rank have higher effective diffusivities. Moreover, it is observed that bright coals (vitrinite-rich coals) diffuse more slowly than dull coals (inertinite-rich coals).

Clarkson and Bustin (1999) conclude that bright coals have a uniform micropore structure and their adsorption rate can be adequately modeled using the classic unipore analytical solution. Clarkson and Bustin (1999), Laxminarayana and Crosdale (1999) use unipore analytical model to fit their experimental data and they submit the

results as effective diffusivity. Effective diffusivity is defined as diffusion coefficient divided by diffusion path length.

$$\frac{V_T}{V_{inf}} = 1 - \frac{6}{\pi^2} \sum_{n=1}^{\infty} \frac{1}{n^2} \exp\left(-\frac{Dn^2\pi^2 t}{r_p^2} \right) \qquad (2.3)$$

$$D_e = \frac{D}{r_p^2} \qquad (2.4)$$

, where V_T is total gas desorbed at time t, (cm^3); V_{inf} is total adsorbed or desorbed volume, (cm^3); n is number of diffusing species; D is diffusion coefficient, (cm^2/s); D_e effective diffusivity, (1/s); t is time, (s); r_p is diffusion path length, (cm).

2.5.2.2 Fracture System in Coal Seams

Cleats are natural fractures in coal that usually occur in two sets, in most instances, mutually perpendicular, and also perpendicular to bedding plane. One set is face cleat, which is more continuous and of larger extent; the other set is butt cleat, which is more discontinuous, shorter extent, and is localized between adjacent face cleats. Cleats generally form in bright coal via tensile fracture. The parameters that control the permeability of coal reservoirs are mainly cleat dimension, frequency, and network pattern (Su et al., 2001).

In Figure 2.24, orientations of face and butt cleats are represented on a plan view of a coal seam. Moreover, the other cleat characterization parameters, namely; cleat aperture, spacing and length are shown.
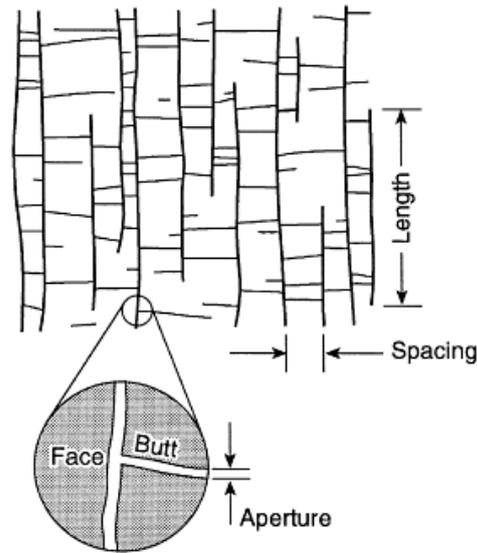
Figure 2.24 The Plan View of a Coal Seam (Laubach et al., 1998).

2.5.2.2.1 Origins of Cleats (Su et al., 2001)

The origins of the cleats are controlled by intrinsic and extrinsic causes. The former include coal constituents, coalification, and the fluid that is formed during coalification; and the latter include tectonic stresses and hydrostatic pressure.

Intrinsic Tensile Forces: During coalification, because plant remains can be gelatinized under the effects of microbes, temperature, and pressure, the coal will become plastic or semi-plastic and produce large amounts of fluids. Along with the fluid formation and discharge from coal, the intrinsic tensile forces arise from matrix shrinkage. When the tectonic stresses are isotropic or weak, an irregular reticular cleat pattern will be formed like mud-cracks or cooling cracks in lava flows. This origin mainly develops at the early stage of coalification. The tectonic stresses superimposed on the intrinsic tensile forces control the cleat geometric patterns.

Fluid Pressure: Along with the coalification, the gas hydrocarbons are formed gradually and held in the isolated matrix pores or connective matrix pores. Due to the formation of the fluid, the fluid pressure in the pore increases. If the fluid pressure in

the matrix pore is less than the extrinsic effective stresses, this situation will be maintained. When the fluid pressure exceeds the extrinsic effective normal stresses and the fracture pressure of coal, the pore will be split along the direction of minimum stresses, and developed into cleats along the direction of maximum stresses as in Figure 2.25. When the fluid pressure is less than or equal to the effective normal stresses, the development of the cleat will terminate. The influence of the fluid pressure on cleat formation mainly develops at the middle and later stages of coalification. The fluid pressure can be superimposed on the intrinsic tensile stresses.
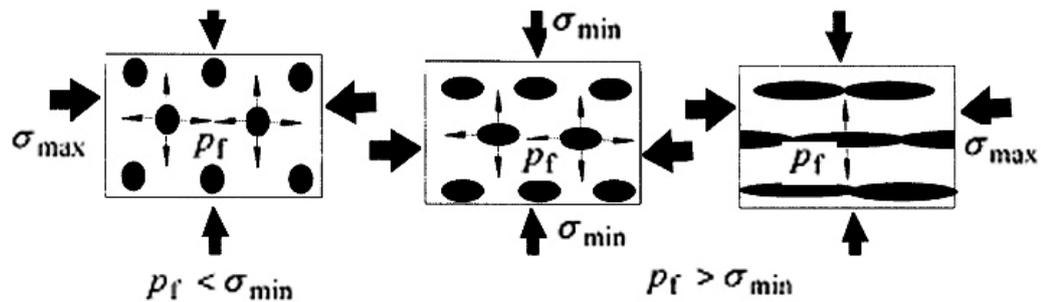
Figure 2.25 Formation of Cleats due to Increasing Fluid Pressure
(Su et al., 2001).

Tectonic Stresses: The tectonic stress field controls the cleat geometric patterns. The control of the tectonic stresses on the cleat formation is based on the intrinsic tensile forces and fluid pressure. In Figure 2.26, (I_1) shows the face cleat extents along the direction of maximum in situ stresses, and the butt cleat along the direction of minimum in situ stresses, so the regular reticular cleat is formed. When the tectonic stresses are isotropic or weak, the irregular reticular cleat like (I_2) in Figure 2.26 will be formed. Furthermore, if the stress is compressive in one direction and tensile in another direction, isolated straight pattern like (II_1) will be formed. The S pattern in Figure 2.26, (II_2) will be formed under shear stresses. Moreover, pattern (III) is formed under multiple tectonic stresses. Therefore, the cleat

network pattern and strike are controlled by the tectonic stresses that are superimposed on the tensile forces and fluid pressure. Preferred fracture orientation is consistent with the principal stresses over wide areas which suggest that the cleat formation is nearly controlled by tectonic stresses.
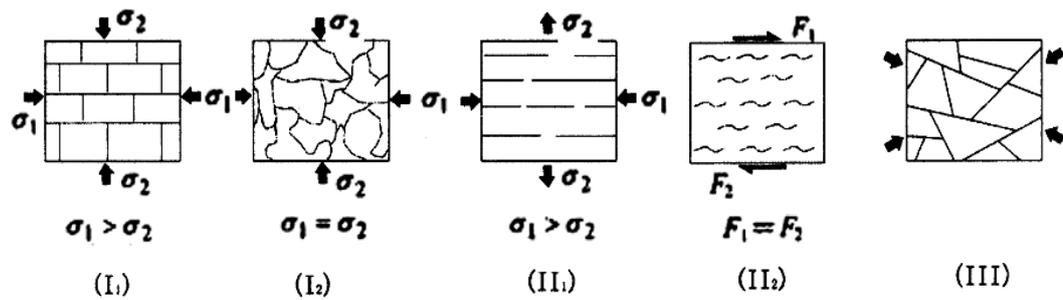
Figure 2.26 Cleat Patterns for Different Stress Fields (Su et al., 2001).

Cleat Annealing: Cleat annealing means that the cleat is filled with secondary maceral in the low rank coal or the cleat disappears in high rank coal such that it cannot be observed on the macro or micro scale. Cleat annealing is different from cleat mineralization of fracture in rocks. It exists in coals of any rank, even in brown coal. There are two mechanisms of cleat annealing namely, secondary maceral filling and agglutination.

Exsudatinite is a secondary maceral, which generally occurs in cleat or as fillings of bedding-plane fractures and occasionally also in empty cell lumens. It is found that the cleat is filled commonly with exsudatinite in brown coal and sub-bituminous coal. Therefore, cleat annealing begins at the initial stage of its formation. Agglutination is another mechanism of cleat annealing. It means that cleat wall pieces fuse together under high temperature and pressure.

2.5.2.2.2 Cleat Properties

Characterization of cleats and fractures is important both for coalbed methane (CBM) exploratory strategies as well as for successful recovery of coalbed gases. To characterize coal fabric (i.e., the geometric arrangement between cleat spacing and aperture width), a description of the cleat system can be made based on abundance of cleats per unit length in a perpendicular direction to face and butt cleats. Such description, together with measurements of cleat direction allows making inferences about the three-dimensional connectivity of the system available for fluid flow (Solano-Acosta et al., 2007).

Various cleat properties such as orientation, spacing and effective porosity are not uniform throughout the coal in a given formation but vary both vertically and laterally as a function of such geologic variables as the depth, coal rank, bed thickness, coal lithotype, ash content, effective stress, and degree of secondary cleat mineralization (Nelson, 2000).

Length and Aperture: The length and height of cleats depend on the distribution of bright coal, since the cleats generally occur in bright coals. The cleat length ranges from several centimeters to several decameters or several hectometers, and the height ranges from several centimeters to several decameters. The unstressed cleat aperture ranges from 0.001 to 20 mm (Su et al., 2001).

Cleat Spacing: The cleat spacing is an important physical reservoir property since this parameter affects the friability of the coal and the magnitude of the bulk reservoir permeability, which vary inversely as a function of the cleat spacing. Cleat spacing is commonly observed to vary inversely with coal rank and bed thickness. For coals of similar rank, the cleat frequency and absolute permeability values are typically greatest in bright, vitrinite-rich lithotypes and lowest in dull, inertinite-rich lithotypes. All other factors being equal, the absolute permeability of coalbed reservoirs typically increases as the cleat spacing decreases (Nelson, 2000).

Relationship between cleat intensity (i.e., a measure of cleat spacing) and coal rank has been discussed in several studies. It was claimed that most cleats are formed in the bituminous rank, and the observed decrease in cleat abundance at high ranks has been attributed to annealing as thermal maturation increases with coalification (Solano-Acosta et al., 2007). In Figure 2.27, Ammosov and Eremin's (1963) cleat intensity vs. coal rank diagram is modified by Solano-Acosta et al. (2007) by changing their metamorphic grade classification to American Society for Testing & Materials (ASTM)'s (2005) coal rank classification scheme.
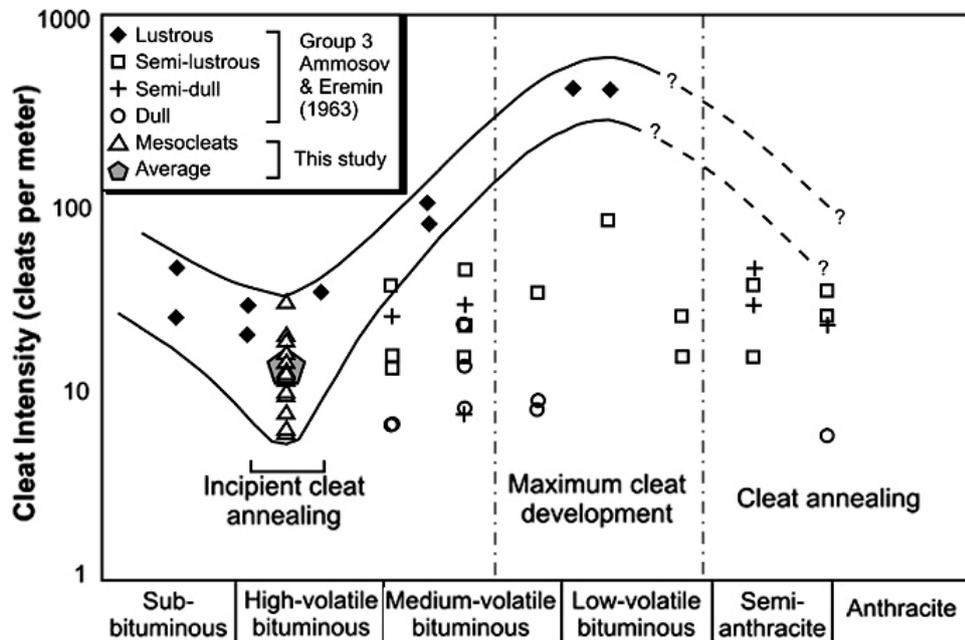
Figure 2.27 Modified Ammosov & Eremin's (1963) Diagram on Cleat Intensity with respect to Coal Rank (Solano-Acosta et al., 2007).

According to data provided by Su et al. (2001), when the vitrinite reflectance is less than 1.35%, the cleat frequency increases with the rise of coal rank. If the vitrinite reflectance is greater than 1.35%, cleat frequency decreases. Vitrinite reflectance of 1.35% is close to the point where medium-volatile bituminous coal rank ends and low-volatile bituminous rank starts. Therefore, the trend of

the data set provided by Su et al. (2001) is nearly the same with Ammosov &
Eremin's (1963) diagram.

Effective Cleat Porosity: The effective cleat porosity is the ratio of the
interconnected cleat void volume to the bulk coal volume. Cleat-fracture porosity
in coal is estimated to be between 0.5% and as much as 2.5% (Laubach et al., 1998).

Cleat Orientation: The cleat orientation is an important physical reservoir
property since it controls the direction of bulk fluid flow. On a regional scale, the
face and butt cleats orientations or strikes in coalbed reservoirs are often aligned
roughly perpendicular and parallel, respectively, to map-scale structures such as faults
and fold axes. Due to the orthogonal orientation and length differences of the face
and butt cleats, there is typically a significant permeability anisotropy in coalbed
reservoirs. The absolute permeability of coalbed reservoirs parallel to the face
cleat direction is generally two to four times greater than that parallel to the butt
cleat direction. This permeability anisotropy causes the drainage area around
horizontal wellbores to have a pronounced elliptical shape (Nelson, 2000).

Cleat Compressibility: Coal cleats are relatively compressible compared to the
bulk coal matrix material. The compressibility is the incremental change in the cleat
void volume per unit change in the compressive stress. Cleat compressibility is an
important physical reservoir property since it affects the cleat aperture width and
effective porosity, which, in turn, affect the bulk reservoir permeability (Nelson, 2000).

Cleat Permeability: As Scott et al. (2002) stated, indirect measurements using drill
stem tests and/or production modeling suggest that cleat permeability is generally
ranges between 0.5 and 100 md. A carbonate study conducted by Lucia (1983)
yielded a relationship between permeability, fracture spacing, and fracture aperture.
This relation indicates that permeability increases with the cube of the fracture aperture
and varies with the inverse of the fracture spacing. This relation can also be used for
coal media by considering the coal matrix as an impermeable media.

$$k_f = 84.4 \cdot 10^8 \cdot \frac{w^3}{z} \tag{2.5}$$

, where k_f is absolute cleat permeability, (md); w is fracture aperture, (cm); z is fracture spacing, (cm).

2.6 Parameters Controlling Initial Methane Content

Gas content in coals is not fixed but changes when equilibrium conditions within the reservoir are disturbed. Major parameters affecting gas content variability include coal rank, gas generation and reservoir conditions.

2.6.1 Coal Rank and Gas Generation

Coal rank has an important effect on the sorptive behavior and storage capacity of coal. The adsorptive capacity of coal is traditionally described as increasing with coal rank. Coal gases are generated through thermogenic and biogenic processes. Coals must reach a certain threshold of thermal maturity (vitrinite reflectance values between 0.8% and 1.0%) before large volumes of thermogenic gases are generated. The amount and types of coal gases generated during coalification are a function of burial history, geothermal gradient, maceral (organic matters in coal) composition, and coal distribution within the thermally mature parts of a basin. Gases in coalbeds may also be formed through the process of secondary biogenic gas generation. Secondary biogenic gases are generated through the metabolic activity of bacteria, introduced by meteoric waters moving through permeable coalbeds or other organic-rich rocks. Thus, secondary biogenic gases differ from primary biogenic gases because the bacteria are introduced into the coalbeds after burial, coalification, and subsequent uplift, exposure, and erosion of basin margins (Scott, 2002). Therefore, thermogenic and biogenic processes control gas content, whereas coal rank determines sorption capacity of coal.

2.6.2 Reservoir Conditions

Gas content decreases with decreasing pressure and temperature, and coalbeds become undersaturated with respect to methane during basin uplift and cooling. Coals are saturated to oversaturated with respect to methane during active gas generation at high temperatures. However, as reservoir temperature decreases during basinal uplift and cooling, gas generation ceases. Coals become undersaturated with respect to methane as the sorption isotherm shifts upward as in Figure 2.28 (Scott, 2002).
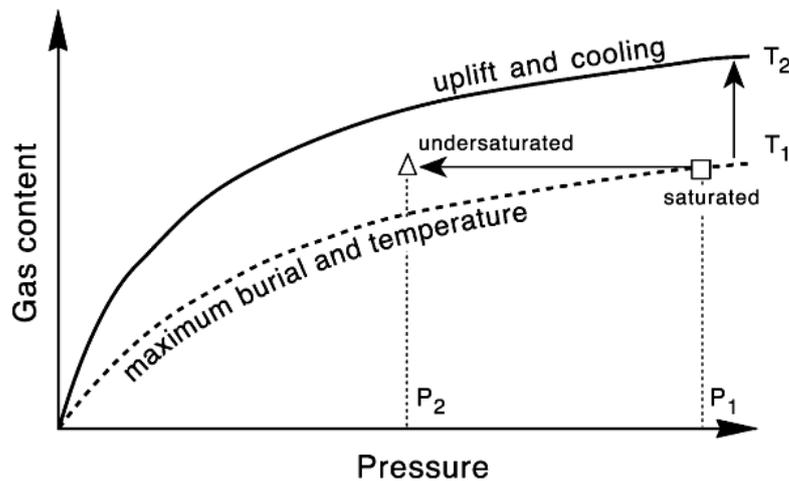
Figure 2.28 Changes in Methane Saturation due to Basinal Uplift and Cooling (Scott, 2002).

The dry coal anomaly stated by Hoch (2005) is related to the change in reservoir pressure and temperature conditions. It is reported that the most unusual feature of the Horseshoe Canyon coal is that the best areas of the formation produce no water. The gas to water ratio is therefore very low, less than 1 bbl/Mscf. The reservoir pressures of the Horseshoe Canyon coals are definitely very low, being in the order of 10 to 50% water-hydrostatic pressure, with the average being less than 30% of water-hydrostatic pressure. Geologists think that after the various layers of the Horseshoe Canyon formation were laid down, further deposition occurred on top of

it. Then the formation of Rocky Mountains caused the overburden on top of the Horseshoe Canyon to reach 16,000 – 20,000 ft (5000-6000 m), squeezing water out of the compacting shale. Gas of thermogenic origin migrated from shale and coal to sandstone where it accumulated. Erosion and uplifting has in time removed 6,500-13,000 ft (2000-4000m) of sediments and this lead to low pressure gradient with low methane content (Hoch, 2005).

Therefore, there are three main types of coal reservoir conditions that are mentioned in the literature. These are methane saturated dry coal, methane undersaturated wet coal and methane saturated wet coal.

2.7 Well Productivity of Coalbed Methane Reservoirs (GRI, 1996)

A typical production profile of coalbed methane well is shown in Figure 2.29. This profile differs significantly from the typical decline of a conventional gas well. Productivity of typical coalbed methane wells can be investigated into three phases. Phase I is characterized by a constant water production rate and declining flowing bottomhole pressure. During this phase, the well is being pumped-off and the gas rate may be inclining, as shown in Figure 2.29. The gas rate may also decline, depending on the near-well relative permeability characteristics of the reservoir. At the end of Phase I, the well reaches its minimum flowing bottomhole pressure.

Phase II is characterized by increase in the gas production rate and a significant decline in the water production rate. Moreover, phase II is characterized by several dynamic changes in reservoir flow conditions:

- Water relative permeability decreases.
- Gas relative permeability increases.
- Outer boundary effects become significant (pseudo-steady state flow).
- Gas desorption rates change dynamically.
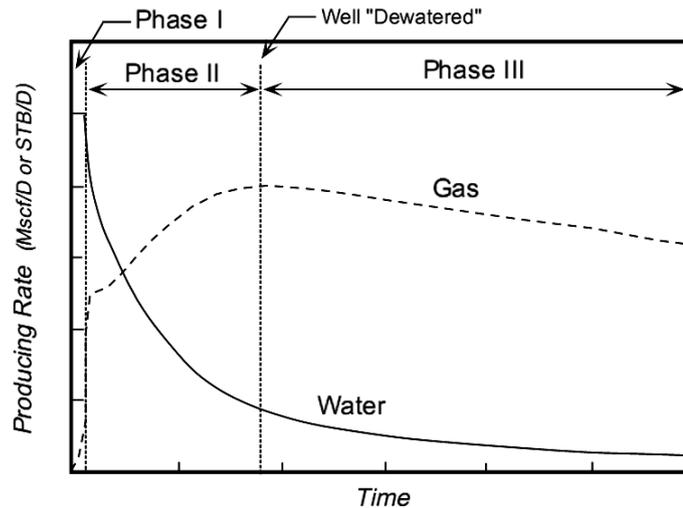
Figure 2.29 Coalbed Methane Production Profiles (GRI, 1996).

As for Phase III, it begins when reservoir flow conditions are stabilized. The well reaches its peak gas rate, and gas production is characterized by a more typical decline trend. During this phase, water production is low and/or negligible, and gas and water relative permeabilities change very little. The well is considered to be dewatered at the beginning of Phase III. At this point, water production reaches a low level and gas and water relative permeabilities change little thereafter. Therefore, pseudo-steady state flow exists for the rest of Phase III.

The length of the dewatering process and the magnitude of the producing rates of gas and water are controlled by the physical properties of the coal as well as project development parameters. This process may take weeks, months, or years depending on the properties of the producing coalbed.

2.8 Transient Processes during ECBM Recovery

There are two principal variants of ECBM recovery, namely N_2 and CO_2 injection, which use two distinct mechanisms to enhance methane desorption and production. Unlike the primary recovery method, ECBM recovery allows the maintenance of reservoir pressure. The mechanism used in N_2 injection is somewhat similar to inert

gas stripping because nitrogen is less adsorbing than methane. Injection of nitrogen reduces the partial pressure of methane in the reservoir, thus promoting methane desorption without lowering the total reservoir pressure. On the other hand, CO_2 injection works on a different mechanism because it is more adsorbing on coal compared with methane. Thus, it has an additional benefit that a potentially large volume of greenhouse gas can be sequestrated in deep coal seams (Shi and Durucan, 2005).

The transient processes occurring around CO_2 injection and CH_4 production wells during application of ECBM recovery technique are different. The permeability that controls gas and water flow is the effective permeability, which is the product of absolute and relative permeability. Around injection wells CO_2 injection pressurizes cleats and can cause the cleat porosity to increase, depending on the average pressure in it. Gas injection does not displace much, if any, water. As a result, while the pore volume increases, the water volume remains relatively constant. The water saturation in the cleats is decreased. This reduces the relative permeability to water and increases the relative permeability to gas. During fill-up with CO_2, there is a period when swelling effects are greater than ballooning effects. Swelling reduces the porosity, while the water saturation is increased, in turn reducing the relative permeability to gas and increasing the relative permeability to water. The reduced effective permeability to gas can be overcome by ballooning. As CO_2 injection continues, the reduction in effective permeability to gas will cause the injection pressure to increase until ballooning effects overcome both swelling and relative permeability effects. Therefore, this allows injection to continue (Mavor and Gunter, 2004).

Around production wells, however, when gas and water are produced, cleat porosity can decrease before matrix-shrinkage effects are significant. Water saturation is reduced by depletion of the water in the cleats and by gas flow from the matrix into the cleats. The reduction in cleat porosity will tend to maintain greater water saturations and, thus, greater relative permeability to water than if the porosity remains unchanged. The effective permeability to water generally will continue to decrease because the absolute permeability variation is a function of the cube of the

porosity ratio, while the water-saturation increase is a linear function of the porosity ratio. Eventually, the porosity may begin increasing because of the shrinkage of the matrix caused by reduced gas content. As the porosity increases, the water saturation is reduced faster than by water production alone. Effective permeability is increased to both water and gas, although the increase in the effective permeability to water is less than that of gas owing to the relative permeability to water reduction. These combined effects cause water-production rates to reduce much faster than can be explained by depletion of the water volume alone (Mavor and Gunter, 2004).

2.9 Cleat Permeability Modeling

Commercial production of gas from coal seams is highly dependent upon cleats, which control the magnitude and distribution of absolute permeability throughout the reservoir. Absolute permeability and porosity of cleats vary as a function of location, pressure within the cleat system, and the composition of gas within the coal matrix. Moreover, variations in cleat porosity cause variations in fluid saturations that in turn cause variations in the relative and effective permeability to gas and water (Mavor and Gunter, 2004).

There are three main processes controlling effective gas permeability in cleats during primary and enhanced coalbed methane recovery namely, effective stress applied on the cleat surface, shrinkage & swelling due to adsorption/desorption processes and relative permeability effect owing to multiphase flow of water and gas.

2.9.1 Effective Stress on Cleat Surfaces

Laboratory studies performed using coal samples compressed under uniaxial strain conditions have shown that the effective porosity and absolute permeability of the coal cleats decrease with increasing effective stress. The effective stress is the difference between the total confining pressure and the pore pressure. Since the pore pressure in coalbed reservoirs progressively decreases over time with gas production, the effective stress gradually increases. This leads to a decrease in effective cleat porosity and absolute permeability (Nelson, 2000).

Seidle (1992) proposed an equation modeling cleat permeability with respect to effective stress. He defined the system with matchstick geometry. The geometry referred to as "matchstick" was a collection of rectangular parallelepipeds. He successfully matched the proposed model with the experimental data.

$$\frac{k_{f2}}{k_{f1}} = \exp\left[-3c_f \cdot \left(\sigma_{h2} - \sigma_{h1}\right)\right] \qquad (2.6)$$

, where k_f is absolute fracture permeability, (md); c_f is fracture compressibility, (1/psi); σ_h is effective stress on fracture surfaces, (psi).

2.9.2 Shrinkage and Swelling Effect

Gray (1987) and Seidle (1992) mentioned about the shrinkage effect during desorption process of methane from coal matrix. As stated by Gray (1987), coal matrix shrinks when the adsorbed gas in coal matrix desorbs and this increases the permeability by rising cleat aperture. Furthermore, as reported by Seidle and Huitt (1995) coal matrix swells and shrinks as gas is first adsorbed then desorbed and the amount of swelling depends on coal rank and sorbed gas composition.

Mavor and Vaughn (1998) reported that there is an increase in permeability during primary recovery of methane due to shrinkage of coal matrix according to well test data obtained from San Juan Basin Fruitland formation of the U.S.A. They tried to fit the well test data with the permeability model proposed by Palmer and Mansoori (1998). Matrix shrinkage, swelling and net confining stress on the cleat surfaces are combined in Palmer and Mansoori (P&M) model to predict the absolute cleat permeability and porosity with respect to reservoir pressure during methane production.

$$\frac{\varphi_f}{\varphi_{fi}} = 1 + c_f \cdot (P - P_i) + \frac{\varepsilon_{inf}}{\varphi_{fi}} \cdot \left(1 - \frac{K}{M}\right) \cdot \left(\frac{P_i}{P_i + P_{inf}} - \frac{P}{P + P_{inf}}\right) \qquad (2.7)$$

$$\frac{K}{M} = \frac{1}{3} \cdot \left(\frac{1+v}{1-v} \right)$$ (2.8)

$$M = E \cdot \frac{1-v}{(1+v)(1-2v)}$$ (2.9)

$$\frac{k_f}{k_{fi}} = \left(\frac{\varphi_f}{\varphi_{fi}} \right)^3$$ (2.10)

$$c_f = \frac{1}{\varphi_{fi} M}$$ (2.11)

, where φ_f is fracture porosity, (fraction); φ_{fi} is initial fracture porosity, (fraction); c_f is fracture compressibility, (1/psi); P is pressure, (psi); P_i is initial pressure, (psi); ε_{inf} is infinite strain; P_{inf} is infinite pressure, (psi); K is bulk modulus, (psi); M is constraint axial modulus, (psi); E is elastic modulus, (psi); v is Poisson's ratio; k_f fracture permeability, (md); k_{fi} initial fracture permeability, (md).

$$\frac{\varepsilon_{inf}}{\varphi_{fi}} \cdot \left(1 - \frac{K}{M} \right) \cdot \left(\frac{P_i}{P_i + P_{inf}} - \frac{P}{P + P_{inf}} \right)$$ (2.12)

The shrinkage and swelling part of P&M model is given above. In this equation, volumetric strain, ε_V at a given pressure, P is defined as below.

$$\varepsilon_V = \frac{\varepsilon_{inf} \cdot P}{P + P_{inf}}$$ (2.13)

P&M model is applicable to one-component gas systems, specifically during primary methane production. However, in ECBM recovery and pollutant storage projects, the injected and produced gas compositions are different from the original in-situ composition. Such changes cause the coal matrix to swell or shrink depending upon changes in the adsorbed gas composition. In addition, as swelling or shrinkage change the cleat porosity, there are changes in the water saturation and relative permeability to gas and water within the cleat that are not accounted for by the P&M theory (Mavor and Gunter, 2004).

47

Shrinkage and swelling of coal matrix is a function of pressure, adsorbed gas component, and rank of coal. Swelling effect of CO_2 is greater than CH_4 and N_2 at the same pressure. The result of an experimental study done by Cui et al. (2007) shows both component and pressure dependency of swelling in Figure 2.30. As the pressure of each pure gas component increases, the volumetric strain due to swelling also increases. Therefore, injection of CO_2 at high pressure may lead to high amount of swelling by decreasing injectivity.
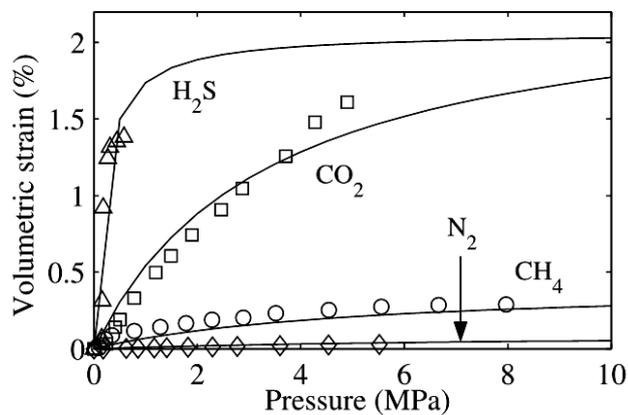
Figure 2.30 Volumetric Strain vs. Pressure for Different Gas Components (Cui et al., 2007)

As it is stated by Mazumder et al. (2006), field evidence suggests that the well injectivity has indeed declined at early stages of CO_2 injection. It has been reported that on a unit of pressure basis, CO_2 is adsorbed in higher concentration by coal than by CH_4. This differential swelling behavior would have extreme consequences for field-injection projects. It may lead to elevated injection pressures, causing uncontrolled fracturing of the reservoir beyond a certain pressure. Moreover, Shi and Durucan (2005) reported that the loss in well injectivity due to CO_2 injection at the Allison pilot field in the San Juan basin of the U.S.A. is attributed to an estimated two order of magnitude reduction in permeability.

The relationship between rank of coal and volumetric strain for different gases are provided by Laxminarayana et al. (2004). Volumetric strain data are obtained at 0.6

MPa and the rank of coal used in that study ranges from sub-bituminous to medium volatile. As rank of coal increases, volumetric strain and swelling effect owing to adsorption of each gas component increases as in Figure 2.31.
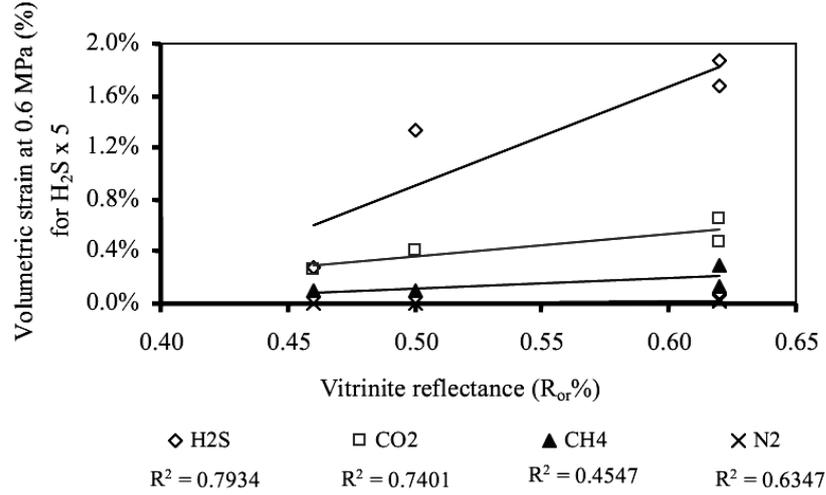
Figure 2.31 Volumetric Strain vs. Rank of Coal for Different Gas Components (Laxminarayana et al., 2004).

P&M model is applicable to one component systems. However, during application of ECBM recovery CH_4, CO_2 and N_2 are mixed in the reservoir environment. Therefore, multicomponent effects should be considered. To be able model the multicomponent swelling and shrinkage effect on cleat permeability, extended P&M model is used, which was first introduced by Mavor and Gunter (2004).

$$\frac{\varphi}{\varphi_i}=1+c_f(P-P_i)+\frac{1}{\varphi_i}\times\left(1-\frac{K}{M}\right)\times\left(\sum_{j=1}^{j=nc}\frac{\varepsilon_{inf,j}\times y_{i,j}\times P_i/P_{inf,j}}{1+P_i\times\sum_{k=1}^{k=nc}y_{i,k}/P_{inf,k}}-\sum_{j=1}^{j=nc}\frac{\varepsilon_{inf,j}\times y_j\times P/P_{inf,j}}{1+P\times\sum_{k=1}^{k=nc}y_k/P_{inf,k}}\right)(2.14)$$

where i is initial condition; k or j represent each gas component; nc is the number of gas components. Names and units of all parameters in the extended P&M model are

the same with the original Palmer and Mansoori (1998) model. Moreover, Equations 2.8, 2.9, 2.10, 2.11 are also valid for extended P&M model. All deformations in P&M model and its extended version are considered as elastic.

2.9.3 Relative Permeability Effect

In addition to effective stress on cleat surfaces and shrinkage & swelling effect, relative permeability has also an important role in production of coalbed methane. As the pressure is reduced in the cleat system by production of water from wells, gas desorbs into the cleat system. At this point, and for the remainder of the life of the producing wells, two-phase flow occurs in the cleat system. Under two-phase flow conditions, the relative permeability relationships between gas and water control the relative flow of gas and water in the reservoir. Thus, it is important to determine the relative permeability characteristics of the coal being analyzed. Furthermore, changes in fracture porosity due to shrinkage and swelling during application of ECBM recovery technique controls fluid saturations that in turn lead to changes in relative and effective gas permeability (GRI, 1996).

2.10 Applicability of ECBM Recovery to Different Coal Ranks

High rank coals exist generally between 300–1500 meters and may be unmineable due to economic and technical reasons. These coals may be ideally suited for ECBM recovery as they have very high methane content and can store very large amounts of CO_2. However, low to medium bituminous coals are considered to be more ideally suited since anthracite coals tend to be less permeable and highly undersaturated with gas, and have a lower surface area per unit mass. Furthermore, low to medium bituminous coals are likely to have a more developed naturally occurring cleat system than higher rank coals because they have smaller unconfined compressive strengths. This increases their permeability and the possibility of more coalbed methane recovery. However, anthracite coals may lead to more stable CO_2 storage as they can provide a higher deep well potential. As a result, the choice of a suitable coal for ECBM recovery is not conclusive and requires further research on technical and economic grounds (Katyal et al., 2007).

CHAPTER 3

STATEMENT OF THE PROBLEM

Complexity in modeling enhanced coalbed methane (ECBM) recovery is not only caused by sorption-controlled behavior of coalbeds but also the interaction between coal media and injected CO_2/N_2 gas mixture, which changes the coal properties controlling gas flow mechanism with respect to injection time. In addition, determination of in-situ coal properties related to transport mechanism is complicated due to having lack of a standardized procedure in the literature.

By considering these difficulties, a new approach will be developed by constructing an input database based on the relationships between coal rank and its physical properties. Parametric simulation studies with the rank classification will provide more representative results for the coal reservoirs rather than the univariate analysis. Besides coal rank, simulation cases will be run for different reservoir types, well-patterns, drainage areas, anisotropies, cleat permeabilities, molar compositions of injected fluid and well types. For all cases, shrinkage and swelling, which is the main transient process controlling cleat permeability during ECBM recovery, will be taken into account by making use of extended version of Palmer and Mansoori (P&M) (1998) permeability model. In addition, effects of shrinkage and swelling on ECBM recovery and CO_2 sequestration will be studied separately with rank-dependent coal properties. Besides to coal rank, different reservoir types, molar compositions of injected fluid, and parameters within the extended P&M permeability model will be considered with a sensitivity analysis. Therefore, the effects of variable coal properties on ECBM recovery will be investigated with various simulation scenarios which will be run with a compositional reservoir simulator of CMG (Computer Modeling Group) /GEM module by primarily considering the maximization of CH_4 recovery.

CHAPTER 4

METHODOLOGY

4.1 Preparation of Simulation Inputs

Most of the rank-dependent coal properties in the literature are provided with respect to vitrinite reflectance and carbon contents of coal. Intervals of these parameters corresponding to a specific rank of coal are provided in Appendix B, Table B.1. Moreover, simulation inputs with respect to the rank of coal are given with their references in Tables B.2, B.3, B.4, and B.5. In this section, construction of the rank-dependent physical coal property database is described, which is used as simulation inputs for a compositional reservoir simulator, Computer Modeling Group (CMG), GEM module.

Coal is a dual-porosity media including cleats and matrix blocks. As Scott (2002) stated, indirect measurements using drill stem tests and/or production modeling suggest that cleat permeability is generally ranges between 0.5 and 100 md. Hence, five different permeability cases are selected in the given range. These are 4, 10, 25, 50 and 100 md. When it is compared to cleat permeability, coal matrix permeability is very small. Laubach et al. (1998) states that over 95% of the gas in coal is stored in micropores of coal matrix ranging from 0.5 to 1 nm, which causes no effective permeability in matrix. Thus, matrix permeability in our model is defined as 0.001 md.

Cleat spacing is an important physical coal property since its magnitude directly affects reservoir permeability. The absolute permeability of coalbed reservoirs typically increases as the cleat spacing decreases (Nelson, 2000). Relationship between cleat spacing and rank of coal has been discussed in several studies. It is claimed that most

cleats are formed in the bituminous rank, and cleat abundance decreases at high ranks (Solano-Acosta et al., 2007). According to the data provided by Su et al. (2001) in Figure 4.1, when the vitrinite reflectance is less than 1.35%, the cleat frequency increases with the rise of the coal rank. If the vitrinite reflectance is greater than 1.35%, cleat frequency decreases. 1.35% vitrinite reflectance is close to the point where medium-volatile bituminous rank ends and low-volatile bituminous rank begins. As the increasing cleat spacing trend is obvious between sub-bituminous and medium-volatile bituminous, this range is preferred in our study. Cleat frequencies in Figure 4.1 are tabulated in Table A.1 and they are converted into cleat spacing.
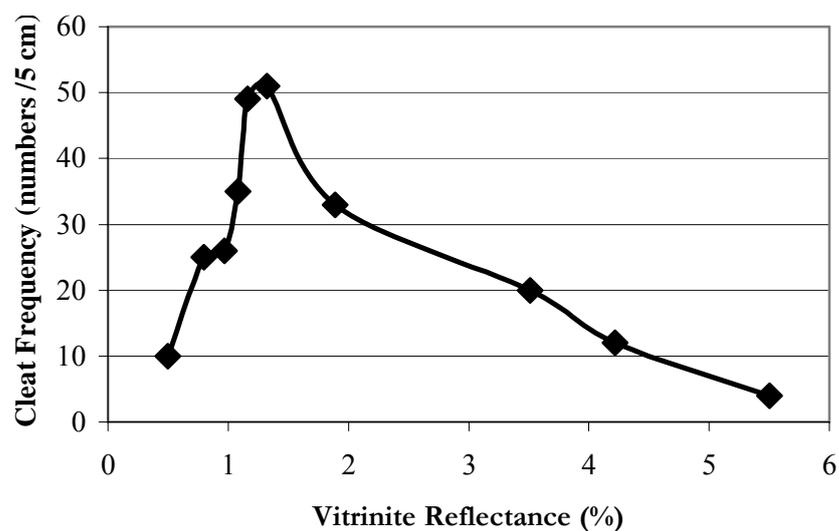
Figure 4.1 Cleat Frequency vs. Vitrinite Reflectance (Su et al., 2001).

From a research on fractured carbonate reservoirs, Lucia (1983) developed an equation relating fracture width and spacing to reservoir permeability assuming that the carbonate matrix is impermeable. Equation 4.1 indicates that k_f, fracture permeability, (md) increases with the cube of w, fracture aperture, (cm) and varies with inverse of z, the fracture spacing, (cm). This relation can also be used for coal by

considering the coal matrix as impermeable media (Solano-Acosta et al., 2007). Therefore, this formula is utilized in this study to calculate cleat apertures for combinations of permeability and cleat spacing. It is realized that computed values ranges from 4 μm to 18 μm in Table B.2. For comparison purposes, the cleat apertures of a coal sample from Zonguldak Basin (Northwestern Turkey) is measured and reported by Karacan and Okandan (2000) in the range of 10–30 μm and the mean size is 20.2 μm. Moreover, Gamson et al. (1993) reported that micro-cleat apertures vary between 0.5 μm and 20 μm. Thus, these two examples confirm the consistency of our data set.

$$k_f = 84.4 \cdot 10^8 \cdot \frac{w^3}{z} \qquad (4.1)$$

Effective cleat porosity is the ratio of the interconnected void volume of cleat to the bulk volume of coal. Matrix porosity, however, is the ratio of interconnected pore volume inside coal matrix to bulk matrix volume. Fracture porosities of coal with respect to cleat aperture, spacing and rank of coal are calculated from Equation 4.2, which is provided by Robertson and Christiansen (2006).

$$\varphi_f = \frac{3w}{z} \qquad (4.2)$$

, where w is fracture aperture (cm); z is the fracture spacing (cm). The effective porosity of the matrix block is assumed to be zero in Equation 4.2, leaving the fracture system to provide the only interconnected void space. Cleat porosity in coal is estimated to be between 0.5% and as much as 2.5% (Laubach et al., 1998). In Table B.3, calculated fracture porosities ranges from 0.37% to 3%.

Total coal porosity, which includes cleat and matrix porosities, with respect to carbon content of coal is provided in Berkowitz's (1979) book. Each matrix porosity in Table B.3 is calculated by subtracting the calculated cleat porosity from rank-dependent total porosity. Since the definitions of cleat and matrix porosities are

different, following equation is derived to define a mathematical relation between these quantities.

$$\varphi_m = \frac{(\varphi_t - \varphi_f)}{(1 - \varphi_f)} \tag{4.3}$$

, where φ_m is matrix porosity; φ_f is fracture porosity; φ_t is total porosity.

Apparent density of coal relating to carbon content of coal is obtained from Williamson's (1967) book. Coal densities for each coal rank are tabulated in Table B.3.

Main strength parameters controlling shrinkage and swelling (SS) are elastic modulus and Poisson's ratio. As it is given in Kural's (1994) book, elastic moduli from different references are plotted with respect to carbon contents of coal. These plots show an increasing trend in elastic modulus from sub-bituminous (~70% carbon content) to medium-volatile bituminous coals (~%85). After medium-volatile bituminous, however, it decreases. By taking into account this trend, a database is constructed by making use of the elastic moduli published in the literature (Berkowitz, 1979; Evans and Pomeroy, 1966; Vaziri et al., 1997; Mavor and Vaughn, 1998; Gentzis, 2000) with respect to coal rank in Table A.2. The same increasing trend is observed and the rank-dependent average elastic moduli are provided in Table B.4. As for Poisson's ratio, it is independent of carbon content of coal according to data published in Berkowitz's (1979) book. Its value is given as 0.35 and constant between sub-bituminous and medium-volatile bituminous. In this study, an average Poisson's ratio of 0.34 is calculated using the published data in Table A.2 (Berkowitz, 1979; Vaziri et al., 1997; Mavor and Vaughn, 1998; Gentzis, 2000). It is very close to the value in Berkowitz's (1979) book. Standard deviation of this data set is found as 0.06. Descriptive statistics of elastic modulus and Poisson's ratio are provided in Table A.3 and A.4.

The compositional simulator used in this study, GEM module of CMG (Computer Modeling Group), utilizes the extended version of Palmer & Mansoori (P&M)

55

(1998) model for simulating multi-component SS effects. Extended P&M model is the modified version of the original P&M model, which is used only for one-component gas systems. Furthermore, derivation of the extended one is available in Mavor and Gunter's (2004) study and equations related to this model are available in Chapter 2. In this model, fracture compressibility is defined as below,

$$c_f = \frac{1}{\varphi_{fi}M} \tag{4.4}$$

$$M = E\frac{1-v}{(1+v)(1-2v)} \tag{4.5}$$

, where c_f is fracture compressibility, (1/psi); M is constraint axial modulus, (psi); φ_{fi} is initial fracture porosity, fraction; E is elastic modulus, (psi); v is Poisson's ratio.

By using the Equations 4.4 and 4.5, fracture compressibilities are calculated for corresponding rank of coal and cleat porosity in Table B.4. Cleat compressibilities available in the literature are nearly in the order of 10^{-4} psia^{-1} in Tables A.5 and A.6 (Mckee et al., 1988; Harpalani and Schraufnagel, 1990; Shi and Durucan, 2005). Thus, ones in Table B.4 calculated with the Equations 4.4, 4.5 are consistent with the published data. As the matrix compressibilities in the literature is in the order of 10^{-6} psia^{-1} in Table A.5 and A.6 (Berkowitz, 1979; Harpalani and Schraufnagel, 1990; Mckee et al., 1990) and the variance of the data set is small, $2.84*10^{-6}$ psia^{-1} is taken as an average value for all ranks of coal.

Shrinkage and swelling of coal matrix is a function of pressure, type of gas adsorbed and rank of coal. Component dependency of swelling is shown with an experimental study done by Cui et al. (2007). Swelling effect of CO_2 is greater than CH_4 and N_2 at the same pressure. Besides, as the pressure of each gas component rises, swelling effect increases. Therefore, injection of CO_2 at high pressures may lead to increase in swelling and decrease in injectivity. Moreover, the relationship between SS and rank of coal is reported by Laxminarayana et al. (2004). In their study, volumetric strain data are obtained at 0.6 MPa and the rank of coal used ranges from sub-bituminous

to medium volatile. As the rank of coal increases, volumetric strain and swelling effect go up. By considering the study of Laxminarayana et al. (2004) and Cui et al. (2007), strain data with respect to rank of coal and gas component are tabulated with their references in Table A.7. Average values of infinite pressures and infinite strains regarding to rank of coal are given in Table B.5. Besides, volumetric strain vs. pressure plots for N_2, CH_4 and CO_2 with respect to rank of coal are shown in Figures A.1, A.2 and A.3 by using the average values in Table B.5.

Gas storage by physical adsorption occurs mainly in the coal matrix (Harpalani and Chen, 1997). Gas storage capacity curve of coal is dependent on type of gas adsorbed and rank of coal. As it is stated by Arri et al. (1992), the amount of CO_2 stored is 2 times greater than CH_4 and nearly 3 times greater than N_2. In addition to component-dependent gas storage capacity of coal, rank of coal has also an important role on the amount of gas stored. Amount of CH_4 stored at the same pressure increases as the rank of coal increases (GRI, 1996). Moreover, the same trend is also observed for CO_2 and N_2 in Reeves and Gonzales's (2005) study. By collecting published sorption data with respect to rank of coal in Tables A.8 and A.9 (Mavor et al., 2003, 2004; Reeves and Gonzales, 2005; OGS, 2007), average values of Langmuir pressures and volumes are assigned for each coal rank and gas composition in Table B.5. Behavior of averaged Langmuir constants with respect to rank and type of gas are the same with aforementioned trends and it is seen in Figures A.4, A.5, and A.6.

Gas transport in coals is considered to occur at two scales: (I) laminar flow through the cleat system, and (II) diffusion through the coal matrix. Flow through the cleat system is pressure-driven and may be described using Darcy's law, whereas flow through the matrix is assumed to be concentration-driven and is modeled using Fick's law of diffusion (Harpalani and Chen, 1997). During gas production, the desorbed gases from the internal pores diffuse through the coal matrix to reach the cleat system and then it flows to the producing well. Thus, the gas diffusion in the coal matrix plays an important role in gas production. With its relatively smaller kinetic diameter, CO_2 can permeate not only macropores but also ultra micropores, which likely block CH_4 and N_2 that have slightly larger kinetic diameters, resulting in

one or two order of magnitude higher diffusivity of CO_2 than those of CH_4 and N_2 in the coal matrix. Hence, there is a strong selective diffusion of CO_2 over CH_4 and N_2 (Cui et al., 2004).

According to the study done by Laxminarayana and Crosdale (1999), CH_4 desorption rate of crushed coals measured at 0.5 MPa indicates that coal rank have important influences and there is a general trend of decreasing diffusion rate with increasing rank. Moreover, it is observed that gas diffusion through bright coals (vitrinite-rich coals) occurs more slowly than dull coals (inertinite-rich coals). In Clarkson and Bustin's (1999) study, it is stated that bright coals have a uniform micropore structure and their adsorption rate are adequately modeled using the classic unipore analytical solution. Both Clarkson and Bustin (1999) and Laxminarayana and Crosdale (1999) used unipore analytical model to fit their experimental data and they submit the results as effective diffusivity. Effective diffusivity is defined as the ratio of diffusion coefficient to the second power of diffusion path length. In this study, unipore diffusion model is used and r_p is defined as the cleat spacing by assuming that diffusion path is equal to coal matrix length. Laxminarayana and Crosdale's (1999) effective diffusivity data are converted to diffusion coefficients for each rank of coal. Since this data set is valid only for CH_4, diffusion coefficients of N_2 and CO_2 are determined by assuming that N_2 diffuses five times and CO_2 diffuses 100 times faster than CH_4 (Cui et al., 2004). Consequently, rank and component-dependent diffusion coefficients are tabulated in Table B.5.

In addition to rank and gas component dependent parameters, relative permeability curves of gas and water are needed to be able to model gas flow through cleat system. Therefore, relative permeability curves of San Juan Basin Fruitland formation data is used in Figure 4.2 (Mavor and Vaughn, 1998). Besides, the numerical values are provided in Table A.10.
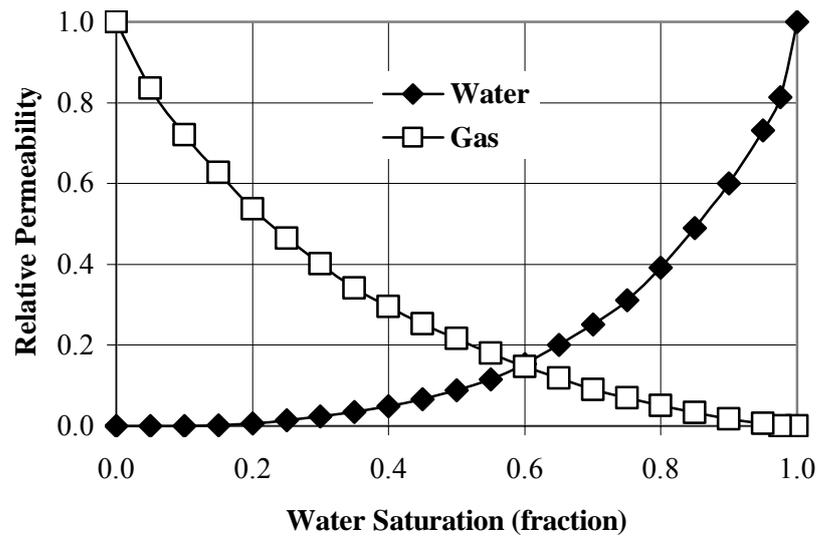
Figure 4.2 Relative Permeability vs. Water Saturation (Mavor and Vaughn, 1998).

4.2 Simulation Cases

Compositional reservoir simulator, GEM which is the product of Computer Modeling Group Ltd., Canada is selected to run the various enhanced coalbed methane simulation cases. This package has capability to simulate coalbed methane reservoirs and multi-compositional effects during injection of CO_2 or CO_2/N_2 gas mixtures. Moreover, it includes the extended P&M model to be able to study in shrinkage and swelling of coal during application of primary and enhanced recovery of methane. Besides, dual-porosity options are available to model cleat and matrix interactions during gas flow (CMG, 2007).

In this study, Gilman and Kazemi type of shape factor are preferred to investigate dual-porosity unsteady state gas transportation. Numerical dispersion control is also used to minimize any errors due to numerical calculations. Pore volume modifiers and transmissibility at the edges of the well patterns are adjusted so that pattern is isolated from the whole reservoir. Pressure, volume and temperature calculations are performed with Peng-Robinson equation of state. One of the codes written for high

volatile bituminous coal rank is provided in Appendix C with the explanations in bold letters.

In Table 4.1, a time schedule for all simulation cases, except methane-saturated dry coal case, is provided. Simulations begin with primary recovery of coalbed methane (CBM), which takes 10 years. After 10 years, ECBM recovery technique is applied. The aim of ten-year primary recovery is to decrease the water saturation in the cleat system and to increase the relative permeability of gas before injection of CO_2 or CO_2/N_2 mixture into the coal reservoir. In all cases water saturations after ten-year CBM recovery are below 40%. As there is no water in the fractures of methane-saturated dry coals, ECBM recovery is applied at the beginning.

Table 4.1 Time Schedule for Simulation Cases.

CBM Recovery	ECBM Recovery	Breakthrough Condition (CO_2 Molar Composition @ Production Wells)
Day	Day	%
0 - 3650	3650 – CO_2 Breakthrough	> 10

In this study depth and net thickness of the coal seam are selected as 3000 ft and 20 ft respectively. Average geothermal gradient is taken as 15 °F/1000 ft. Initial reservoir temperature is calculated as 113 °F. Pressure gradient is set to 0.39 psi/ft, which is the pressure gradient of the coal reservoir in Black Warrior Basin, USA (Pashin and Mcintyre, 2003). Initial molar gas composition of the coal reservoir is assumed as 100% CH_4.

As for production and injection conditions, bottomhole flowing pressure is set to 50 psia for production wells. Moreover, CO_2 is injected above supercritical point (88 °F and 1074 psia) in order to avoid adverse effects from CO_2 separating into liquid and gas phases in the injection system. Therefore, bottomhole injection pressure is set to

1170 psia, which is the pressure at 3000 ft depth due to 0.39 psi/ft pressure gradient, so that injection pressure and reservoir temperature are in supercritical region. Furthermore, radii of the injection and production wells are set to 0.25 ft.

Table 4.2 Constants for Simulation Cases.

Names	*Symbols*	*Value*
Reservoir Type	Rt	Methane Saturated Wet Coal (S_{wi} = 100%)
Coal Rank	Cr	High-Volatile
Well - Pattern	Wp	Inverse 5 - Spot
Drainage Area	Da	100 Acre
Cleat Permeability	k_f	10 md
Anisotropy	An	1 : 1
Molar Composition of Injected Fluid	Mo	100 % CO_2

In Table 4.2, values of constants used in simulations and their symbols are provided. Before giving information about each simulation case, it would be better to summarize some important assumptions in coal reservoir model.

- No permeability in coal matrix. After desorption, methane is transported from coal matrix to cleats by diffusion.
- Water presents only in cleats, there is no water in matrix pores. Therefore, water saturation is defined as ratio of the volume of water in cleats to cleat volume.
- Coal grains are incompressible.
- Pores in coal matrix are uniform.

Simulation cases are composed of two sections. In the first section, effects of physical coal properties and some operational parameters on the total methane recovery at the CO_2 breakthrough (TMRB), displacement ratio, CO_2 breakthrough

and CO_2 storage are studied. In the second part, how shrinkage and swelling affects the aforementioned parameters is examined. For all simulation cases, cartesian grid size is set to 75x75 ft to be able to observe the transient processes in detail. As an example, cartesian grid for inverted 5-spot pattern with 100 acre drainage area is shown in Figure 4.3.
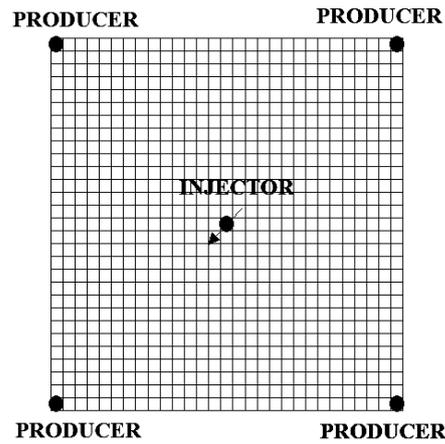
Figure 4.3 75x75 ft Cartesian Grid for Inverted 5-Spot Pattern.

4.2.1 Coal Properties and Operational Parameters

In this section, seven different vertical well cases are run to observe their effects on TMRB and CO_2 sequestration. Different coal ranks, reservoir types, well-patterns, drainage areas, cleat permeabilities, anisotropies, molar compositions of injected fluid are considered. The variable and constant parameters used in each case are tabulated in Table 4.3. In addition, horizontal well cases are simulated and compared to vertical well cases.

Table 4.3 Variables and Constants Used for Simulation of Vertical Well Cases.

Case #	Variables	Constants					
1	Cr	Rt	Wp	Da	k_f	An	Mo
2	Rt	Cr	Wp	Da	k_f	An	Mo
3	Wp	Rt	Cr	Da	k_f	An	Mo
4	Da	Rt	Cr	Wp	k_f	An	Mo
5	k_f	Rt	Cr	Wp	Da	An	Mo
6	An	Rt	Cr	Wp	Da	k_f	Mo
7	Mo	Rt	Cr	Wp	Da	k_f	An

Table 4.4 Case # 1 (Rank of Coal).

Rank of Coal	Symbol	Initial CH_4 in Place
-	-	10^6 Scf
Medium-volatile Bituminous	Mvb	1396
High-volatile Bituminous	Hvb	1264
Sub-bituminous	Sb	967

In case #1, all parameters except coal rank are constants. In Table 4.4, three different coal ranks are defined according to the information given in the "Preparation of Simulation Inputs" Section. For each coal rank initial CH_4 in place are calculated by the simulator according to Equation 4.6, which is the volumetric reserve estimation equation including both free gas in place in the cleats and adsorbed gas in place in the coal matrix.

$$G_i = Da \cdot h \cdot \left[\frac{43560 \cdot \varphi_{fi} \cdot (1-S_{wi})}{B_{gi}} + 1.359 \cdot C_{gi} \cdot \rho_c \cdot (1-a-m) \right] \qquad (4.6)$$

, where G_i is gas in place at initial reservoir conditions, (Mscf); Da is drainage area, (acre); h is net coal thickness, (ft); φ_{fi} is initial fracture porosity, (fraction); S_{wi} is initial water saturation in cleats, (fraction); B_{gi} is gas formation volume factor at initial pressure, (rcf/Mscf); C_{gi} is initial sorbed gas concentration, (scf/ton, dry, ash-free

coal); ϱ_c is coal pure density, (g/cm^3); a is ash-content, (weight fraction); m is moisture content, (weight fraction).

In case #2, all parameters except reservoir type are constants. In Table 4.5, seven different reservoir types are defined depending on their initial adsorbed methane saturation in coal matrix and water saturation in the cleats. Furthermore, the initial CH$_4$ in place for each reservoir type is also provided in Table 4.5.

Table 4.5 Case #2 (Reservoir Type).

Reservoir Types				
Coal Type	Adsorbed CH$_4$ Saturation	Initial Water Saturation in Cleats	Symbol	Initial CH$_4$ in Place
-	-	%	-	10^6 Scf
Dry	S[1]	0	DS	722
Wet	S	30	W30S	1308
Wet	S	60	W60S	1289
Wet	S	100	W100S	1264
Wet	10 % US[2]	100	WUS10	1120
Wet	20 % US	100	WUS20	989
Wet	40 % US	100	WUS40	748

[1] Saturated, [2] Undersaturated

Initial pressure conditions of each reservoir type are tabulated in Table B.6 with their references. In dry coal reservoirs, as it is stated by Hoch (2005) pressure is very low with the average being less than 30% of water-hydrostatic pressure (0.43 psi/ft). By using this information a methane-saturated dry coal reservoir type is defined. Furthermore, three different methane undersaturation cases are defined in Table B.6 as 10%, 20%, and 40% with the following equations (Seidle and O'connor, 2007).

$$\text{Undersaturation (\%)} = 100 - 100 \times \frac{V_{measured}}{G_s} \qquad (4.7)$$

$$G_S = V_L \frac{P}{P+P_L} \tag{4.8}$$

,where $V_{measured}$ is actual initial gas content in coal matrix at reservoir conditions, (scf/ton); G_s is gas storage capacity of coal matrix at reservoir conditions, (scf/ton); V_L Langmuir volume, (scf/ton); P_L is Langmuir pressure, (psi); P is pressure, (psi).

During primary methane recovery from undersaturated coal reservoirs, produced fluid is only water until the reservoir pressure decreases to a value at which desorption of methane begins in coal matrix. It is called the critical desorption pressure. In order to model this phenomenon, matrix pressures and the cleat pressures are defined separately to the simulator. For instance, if undersaturation is 10%, fracture (cleat) pressure is defined as 1170 psia and the matrix pressure is calculated as 850 psia from Equations 4.7 and 4.8. Therefore, the simulator produced water between the pressures 1170 and 850 psia. Below 850 psia, however, water is produced with methane.

In addition to dry and undersaturated coal reservoir types, methane-saturated wet coals are also simulated. In this type of reservoirs, three different initial water saturations are selected as 30%, 60%, 100%.

In case #3, seven different well-patterns are simulated by taking other parameters as constant to determine which well-pattern is the best in terms of ECBM recovery and CO_2 sequestration. The name and symbol of each well-pattern are provided in Table 4.6. Furthermore, locations of production and injection wells for each well-pattern are illustrated in Figure 4.4.

Table 4.6 Case #3 (Well-Pattern)

Well Pattern	Symbol
Direct Line Drive	DLD
Staggered Line Drive	SLD
Inverted 5-spot	Inv.5
Inverted 9-spot	Inv.9
Normal 9-spot	N.9
Inverted Hexagonal 7-spot	Inv.Hex.7
Normal Hexagonal 7-spot	N.Hex.7
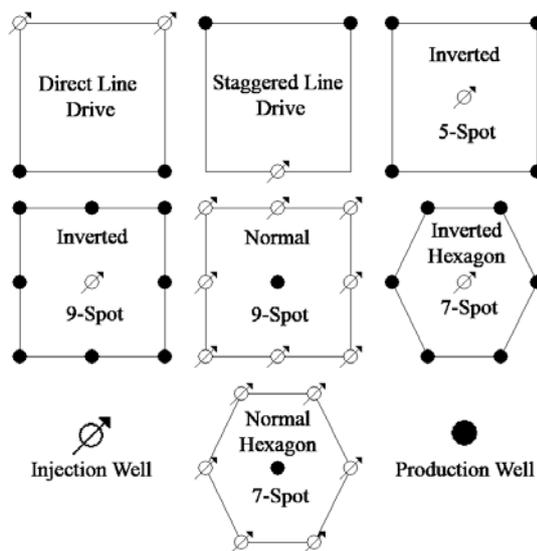
Figure 4.4 Well Patterns in Case #3.

In case #4, the effect of drainage area on TMRB and CO_2 sequestration is investigated by defining four different values. These are 50, 100, 150 and 200 acres.

As it is stated before cleat permeability generally ranges between 0.5 and 100 md. Hence, five different permeabilities are selected for case #5, which are 4, 10, 25, 50 and 100 md. Furthermore, there are two types of cleats in the coal seams, namely, butt and face cleats. These are generally orthogonal to each other. Permeability of face cleats is larger than butt cleats, which leads to permeability anisotropy in the coal seams. In order to simulate the possible effects of permeability anisotropy on TMRB and CO_2 sequestration, six different anisotropies are chosen for case #6. These are

1:1, 1:2, 1:4, 1:9, 1:16 and 1:25 anisotropies. 4 md is selected as a constant value for butt cleat. For instance, if anisotropy is 1:4, then face cleat permeability is defined as 16 md.

Furthermore, effect of the molar composition of injected fluid on the TMRB and CO_2 sequestration is examined in case #7. Four different molar compositions of CO_2/N_2 mixtures are selected as 100/0 %, 75/25 %, 50/50 % and 25/75 %.

In addition to vertical well cases, two horizontal wells, one is a production and the other is an injection well, which are parallel to each other in Figure 4.5 are simulated. By keeping the drainage area (100 Acre) constant between these horizontal wells, distance between them is decreased for each run. As the distance decreases, the length of the horizontal wells increases. Optimum distance between horizontal production and injection wells is investigated. In addition, performance of horizontal well cases is compared to vertical well cases.
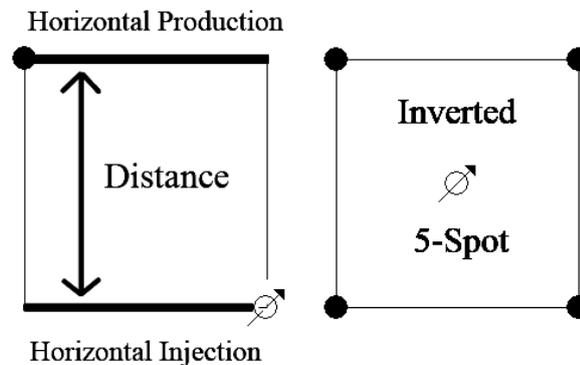
Figure 4.5 Horizontal vs. Vertical Well Cases.

4.2.2 Shrinkage and Swelling Effect

After determining rank and component dependent simulation parameters, three different cases namely, rank of coal, reservoir types and molar compositions of

67

injected fluid are run to observe the effect of shrinkage and swelling on TMRB, displacement ratio, CO_2 breakthrough and CO_2 storage. In addition, parameters in the extended version of Palmer and Mansoori (P&M) (1998) permeability model is collected from the published papers and high, medium, low cases are defined for each parameter to make a sensitivity analysis. In all simulation cases, well-pattern, drainage area, fracture permeability and anisotropy are taken constants as inverted 5-spot, 100 acre, 10 md and isotropic. Values of the parameters corresponding to 10 md case are highlighted with bold letters in Tables B.2, B.3, and B.4. The variable and constant parameters used in the first-three cases are tabulated in Tables 4.7 and 4.8.

Table 4.7 Constants of First Three Cases.

Names	*Symbols*	*Value*
Reservoir Type	Rt	Methane Saturated Wet Coal (S_{wi} = 100%)
Coal Rank	Cr	High-Volatile
Well - Pattern	Wp	Inverse 5 - Spot
Drainage Area	Da	100 Acre
Cleat Permeability	k_f	10 md
Anisotropy	An	1 : 1
Molar Composition of Injected Fluid	Mo	100 % CO_2

Table 4.8 Variables and Constants Used for the First Three Cases.

Case #	*Variables*	*Constants*					
1	Cr	Rt	Wp	Da	k_f	An	Mo
2	Rt	Cr	Wp	Da	k_f	An	Mo
3	Mo	Rt	Wp	Da	k_f	An	Cr

In addition to cases in Table 4.8, a sensitivity study is done for the parameters in the extended P&M model. Their associated values (high, low and medium) are tabulated

in Tables 4.9 and 4.10 with their references. Low and high cases are determined by collecting data from various references. Medium values, however, are calculated by taking average of all.

Table 4.9 Case #4 (Component Dependent Infinite Pressure and Strain).

References	Cases	P_{inf}			ε_{inf}		
		psi			10^{-2}		
-	-	N_2	CH_4	CO_2	N_2	CH_4	CO_2
(Mavor and Vaughn, 1998) (Mavor and Gunter, 2004)	Low	750	168	142	0.09	0.35	1.48
(Shi et al., 2004) (Robertson and Christiansen, 2005) (Mazumder et al., 2006)	Medium	1271	555	711	0.313	0.842	3.14
(Cui et al, 2007) (Wong et al., 2007)	High	2636	886	1527	0.774	1.3	6.74

Table 4.10 Case #5 (Elastic Modulus and Poisson's Ratio).

References	Cases	E	Calculated Cleat Compressibility	v	Calculated Cleat Compressibility
-	-	10^5 psi	10^{-4} psi^{-1}	-	10^{-4} psi^{-1}
(Evans and Pomeroy, 1966) (Berkowitz, 1979)	Low	1.24	6.2	0.21	1.8
(Vaziri et al., 1997) (Mavor and Vaughn, 1998)	Medium	5.95	1.3	0.35	1.2
(Gentzis, 2000) (Robertson and Christiansen, 2005)	High	8.85	0.87	0.48	0.23

CHAPTER 5

RESULTS AND DISCUSSION

There are mainly two simulation studies investigating the effects of coal properties & operational parameters, and shrinkage & swelling (SS) on total methane recovery at CO_2 breakthrough (TMRB), displacement ratio, CO_2 breakthrough and CO_2 storage. In the coal properties and operational parameters section, simulations are run for different coal ranks, reservoir types, well-patterns, drainage areas, cleat permeabilities, anisotropy, molar compositions of injected fluid and well types. In the second section, simulations are run for different coal ranks, reservoir types and molar compositions of injected gas mixture to observe shrinkage & swelling effects. In addition to aforementioned simulation cases, a sensitivity study is done with the parameters in the extended version of Palmer & Mansoori (P&M) (1998) permeability model. The compositional GEM module of CMG simulator (Computer Modeling Group) is used for this study, which utilizes the extended P&M model for simulating multi-component shrinkage and swelling. All the simulation cases and their conditions are given in Chapter 4 and their numerical results are provided in Appendix D.

The following definitions will be done here for easy follow up the chapter. The ***total methane recovery at CO_2 breakthrough*** (TMRB) includes ten-year primary coalbed methane (CBM) recovery and succeeding enhanced coalbed methane (ECBM) recovery up to CO_2 breakthrough for all simulation cases, except methane-saturated dry coal reservoir case. Moreover, ***displacement ratio*** is defined as the ratio of the amount of CO_2 injected to the amount of CH_4 produced throughout the injection period. Owing to economical reasons, it is better to obtain a lower displacement ratio, since reduction in the amount of CO_2 injected directly decrease the cost. But if the project is evaluated in terms of CO_2 sequestration, it is better to

have a higher displacement ratio. In this study, former one is considered. Furthermore, **CO_2 breakthrough** is defined as the time at which the molar composition of CO_2 in the produced gas stream is higher than 10 percent. It also includes ten-year CBM recovery period.

5.1 Coal Properties and Operational Parameters

After applying ten-year CBM recovery and succeeding ECBM recovery, CO_2 breakthrough time is determined for each case and then the same cases are also run up to this time by applying only CBM recovery technique. Therefore, in this section CBM recovery is defined as the primary methane recovery at the predetermined CO_2 breakthrough time. The difference between TMRB and CBM recoveries at CO_2 breakthrough time shows the success of ECBM recovery. Besides, displacement ratio, CO_2 breakthrough and CO_2 storage are other important parameters affecting the success of the project which are examined with respect to different coal ranks, reservoir types, well-patterns, drainage areas, cleat permeabilities, anisotropy, molar compositions of injected fluid and well types.

5.1.1 Case #1 (Coal Rank)

Methane recovery vs. time is plotted for different ranks of coal (Figure 5.1). During ten-year primary recovery of methane, highest recovery belongs to sub-bituminous coals. In this period, as the coal rank increases, primary methane recovery decreases. After ten years, however, methane recovery from medium volatile bituminous coals increases abruptly with the CO_2 injection and CO_2 breakthrough occurs earlier than lower ranks. Furthermore, TMRB for medium volatile bituminous coal is smaller than lower ranks and TMRB for all ranks are higher than ~95 % (Table D.1).

The difference between TMRB and CBM recovery is the biggest for medium volatile bituminous coals (Figure 5.2). As the coal rank decreases this difference also decreases. The same trend is also valid for displacement ratio. Moreover, the amount of CO_2 stored in coal media goes up as the coal rank increases (Figure 5.3). CO_2 breakthrough time, however, gets shorter with increasing coal rank.
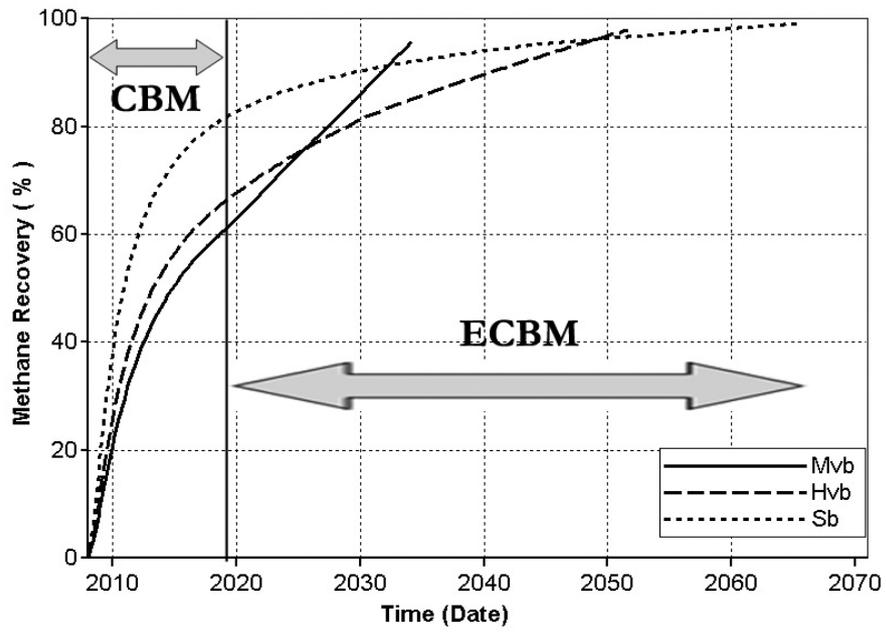
(Mvb: Medium-volatile bituminous, Hvb: High-volatile bituminous, Sb: Sub-bituminous)

Figure 5.1 Methane Recovery vs. Time for Different Coal Ranks.
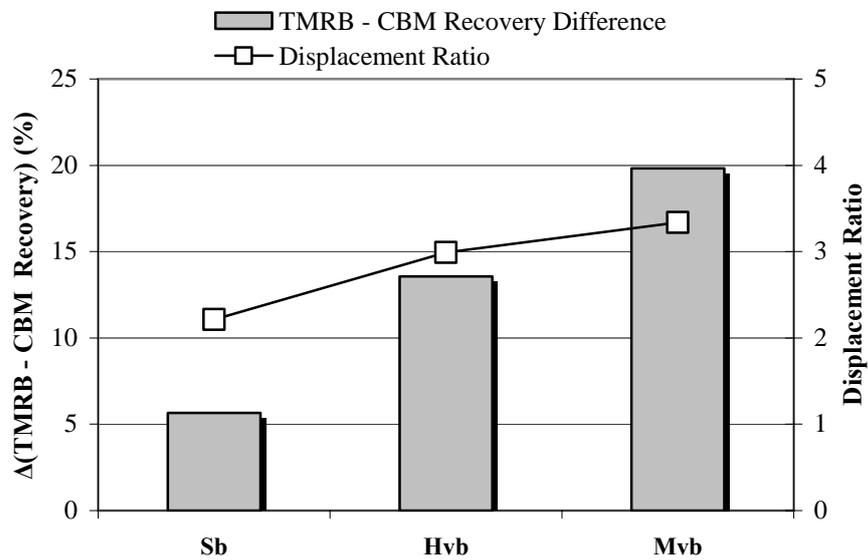
Figure 5.2 Δ(TMRB - CBM Recovery) and Displacement Ratio vs. Coal Rank.
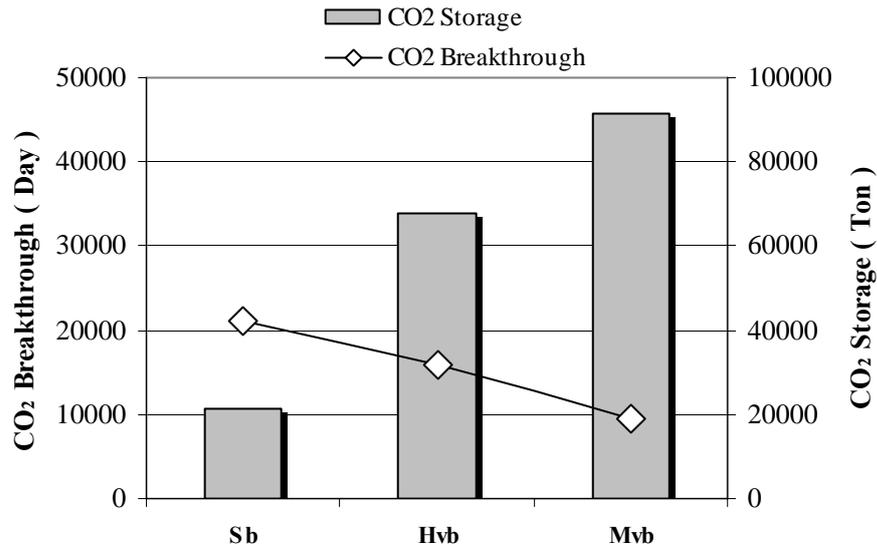
Figure 5.3 CO₂ Breakthrough and CO₂ Storage vs. Coal Rank.

As a result, medium volatile bituminous coal rank is more suitable for ECBM recovery with shortest breakthrough time, highest CO_2 storage and biggest TMRB-CBM recovery difference. Another reason is that production of CH_4 with primary recovery technique from lower rank coals such as sub-bituminous coals enables to recover over 80% of the initial CH_4 in place in the first ten-year. Therefore, this makes the application of ECBM recovery unfavorable for lower rank coals. Moreover, medium volatile bituminous coals contain more CH_4 in place than the lower ranks of coal if all other parameters are the same (Table 4.4 in Chapter 4). The reason why displacement ratio is highest for medium volatile coals is that its CO_2 storage capacity is higher than lower ranks.

5.1.2 Case #2 (Reservoir Type)

Table 4.5 in Chapter 4 summarizes all the reservoir types with initial CH_4 in place. D, W, S and US refers to dry, wet, methane-saturated and methane-undersaturated reservoirs, respectively. The number after W shows the initial water saturation in cleats and the number after S or US shows undersaturation of methane in percentages.
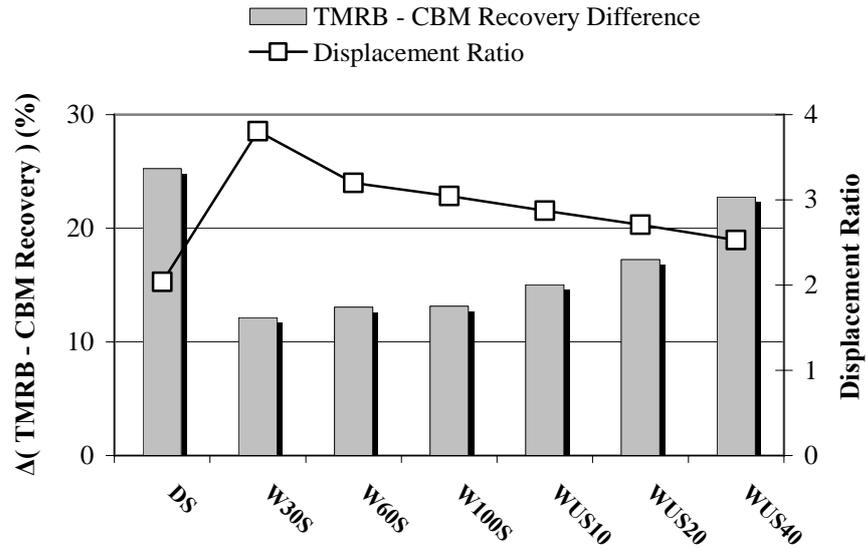
Figure 5.4 Δ(TMRB - CBM Recovery) and Displacement Ratio vs. Reservoir Type.

The difference between TMRB and CBM recoveries at CO_2 breakthrough is the biggest for methane saturated dry coals (Figure 5.4). Undersaturated wet and saturated wet coals follow the dry coals. Displacement ratio is the lowest for methane-saturated dry coal case. As the undersaturation increases, recovery difference increases and displacement ratio decreases. Highest displacement ratio belongs to the methane-saturated wet coal with initial water saturation of 30%. Moreover, effect of initial water saturation on recovery difference is negligible for methane-saturated wet coals.

CO_2 breakthrough occurs earlier in methane-saturated dry coals than any other coal reservoir types (Figure 5.5). While initial water saturation does not have any effect on it, increasing undersaturation leads to later CO_2 breakthroughs. In addition, reservoir type does not affect the amount of CO_2 stored (Figure 5.5). Moreover, TMRB for all reservoir types are calculated as higher than 97 % (Table D.2).
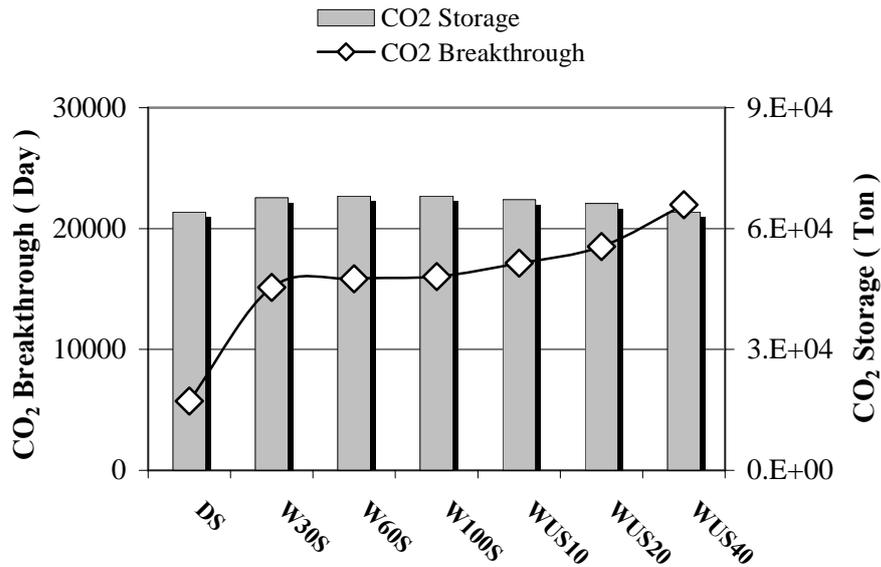
Figure 5.5 CO$_2$ Breakthrough and CO$_2$ Storage vs. Reservoir Type.

At first glance it can be concluded that dry coal reservoirs are more suitable for ECBM recovery with lowest displacement ratio, shortest CO$_2$ breakthrough time and biggest recovery difference. Also the amount of CO$_2$ stored is nearly the same as other reservoir types. In addition, there is no water to produce, which directly decrease the field expenses. However, low initial CH$_4$ content of dry coal reservoirs due to low initial reservoir pressure is a drawback and it may change all of the positive things mentioned above to negative. Therefore, to be able to decide on which coal reservoir is more suitable than others a detailed economical analysis is required.

5.1.3 Case #3 (Well-Pattern)

Main methane production mechanism is desorption in coalbed methane reservoirs, therefore capability of well-patterns to decrease reservoir pressure is very important. Table 4.6 and Figure 4.4 in Chapter 4 show the all well-patterns used in this study. In Figure 5.6, decrease in average reservoir pressure during primary recovery of methane for different well patterns is shown. Drainage of 100 acre area with inverted

9-spot and inverted hexagonal 7-spot patterns give the best results. However, it seems that inverted 5-spot pattern is a better choice than others, since the total number of wells drilled is smaller and its drainage capability is pretty good.
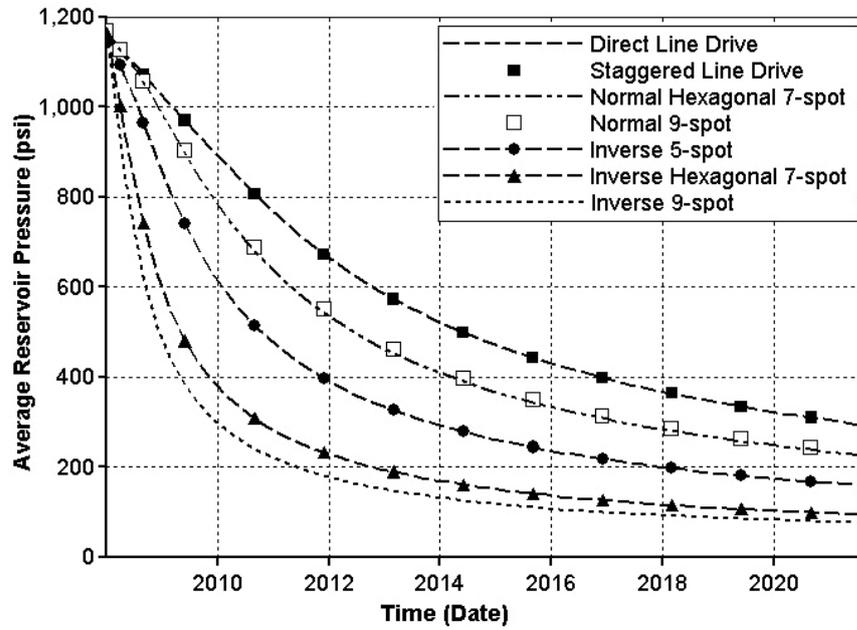
Figure 5.6 Average Reservoir Pressure during CBM Recovery vs. Time for Different Well Patterns.

Figures 5.7 and 5.8 confirm the primary evaluation for the selection of a proper well-pattern for ECBM recovery. The displacement ratio of inverted 5-spot pattern is lower than 7-spot and 9-spot well patterns and its TMRB - CBM recovery difference is bigger than inverted 9-spot and inverted hexagonal 7-spot patterns (Figure 5.7). Furthermore, CO_2 breakthrough with inverted 5-spot pattern occurs as early as 7-spot and 9-spot patterns (Figure 5.8). Moreover, it is realized that the amount of CO_2 stored with inverted 5-spot is good enough when it is compared to others. To sum up, inverted 5-spot pattern has good drainage and CO_2 storage capabilities. It causes short CO_2 breakthrough time with TMRB up to 98% (Table D.3).
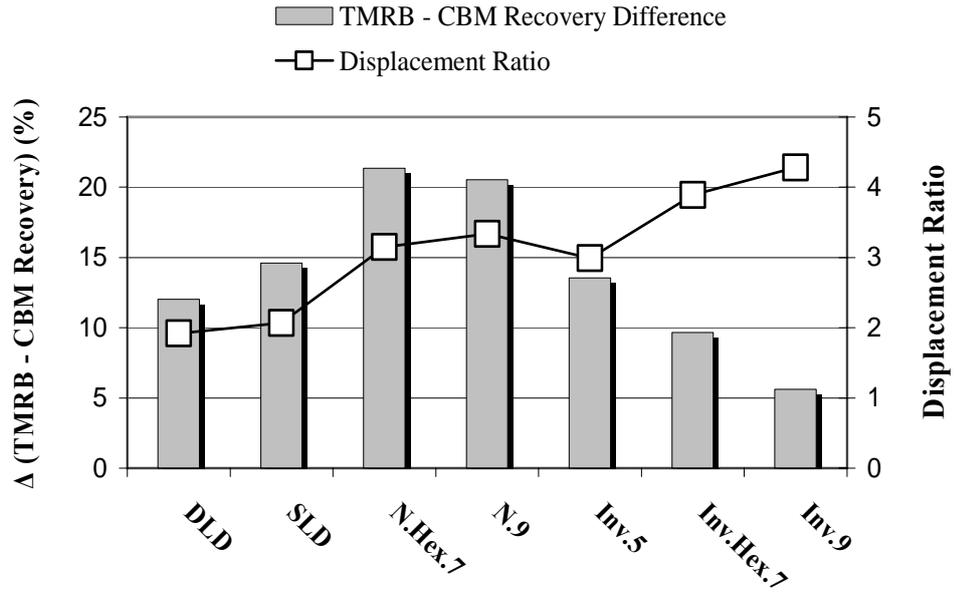
Figure 5.7 Δ(TMRB - CBM Recovery) and Displacement Ratio vs. Well Pattern.
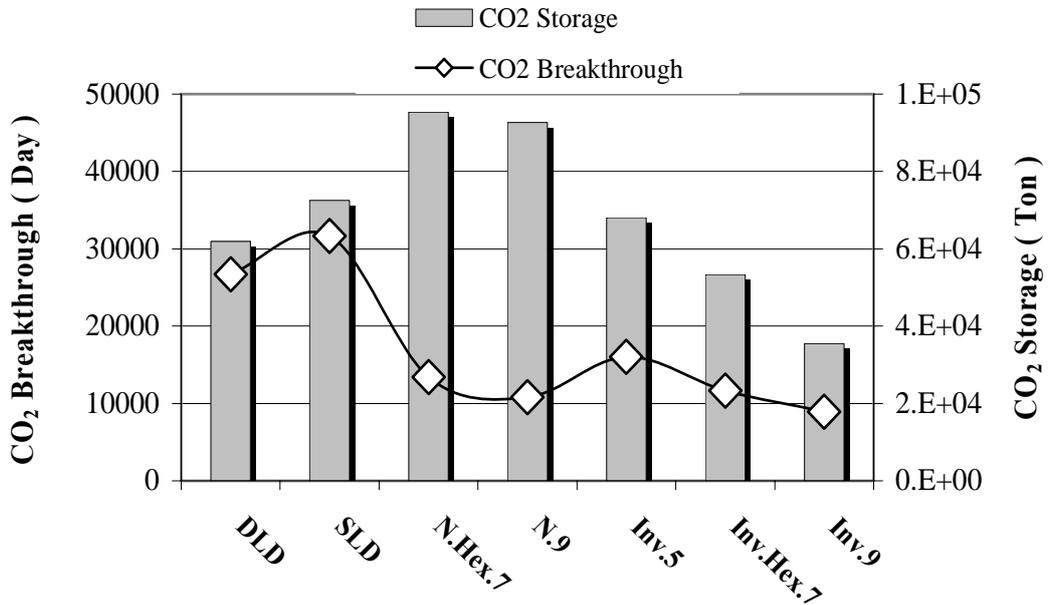
Figure 5.8 CO$_2$ Breakthrough and CO$_2$ Storage vs. Well Pattern.

5.1.4 Case #4 (Drainage Area)

The drainage capability of inverted 5-spot pattern during primary recovery of CH_4 from four different drainage areas is illustrated in Figure 5.9. As the drainage area decreases, reservoir pressure falls more sharply and desorption of CH_4 with respect to time occurs more quickly. In conventional oil and gas reservoirs, however, decrease in drainage area after a certain value may decrease the total flow rate due to intersection of drainage zones of the wells.
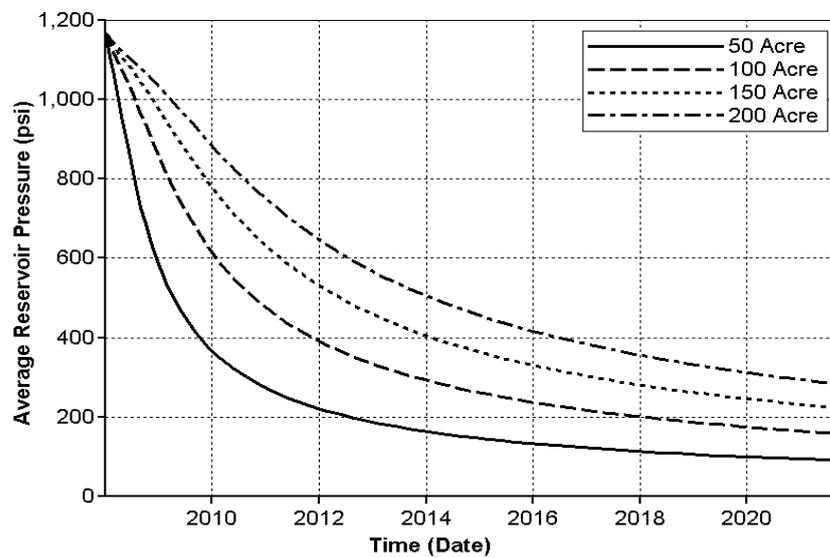
Figure 5.9 Average Reservoir Pressure during CBM Recovery vs. Time for Different Drainage Area.

As the drainage area increases, difference between TMRB and CBM recovery increases slightly and displacement ratio decreases sharply (Figure 5.10). Moreover, both CO_2 storage and CO_2 breakthrough time are directly related to drainage area (Figure 5.11).
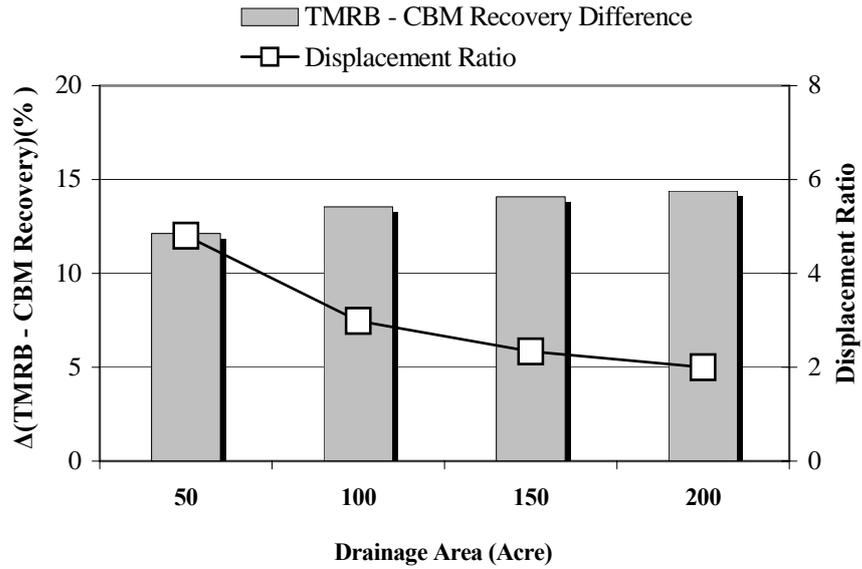
Figure 5.10 Δ(TMRB - CBM Recovery) and Displacement Ratio vs. Drainage Area.
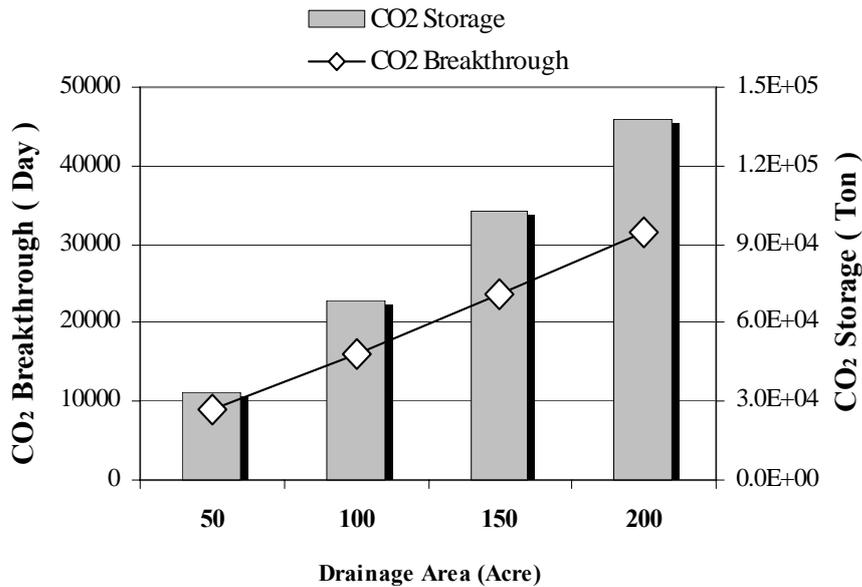
Figure 5.11 CO_2 Breakthrough and CO_2 Storage vs. Drainage Area.

At first glance 100 acre drainage area seems to be better choice for ECBM recovery than others, since its displacement ratio is as low as larger drainage areas and CO_2 breakthrough occurs as early as smaller drainage areas. Moreover, TMRB for all

79

drainage areas are equal to 98% (Table D.4). If the drainage area decreases, the number of wells needed for a field increases. If the drainage area increases, however, CO_2 breakthrough time gets longer. Therefore, the best choice should be determined after an economical analysis considering this trade-off.

5.1.5 Case #5 (Cleat Permeability)

The displacement ratio increases as the cleat permeability increases up to 50 md (Figure 5.12). After 50 md, a decrease is observed. Moreover, biggest TMRB - CBM recovery difference is obtained at 10 and 25 md cases.
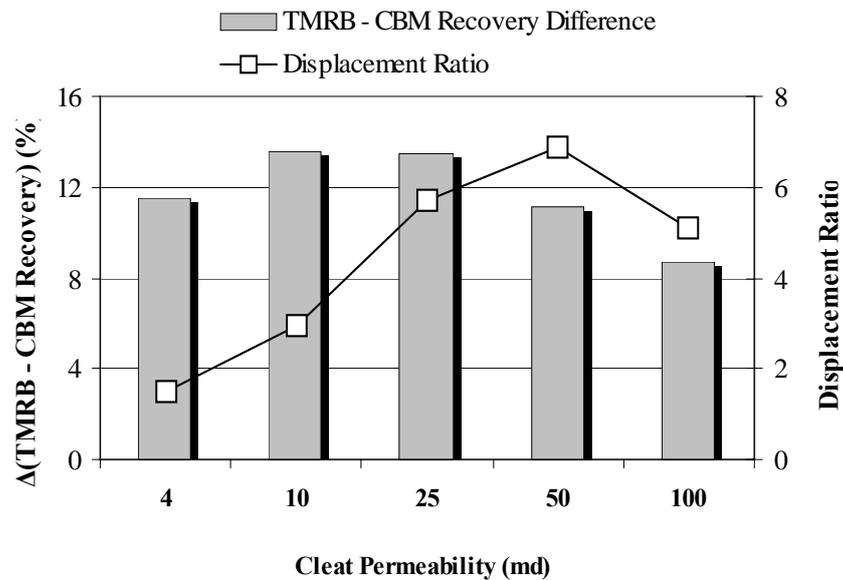
Figure 5.12 Δ (TMRB - CBM Recovery) and Displacement Ratio vs. Cleat Permeability.

CO_2 breakthrough time decreases sharply from 4 to 25 md (Figure 5.13). Between 25 and 100 md, however, decrease in breakthrough time is negligible. In addition, CO_2 storage increases with increasing cleat permeability. Furthermore, TMRB rises up slightly as the cleat permeability decreases and it ranges from 96% to 99% (Table D.5).

80
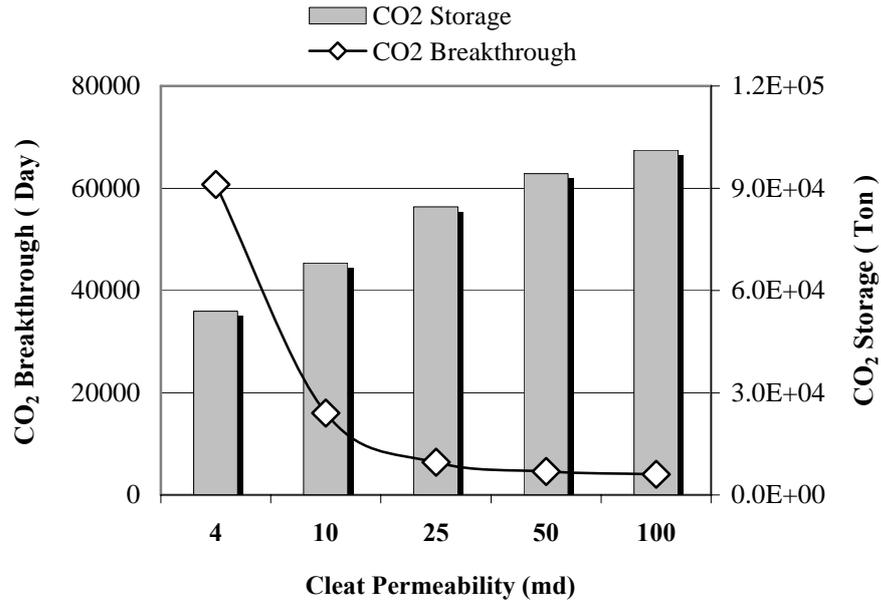
Figure 5.13 CO$_2$ Breakthrough and CO$_2$ Storage vs. Cleat Permeability.

It can be concluded that cleat permeability between 10 and 25 md is the best for ECBM recovery, because displacement ratio is low, CO$_2$ breakthrough is short, while recovery difference is big.

5.1.6 Case #6 (Anisotropy)

The butt and face cleats are generally orthogonal to each other. Permeability of face cleats is larger than butt cleats, which leads to permeability anisotropy in the coal seams. In order to simulate the possible effects of permeability anisotropy on TMRB and CO$_2$ sequestration, six different anisotropies are defined as 1:1, 1:2, 1:4, 1:9, 1:16 and 1:25. The butt cleat permeability is a constant value of 4 md. For instance, if anisotropy is 1:4, then face cleat permeability is defined as 16 md.

TMRB calculated for all anisotropy values by the simulator are nearly equal to 98% (Table D.6). Therefore, anisotropy in cleat permeability has no effect on TMRB. Moreover, the difference between TMRB and CBM recovery declines and displacement ratio goes up as the anisotropy increases (Figure 5.14). It is realized that

81

CO_2 breakthrough time gets shorter with increasing anisotropy. However, the change in CO_2 storage due to anisotropy is negligible (Figure 5.15).
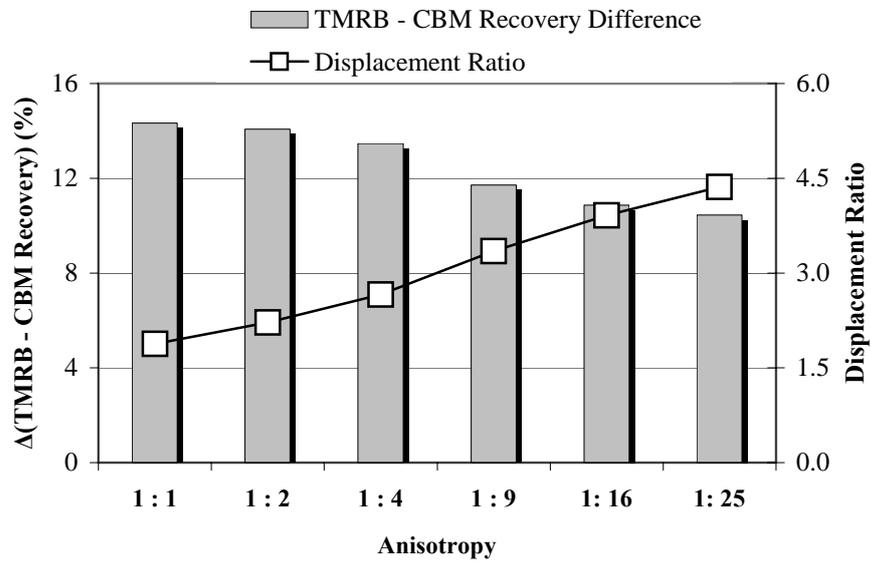
Figure 5.14 Δ (TMRB - CBM Recovery) and Displacement Ratio vs. Permeability Anisotropy.
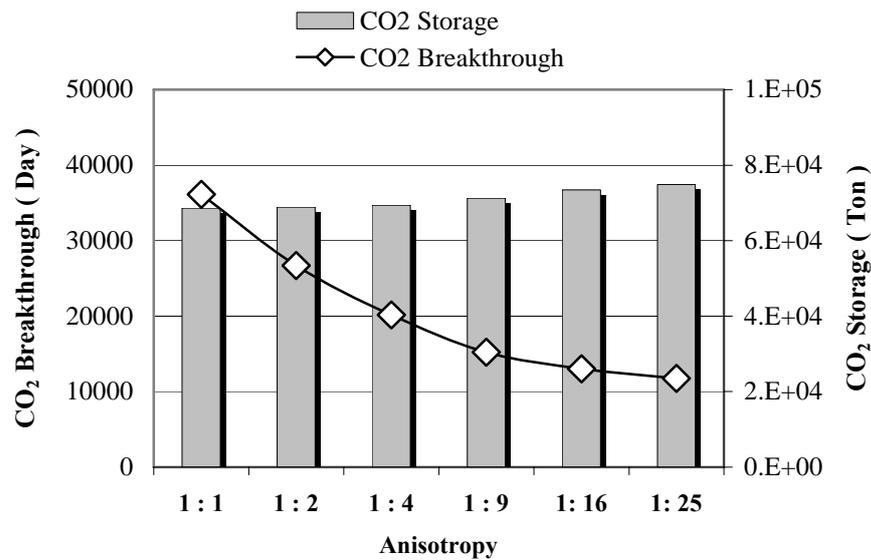
Figure 5.15 CO_2 Breakthrough and CO_2 Storage vs. Permeability Anisotropy.

5.1.7 Case #7 (Molar Composition of Injected Fluid)

Four different molar compositions of CO_2/N_2 mixtures are selected as 100/0 %, 75/25 %, 50/50 % and 25/75 %. Total methane recoveries at CO_2 breakthrough for all molar compositions of injected CO_2/N_2 gas mixture are bigger than 98% (Table D.7). Therefore, molar composition has no effect on TMRB. As the molar percentage of N_2 in CO_2/N_2 mixture increases, difference between TMRB and CBM recovery increases, but the displacement ratio declines (Figure 5.16). Furthermore, CO_2 breakthrough and storage decline as the amount of N_2 in CO_2/N_2 mixture increases (Figure 5.17).
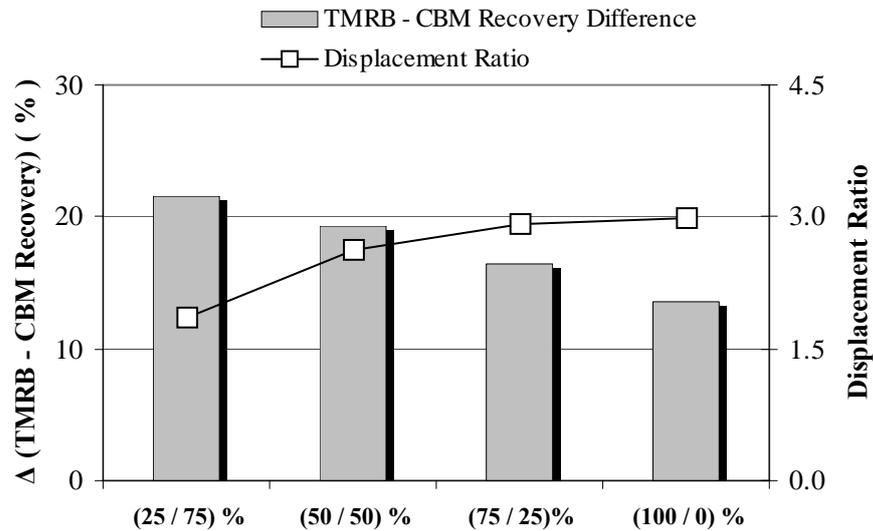
Figure 5.16 Δ (TMRB - CBM Recovery) and Displacement Ratio vs. Molar Composition of Injected (CO_2/N_2) Gas Mixture.

At first glance it may seem that it is better to inject more N_2 than CO_2, but one should also consider N_2 breakthrough, which occurs earlier than CO_2 breakthrough. Therefore, the money that would be spent for separation CH_4 from N_2 is also very important. As a result, the CO_2/N_2 composition between (50/50)% and (75/25)% is better than other compositions, since CO_2 storage is as high as (100/0)% case, CO_2

breakthrough time is as short as (25/75)% and displacement ratio is smaller than (100/0)% case.
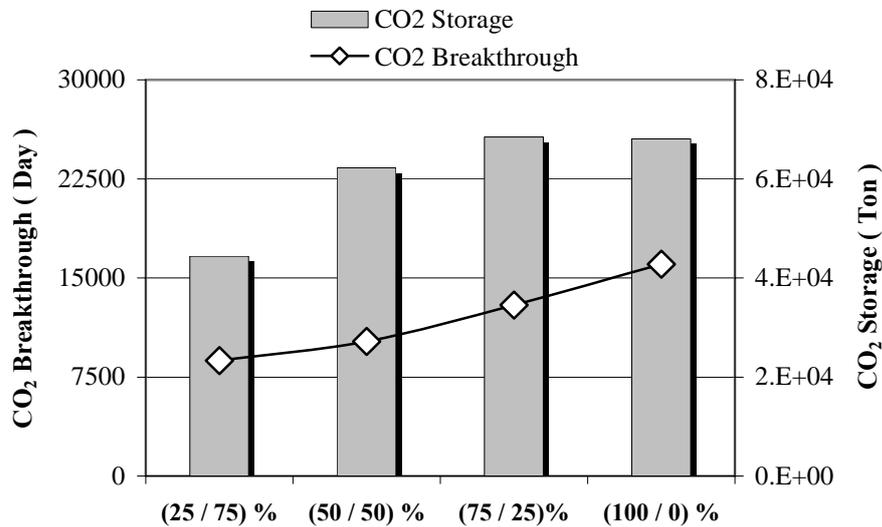
Figure 5.17 CO$_2$ Breakthrough and CO$_2$ Storage vs. Molar Composition of Injected (CO$_2$/N$_2$) Gas Mixture.

5.1.8 Case #8 (Well Types)

Figure 4.5 in Chapter 4 shows the well types used in case #8. The decrease in spacing between horizontal production and horizontal injection wells by keeping 100 acre drainage area constant leads to earlier CO$_2$ breakthrough (Figure 5.18). However, in the same figure TMRB for all cases are the same at the CO$_2$ breakthrough time.

In Figure 5.19, three different simulation runs are discussed. In all cases permeability is isotropic, drainage area is equal to 100 acre and its shape is square. If horizontal injection and production wells are drilled through the face cleat direction as in Case B, methane flows to well through butt cleats. Permeability of butt cleats is smaller than face cleats. Therefore, CO$_2$ breakthrough time gets longer in Case B than the vertical well case. If they are drilled through butt cleat direction, however, flow of

methane occurs through face cleats as in Case A. Thus, CO_2 breakthrough occurs earlier with high methane recovery than vertical well case. In conclusion, determination of the butt and face cleat direction is very important before drilling horizontal wells.
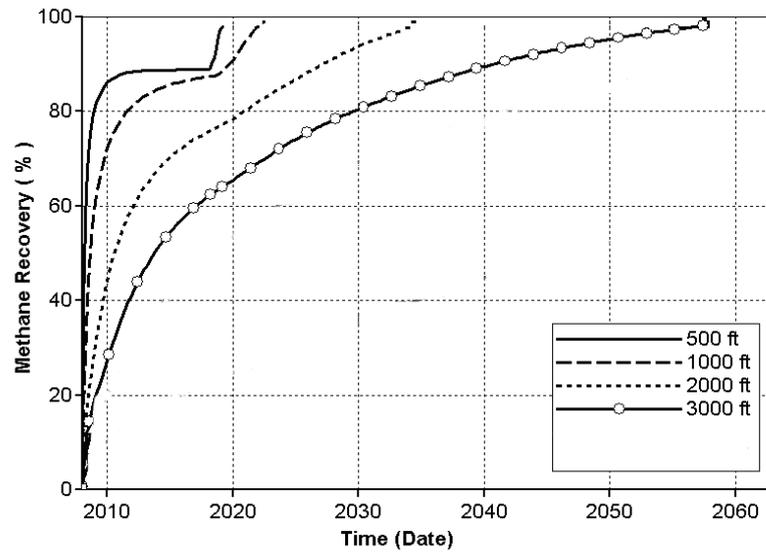
Figure 5.18 Methane Recovery vs. Time for Different Horizontal Well Spacing.
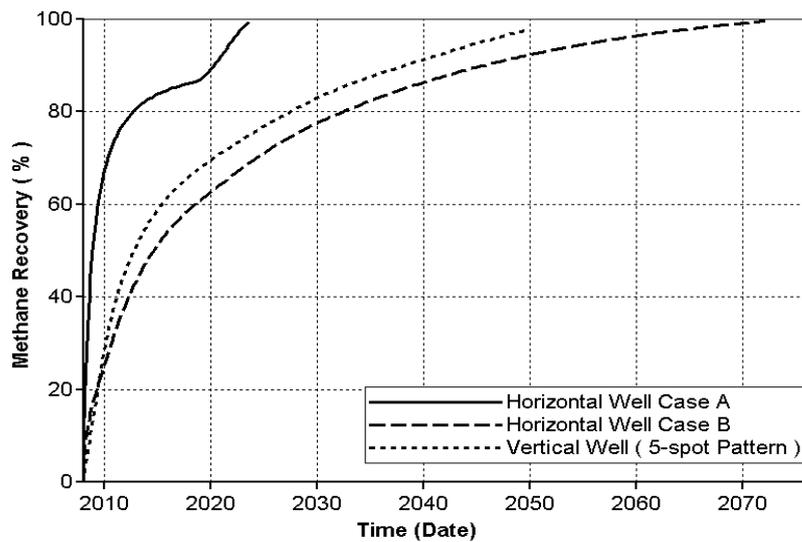
Figure 5.19 Comparison of Horizontal Well Case A and B with a Vertical Well Case.

5.2 Shrinkage and Swelling Effect

In order to examine the shrinkage and swelling (SS) effect on total methane recovery at CO_2 breakthrough (TMRB), displacement ratio, CO_2 breakthrough time and CO_2 storage, simulations are run up to the CO_2 breakthrough time with and without SS. The difference between these cases shows the magnitude of SS effect and it is represented by a multiplier. The ***multiplier*** is defined as a ratio indicating the change in a parameter due to SS effect. If multiplier is bigger than one, SS leads to an increase in that parameter. Otherwise, it leads to a decrease. Each multiplier plot is accompanied by a legend showing the values of corresponding parameters without SS effect.

In addition to multiplier plots, absolute permeabilities were plotted for some cases at the injection well block, so that the decrease in injectivity (swelling effect) due to injection of CO_2 or CO_2/N_2 gas mixture can be clearly seen. In this section, CBM recovery is defined by a different procedure than the aforementioned one in Section 5.1, since it is obtained at the end of ten years. This enables to examine shrinkage effect in the first ten years separately.

Rank of coal, reservoir type and molar composition of injected gas mixture are the main variable parameters in the first three cases of this section. In the sensitivity analysis part, simulation cases with SS effects were examined by plotting methane recovery vs. time plots for high, medium and low values of each parameter forming the extended version of Palmer and Mansoori (P&M) (1998) permeability model. For comparison purposes simulation cases without SS were also run and plotted on the same graphs.

5.2.1 Case #1 (Rank of Coal)

Simulation results of this case are shown in Figures 5.20, 5.21, 5.22 and 5.23. Also numerical results are provided in Table D.8. The increase in TMRB due to shrinkage and swelling is the highest for high-volatile bituminous (Hvb) coals (Figure 5.20). Its multiplier is 1.088, which corresponds to 8.8% increase. Moreover, the smallest

increase in TMRB belongs to sub-bituminous (Sb) coals. Although there is a decrease in CBM recovery for Sb and Hvb coal ranks due to shrinkage and relative permeability effect, TMRB increases. Therefore, swelling during ECBM recovery period has an increasing effect on total methane recovery. For Medium-volatile bituminous (Mvb) case the increase in CBM recovery is smaller than the increase in TMRB, so there is again some swelling effect increasing the total methane recovery. The difference between TMRB and CBM recovery shows that swelling effect on ECBM recovery increases as the rank of coal decreases from Mvb to Sb. Moreover, the decline in displacement ratio owing to swelling gets smaller as the rank of coal increases. Biggest negative change in displacement ratio belongs to sub-bituminous coals with the multiplier of 0.17. The reason why ECBM recovery increases and displacement ratio declines due to SS effects is that flow of CO_2 through cleats is retarded by swelling effect, which decreases the absolute cleat permeability. This provides extra time to CH_4 to be replaced by CO_2 and causes increased sweep efficiency.
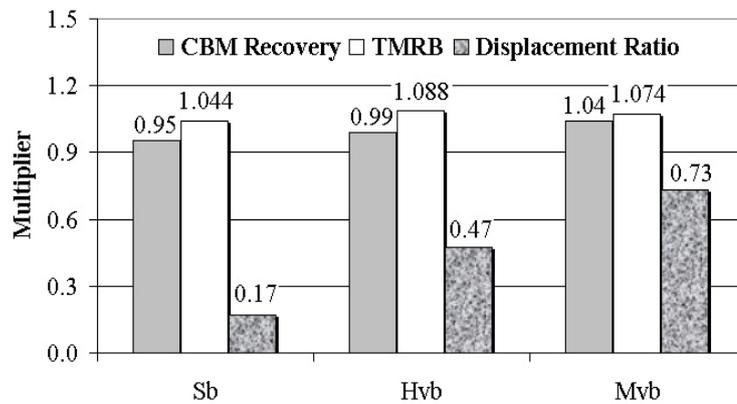
Coal Rank	CBM Recovery	TMRB	Displacement Ratio
-	%	%	%
Sb	83.7	95.3	12.7
Hvb	64.5	90.2	6.3
Mvb	56.2	89.4	4.6

(Mvb: Medium-volatile bituminous, Hvb: High-volatile bituminous, Sb: Sub-bituminous)

Figure 5.20 Multiplier of CBM Recovery, TMRB and Displacement Ratio vs. Coal Rank.

CBM recovery at the end of the ten years, TMRB and displacement ratio without SS effect are provided at the bottom of Figure 5.20. The rise or fall in CBM recovery cannot be explained only by shrinkage effect (Figure 5.20), since there is another parameter controlling primary recovery, which is the gas relative permeability with respect to water saturation. In the ECBM recovery period, however, water saturation is nearly constant (~30%) and relative permeability effects are small.

In Figure 5.21, it is realized that as the rank of coal increases from Sb to Mvb, increase in CO_2 breakthrough time and the decrease in the amount of CO_2 stored owing to swelling declines. Decrease in CO_2 storage due to SS is a direct result of the decrease in displacement ratio. Furthermore, CO_2 breakthrough time increases owing to reduction in absolute permeability (swelling effect) during CO_2 injection.

Coal Rank	CO_2 Breakthrough	CO_2 Storage
-	Days	10^4 Ton
Sb	4535	7.49
Hvb	4992	10.8
Mvb	5173	11.2
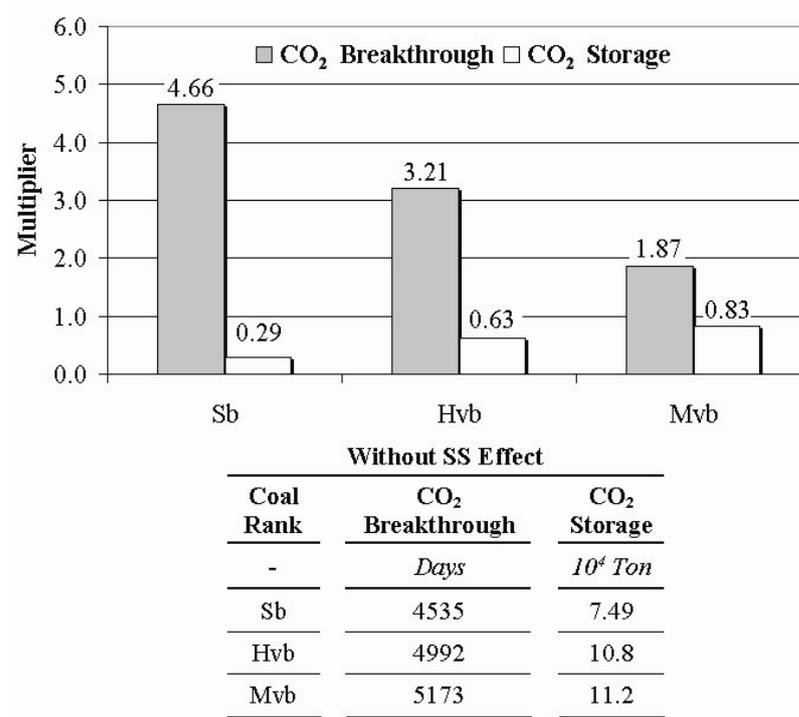
Figure 5.21 Multiplier of CO₂ Breakthrough and CO₂ Storage vs. Coal Rank.

As a result, it can be concluded that SS leads to an increase in TMRB for all ranks of coal, but there is no relationship between rank of coal and the magnitude of increase. Although SS lead to an increase in TMRB, its multiplier is not considerably high which is ranging from 1.044 to 1.088. However, change in displacement ratio, CO_2 storage and CO_2 breakthrough are highly affected by the rank of coal and their multipliers ranges from 0.17 to 4.66. It can be concluded from Figures 5.20 and 5.21 that low-rank coals are affected more than high-rank coals by SS. The reason is that decrease in displacement ratio, increase in breakthrough time and decrease in CO_2 storage owing to SS are the highest for low-rank coals.
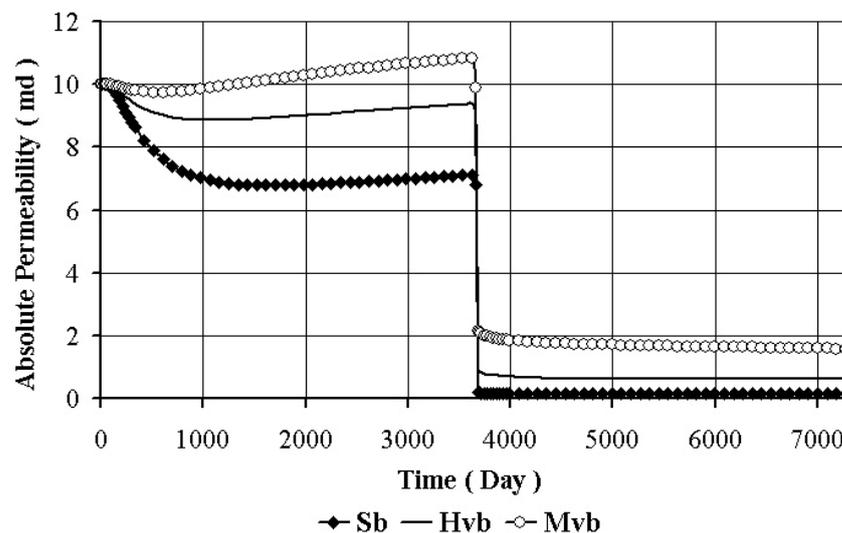
Figure 5.22 Absolute Permeability of Different Coal Ranks at the Injection Well Block vs. Time.

The conclusion above can also be verified by the absolute permeability calculated at the injection well block (Figure 5.22). At the beginning, absolute permeability decreases due to increase in effective stress across cleat surfaces with water and CH_4 production. After a while, shrinkage due to desorption of CH_4 from coal matrix becomes more dominant and an increasing trend in absolute permeability is observed. First ten-year period is obviously different for each ranks of coal according

to their properties. After 10 years, CO_2 is injected and the decrease in the absolute permeabilities due to swelling is clearly seen in this figure. As the rank of coal decreases, cleat permeability after CO_2 injection gets smaller.
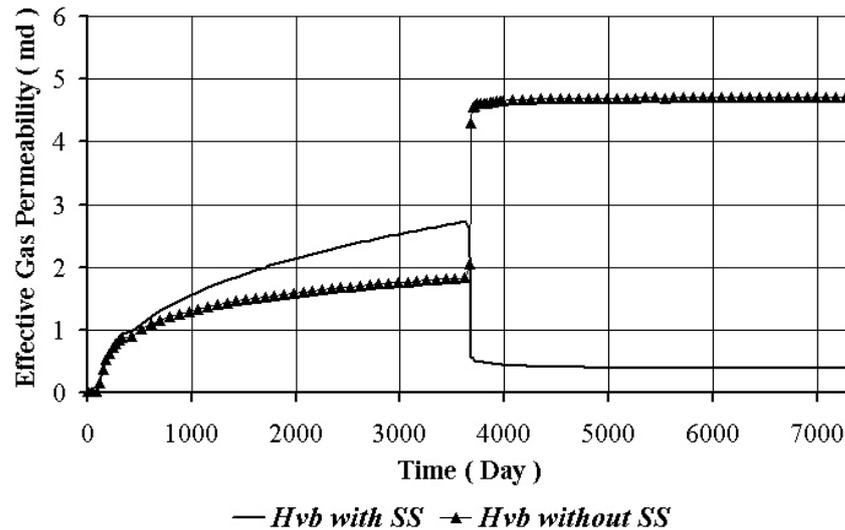
Figure 5.23 Effective Gas Permeability of Hvb Coal Rank at the Injection Well Block with and without SS vs. Time.

One should also consider the relative permeability curves for reservoir management purposes, since effective permeabilities are considerably smaller than absolute ones. In Figure 5.23, as an example for high-volatile bituminous case, effective gas permeability at the injection well block vs. time plot is shown for twenty-year period, which includes ten-years CBM recovery and succeeding ten-year ECBM recovery. During CBM recovery, effective gas permeability with SS effect is higher than without SS case, since shrinkage is the dominant process in this region and it has an increasing effect on absolute permeability. In addition, the increasing trend in effective gas permeability during CBM recovery with and without SS can be explained with the increasing relative gas permeability during production of water inside cleat system. During ECBM recovery, however, effective gas permeability with SS is smaller than without SS case, as swelling is the dominant process causing a

decrease in absolute permeability. However, the relative permeability effect is small after CO_2 injection, since most of the water is produced during CBM recovery.

5.2.2 Case #2 (Coal Reservoir Types)
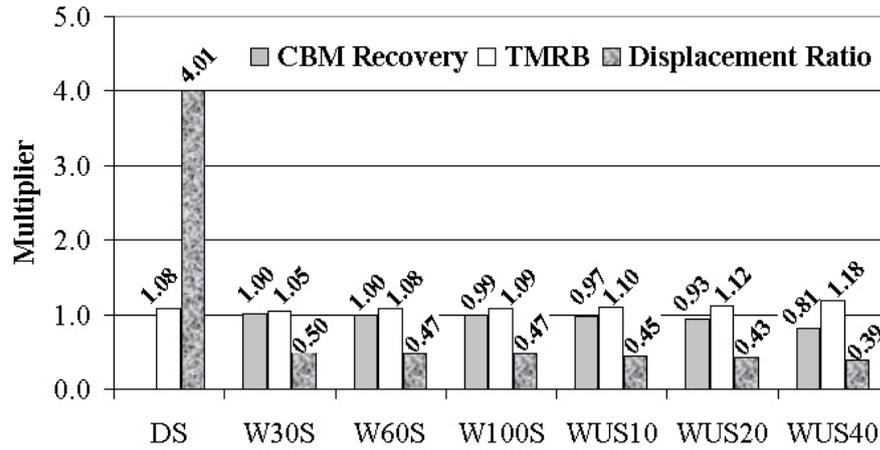
Without SS Effect

Reservoir Types	CBM Recovery	TMRB	Displacement Ratio
-	%	%	%
DS	0.00	92.0	2.97
W30S	72.8	94.2	7.51
W60S	67.1	91.0	6.72
W100S	64.5	90.2	6.33
WUS10	59.7	88.8	6.32
WUS20	54.2	87.0	6.32
WUS40	39.9	82.1	6.49

Figure 5.24 Multiplier of CBM Recovery, TMRB and Displacement Ratio vs. Reservoir Type.

Numerical results of this case are given in Table D.9. As it is seen in Figure 5.24, shrinkage and swelling leads to an increase in TMRB for all reservoir types. Highest increase belongs to undersaturated wet coals. As the undersaturation increases,

positive change in TMRB gets bigger. It is realized that increase in the TMRB for dry coal is equal to methane-saturated wet coal with 60% initial water saturation. Moreover, shrinkage and relative permeability effect becomes more dominant as the undersaturation of coal increases according to CBM recoveries. Difference between TMRB and CBM recovery shows that swelling effect on ECBM recovery increases as the initial water saturation and undersaturation in methane increase. Besides, there is a reduction in displacement ratio due to SS effect for all cases, except methane-saturated dry coals. Multiplier of displacement ratio for dry coals is equal to 4.01. As it is identified in Figure 5.25, fall in CO_2 storage owing to swelling does not depend on reservoir type. However, rise in CO_2 breakthrough time is highest for dry coals.

Reservoir Types	CO_2 Breakthrough	CO_2 Storage
-	Days	10^5 Ton
DS	882	1.04
W30S	4992	1.11
W60S	4992	1.09
W100S	4992	1.08
WUS10	4992	1.08
WUS20	4992	1.08
WUS40	5083	1.08

Figure 5.25 Multiplier of CO_2 Breakthrough and CO_2 Storage vs. Reservoir Type.

It is concluded that dry coal reservoirs are affected more by swelling than others, since increase in CO_2 breakthrough time is biggest and displacement ratio rises by a factor of 4. But one should also consider that injection of CO_2 starts at the beginning of production and initial water saturation is close to zero for dry coals. It seems that methane-saturated wet coals are more suitable for eliminating the negative effects of CO_2 injection.

5.2.3 Case #3 (Molar Composition of Injected Fluid)

Molar Composition of Injected Fluid	CBM Recovery	TMRB	Displacement Ratio
-	%	%	%
25 % CO_2 - 75 % N_2	64.5	99.5	1.91
50 % CO_2 - 50 % N_2	64.5	97.8	3.19
75 % CO_2 - 25 % N_2	64.5	94.8	4.53
100 % CO_2	64.5	90.2	6.33
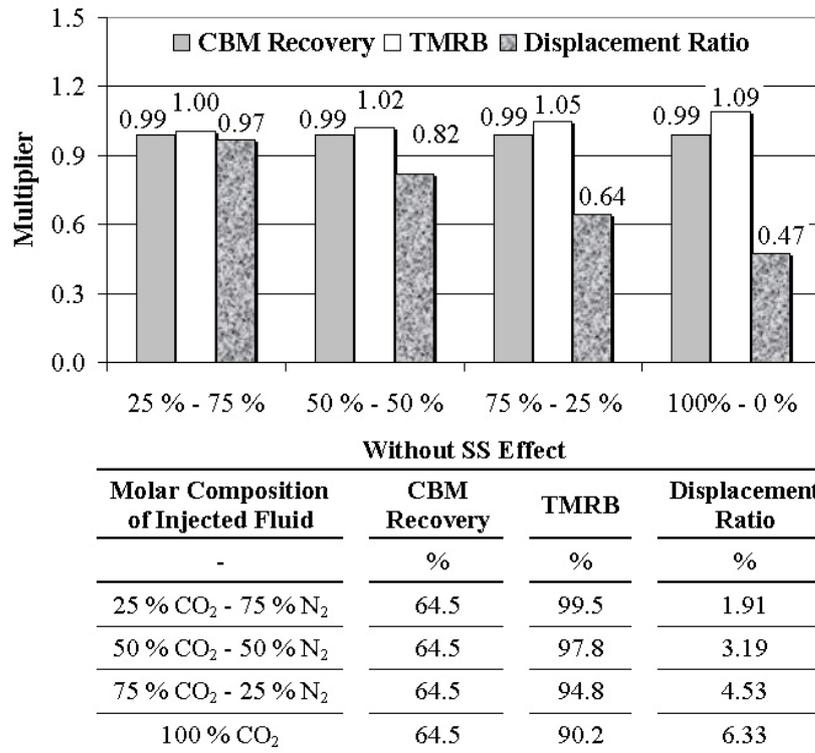
Figure 5.26 Multiplier of CBM Recovery, TMRB and Displacement Ratio vs. Molar Composition of Injected (CO_2/N_2) Gas Mixture.

Numerical results of this case are given in Table D.10. In Figure 5.26, multiplier of TMRB, CBM recovery and displacement ratio owing to SS effect are plotted with

respect to different molar compositions of injected fluid. As the molar percentage of CO_2 in the CO_2/N_2 mixture rises, increase in TMRB also goes up and the difference between TMRB and CBM recovery shows that swelling effect on ECBM recovery increases. Moreover, decrease in displacement ratio ascends, as the molar percentage of CO_2 increases. Decreases in CBM recoveries due to shrinkage and relative permeability effect are the same for all cases, since coal rank and reservoir type are identical. In Figure 5.27 positive change in CO_2 breakthrough time and negative change in CO_2 storage due to swelling get bigger as molar percentage of CO_2 in the mixture increases.
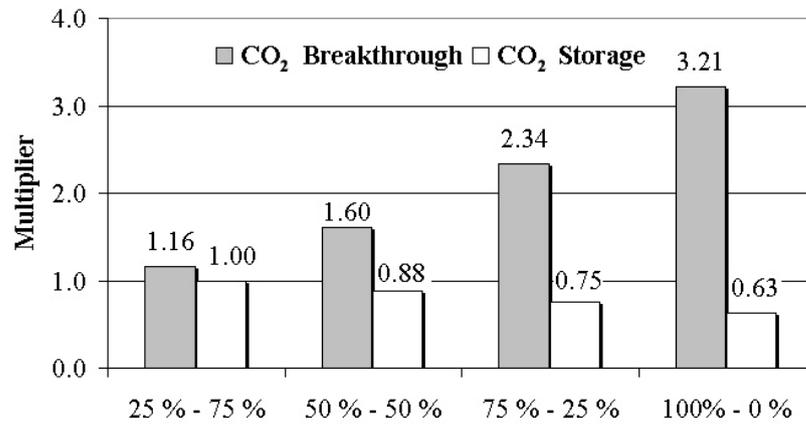
Without SS Effect

Molar Composition of Injected Fluid	CO_2 Breakthrough	CO_2 Storage
-	*Days*	*Ton*
25 % CO_2 - 75 % N_2	7549	44556
50 % CO_2 - 50 % N_2	6361	70889
75 % CO_2 - 25 % N_2	5538	91452
100 % CO_2	4992	108387

Figure 5.27 Multiplier of CO_2 Breakthrough and CO_2 Storage vs. Molar Composition of (CO_2/N_2) Gas Mixture.

Thus, it can be concluded that swelling effect may be reduced by mixing CO_2 with N_2, which is a stripping gas whose adsorption onto coal surface is smaller than CH_4 and CO_2. In order to find the optimum molar composition of the mixture, one should consider increase in CO_2 breakthrough time and decrease in displacement ratio due to SS. Both of them affect the project life and economics.

In Figure 5.28, SS effect on the absolute permeability at the injection well block for two different molar compositions of injected fluids, which are (50% CO_2 - 50% N_2) and (100% CO_2), are plotted. It is clear that as the molar percentage of CO_2 decreases in the mixture, the decrease in absolute permeability due to swelling lessen. Therefore, injection of CO_2 with N_2 may eliminate the reduction in well injectivity.
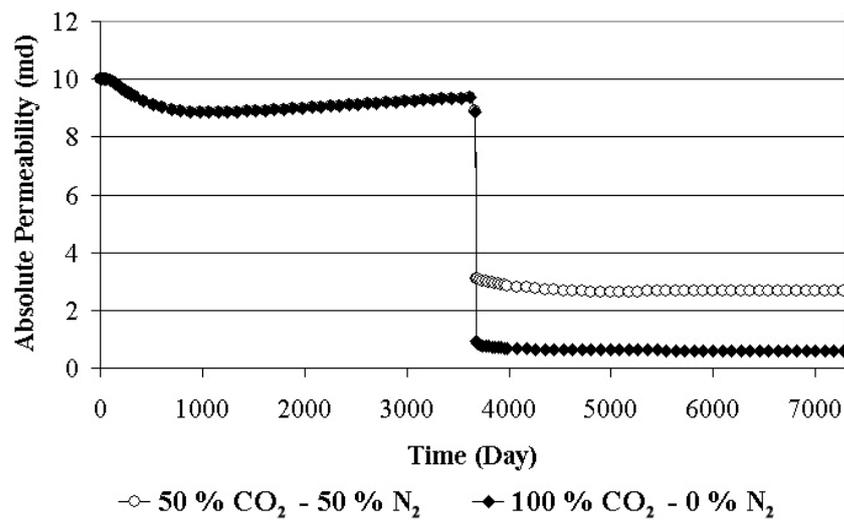
Figure 5.28 Absolute Permeability at the Injection Well Block with Different Molar Compositions of (CO_2/N_2) Gas Mixture vs. Time.

5.2.4 Case #4 (Sensitivity of Model to Infinite Pressure and Infinite Strain)

In case #4, importance of infinite pressure and infinite strain in the extended Palmer and Mansoori (1998) permeability model were investigated by using their high,

medium and low values gathered from literature (Tables 4.9 in Chapter 4). These three cases were also compared to the case without SS effect. As it is seen in Figure 5.29, during CBM recovery (first ten-year) all cases are nearly identical, which means that shrinkage and relative permeability effect do not depend on infinite pressure. Beginning from CO_2 injection it is realized that swelling effect increases as the infinite pressure gets smaller. Without SS effect, CO_2 breakthrough occurs earlier and TMRB is smaller than others.
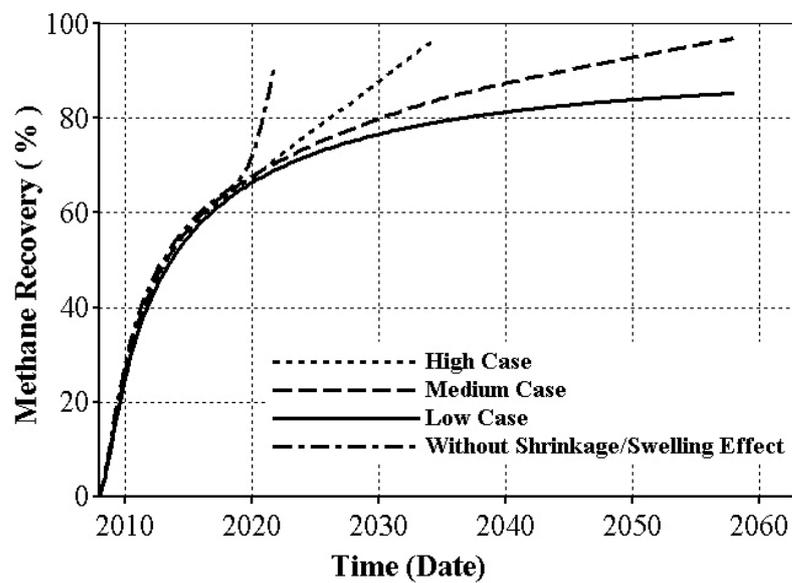
Figure 5.29 Methane Recoveries with Different Infinite Pressures vs. Time.

In Figure 5.30, high case for infinite strain provides the highest recovery at a selected date in CBM recovery period. During ECBM recovery, high case is affected more than other cases by swelling. It has the longest CO_2 breakthrough time and highest TMRB. As a result, both infinite pressure and strain has important effect on swelling, and ECBM recovery. While infinite strain has some effect on CBM recovery, infinite pressure has no effect.
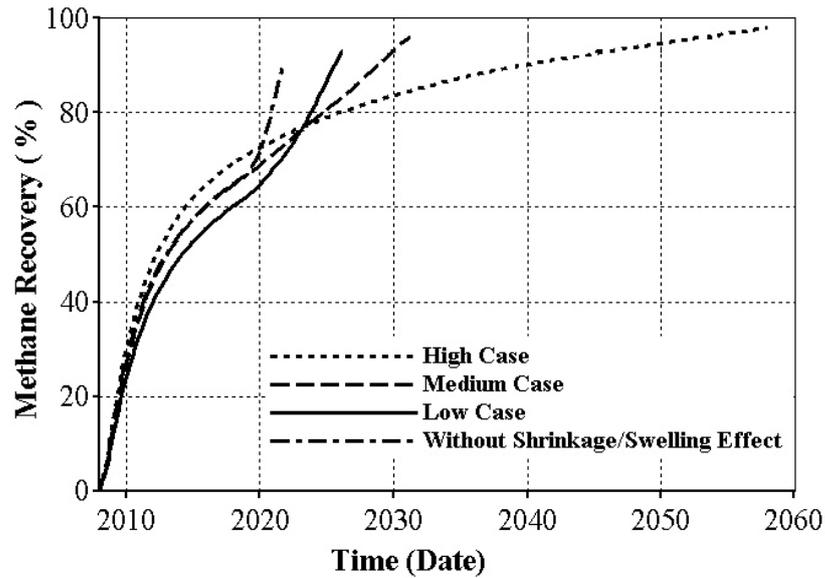
Figure 5.30 Methane Recoveries with Different Infinite Strains vs. Time.

5.2.5 Case #5 (Sensitivity of Model to Poisson's Ratio and Elastic Modulus)

In case #5, high, medium and low values of Poisson's ratio and elastic modulus were used to understand sensitivity of each parameter on TMRB vs. time. These cases were compared to the case without SS effect. Fracture compressibility is a function of both Poisson's ratio and elastic modulus according to extended P&M (1998) model. Therefore, for each case, cleat compressibilities were calculated and entered as input to simulator. Elastic modulus, Poisson's ratio and their associated cleat compressibilities are provided in Table 4.10 of Chapter 4.

In Figure 5.31, as the Poisson's ratio increases, cleat compressibility decreases and therefore swelling effects are reduced. High case for Poisson's ratio is close to the case without SS effect. Moreover, it is realized that Poisson's ratio has no effect on CBM recovery. In Figure 5.32, as the elastic modulus increases, cleat compressibility decreases. This leads to reduction in SS effects. High case for elastic modulus is closer to the case without SS effect than others. Between high and medium cases, methane recovery curve do not vary very much. However, between medium and low

cases, there is a difference. It can be concluded from sensitivity analysis that elastic modulus is the most important parameter affecting both CBM and ECBM recovery.
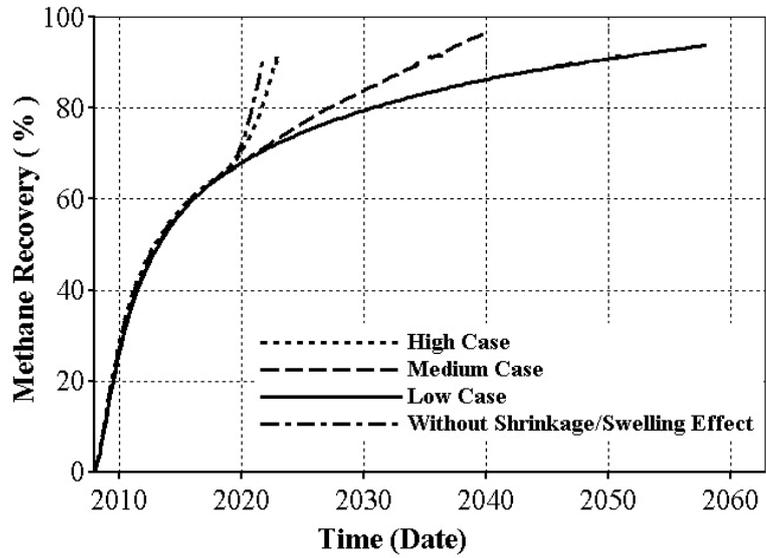
Figure 5.31 Methane Recoveries with Different Poisson's Ratios vs. Time.
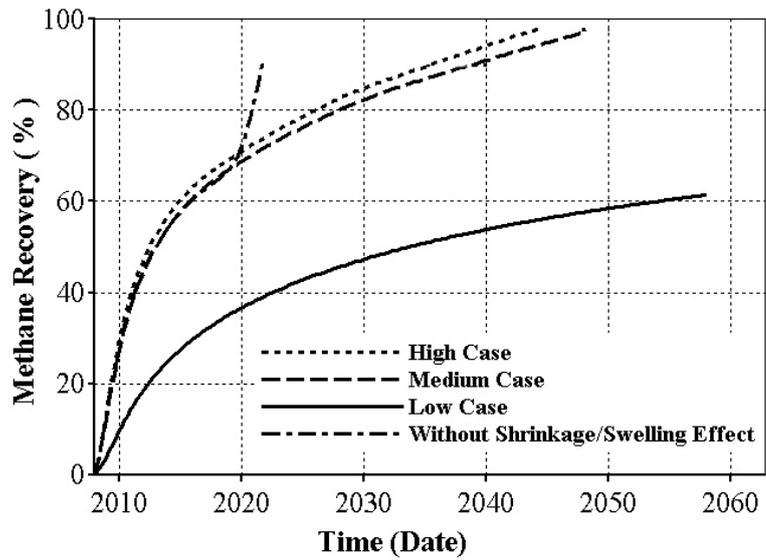
Figure 5.32 Methane Recoveries with Different Elastic Modulus vs. Time

98

CHAPTER 6

CONCLUSIONS

In this study, it was shown that it is possible to construct a rank-dependent coal property database which is used as an input file for enhanced coalbed methane recovery simulations. With this data set, various simulation cases investigating the effects of coal properties, operational parameters, shrinkage and swelling on total methane recovery at CO_2 breakthrough, displacement ratio, CO_2 breakthrough time and CO_2 storage were run and some major conclusions were drawn as:

Coal Properties and Operational Parameters:

- Medium volatile bituminous coals are more suitable for ECBM recovery than lower rank coals because of its shortest CO_2 breakthrough time, highest CO_2 storage capacity and biggest difference between total methane recovery at CO_2 breakthrough and primary coalbed methane recovery (TMRB – CBM). Moreover, its initial amount of CH_4 in place is bigger than low-rank coals.

- Production of CH_4 with primary recovery technique from lower rank coals enables to recover over 80% of the initial CH_4 in place in the first ten-year. Therefore, this makes the application of ECBM recovery unfavorable for lower rank coals.

- Dry coal reservoirs are more suitable for ECBM recovery with lowest displacement ratio (amount of CO_2 injected per CH_4 produced), shortest CO_2 breakthrough time and biggest recovery difference. Another advantage is that no water presents in the cleats. But its low CH_4 content should also be taken into account before making decision.

- Inverted 5-spot pattern has good drainage and CO_2 storage capabilities. It causes short CO_2 breakthrough time with high TMRB up to 98%.

- 100 acre drainage area seems to be better choice for ECBM recovery than others, since its displacement ratio is as low as larger drainage areas and CO_2 breakthrough occurs early enough with 98% total methane recovery. However, further economical analysis is also needed before selecting the optimized one.

- For the range of cleat permeability studied, between 10 and 25 md is the best for ECBM recovery, because displacement ratio is low, CO_2 breakthrough is short, while recovery difference is high.

- Molar composition of injected fluid has an important role on CO_2 breakthrough, displacement ratio and difference between TMRB and CBM recovery at breakthrough. Without any economical analysis, CO_2/N_2 molar composition between (50/50) % and (75/25) % is a better choice, since CO_2 storage is as high as (100/0) % case, CO_2 breakthrough time is as short as (25/75) % and displacement ratio is smaller than (100/0) % case.

- In general, horizontal wells for ECBM recovery are better than vertical wells. Determination of the butt and face cleat direction is also very important before drilling horizontal wells. This directly affects the success of operation. Moreover, distance between horizontal production and injection wells should be optimized to obtain improved results.

Shrinkage and Swelling Effect:

- Shrinkage and swelling effects lead to an increase in total methane recovery at CO_2 breakthrough for all ranks of coal, but there is no relationship between rank of coal and the magnitude of increase. However, change in displacement ratio, CO_2 storage and CO_2 breakthrough are highly affected by the rank of coal.

- Increase in ECBM recovery due to swelling increases as the rank of coal decreases. However, the decrease or increase in CBM recovery cannot be explained solely by shrinkage effect, since there is another parameter controlling recovery, which is relative gas permeability with respect to water saturation. In the ECBM period, however, water saturation is nearly constant and relative permeability effects are small. Therefore, swelling effect can clearly be understood.

- Decrease in displacement ratio owing to swelling gets smaller as the rank of coal increases.

- As the rank of coal from sub bituminous, high volatile bituminous to medium volatile bituminous increases, increase in CO_2 breakthrough time and the decrease in the amount of CO_2 stored due to swelling declines.

- Low-rank coals are affected more negatively than high-ranks by shrinkage and swelling. Earlier breakthrough of CO_2 for high-rank coals than low-rank coals can be explained with this conclusion. Lower swelling effect leads to higher absolute cleat permeability.

- Shrinkage and swelling leads to an increase in total methane recovery at CO_2 breakthrough for all reservoir types. Highest increase belongs to undersaturated wet coals.

- Methane-saturated dry coal reservoirs are more affected by swelling than others. But one should also consider that injection of CO_2 starts at the beginning and initial water saturation is close to zero for dry coals.

- Shrinkage and relative permeability effect becomes more dominant as the undersaturation of coal increases according to CBM recoveries. Swelling effect on ECBM recovery increases as the initial water saturation and undersaturation in methane increase.

- As the molar percentage of CO_2 in the CO_2/N_2 mixture rises, swelling effect on ECBM recovery increases. Swelling effect may be reduced by mixing CO_2 with N_2. In order to find the optimum molar composition of the mixture, one should consider increase in CO_2 breakthrough time and decrease in displacement ratio due to shrinkage and swelling. Both effect the project life and economics.

- Both infinite pressure and strain has important effect on swelling, and therefore ECBM recovery. While infinite strain has some effect on CBM recovery, infinite pressure has no effect on it. Elastic modulus is the most important parameter in the extended Palmer and Mansoori permeability model controlling shrinkage and swelling.

CHAPTER 7

RECOMMENDATIONS

In this study, a new approach was developed by constructing a simulation input database with rank-dependent coal properties published in the literature. The effects of variable coal properties on the total methane recovery at CO_2 breakthrough, displacement ratio, CO_2 breakthrough time and CO_2 storage were investigated with various ECBM recovery simulation scenarios which were run with a compositional reservoir simulator of CMG (Computer Modeling Group) /GEM module. However, further simulation studies are needed to observe effects of the other simulation alternatives on aforementioned parameters. The recommendations for future works are as follows.

- The wells are not defined as stimulated in this study. It is known that hydraulic fracturing has an important impact on the primary recovery of methane. A simulation study can be done with different hydraulic fracturing scenarios so that its effects on enhanced coalbed methane recovery and CO_2 sequestration can be observed.

- In this study, different vertical well-patterns were studied. In addition to this, different horizontal well patterns can also be studied.

- New simulation cases can be defined for different dip angles of coal seams and net coal thicknesses. Furthermore, applicability of multi-seam completions for enhanced coalbed methane recovery can be examined.

- Although most of the parameters affecting ECBM recovery have been studied throughout this study, economical analysis part is missing. By making an economical sensitivity analysis for each simulation case, results will be more meaningful both technically and financially.

- Enhanced coalbed methane recovery simulation study done by Sinayuc (2007), which was applied to Amasra coal field in Zonguldak, Turkey can be optimized with the light of the information obtained from this study.

REFERENCES

Ammosov, I.I., Eremin, I.V., (1963) Fracturing in Coal, Translated Version from Russian, *U.S. Department of Commerce*, Washington D.C., U.S.A..

Arri, L.E., Yee, D., Morgan W.D., Jeansonne, M.W., (1992) Modeling Coalbed Methane Production with Binary Gas Sorption, SPE Paper No. 24363, *Society of Petroleum Engineers Rocky Mountain Regional Meeting*, Casper, Wyoming, 18 -21 May.

ASTM, (2005) Standard Classification of Coals by Rank, Designation No. D 388 – 05, *American Society for Testing and Materials*.

Berkowitz, N., (1979) An Introduction to Coal Technology, *Academic Press*, New York.

Busch, A., Gensterblum, Y., Krooss, M.K., Little R., (2004) Methane and Carbon Dioxide Adsorption - Diffusion Experiments on Coal: Upscaling and Modeling, *International Journal of Coal Geology*, Vol. 60, pp. 151 - 168.

Clarkson, C.R., Bustin, R.M. (1999) The Effect of Pore Structure and Gas Pressure upon the Transport Properties of Coal: a Laboratory and Modeling Study. 2. Adsorption Rate Modeling, *Fuel*, Vol. 78, pp. 1345 - 1362.

CMG, (2007) User's Guide, GEM Advanced Compositional Reservoir Simulator, *Computer Modeling Group Ltd.*, Calgary, Canada.

Cui, X., Bustin, R.M., Dipple, G., (2004) Selective Transport of CO_2, CH_4, and N_2 in Coals: Insights from Modeling of Experiment Gas Adsorption Data, *Fuel*, Vol. 83, pp. 293 - 303.

Cui, X., Bustin, R.M., Chikatamarla, L., (2007) Adsorption-Induced Coal Swelling and Stress: Implications for Methane Production and Acid Gas Sequestration into Coal Seams, *Journal of Geophysical Research*, Vol. 112, B10202.

Davis, D., Oudinot, A., Sultana, A., Reeves, S., (2004) Coal-Seq V2.2: A Screening Model for ECBM Recovery and CO_2 Sequestration in Coal; Topical Report and User's Manual, *U.S. Department of Energy and Advanced Resources International.*

Ebbing, D.D., Gammon, S.D., (1999) General Chemistry, *Houghton Mifflin Company*, 6th Edition.

EIA, International Energy Outlook 2007, *Energy Information Administration, U.S. Department of Energy* (last accessed 20 January, 2007) http://tonto.eia.doe.gov/FTPROOT/forecasting/0484(2007).pdf.

EIA, What Are Greenhouse Gases?, *Energy Information Administration*, *U.S. Department of Energy* (last accessed 15 February, 2008) http://www.eia.doe.gov/oiaf/1605/ggrpt/figure_1.html

Espie, A.A., (2005) CO_2 Capture and Storage: Contributing to Sustainable World Growth, IPTC 10936, *International Petroleum Technology Conference*, Doha, Qatar, 21 - 23 November.

Evans, I., Pomeroy, C.D., (1966) The Strength, Fracture and Workability of Coal, *Perhamon Press*, Oxford, London.

Franklin, M.O., (2004) Storage of Carbon Dioxide in Geologic Formations, SPE Paper No. 88842, *Society of Petroleum Engineers Distinguished Author Series.*

Gale, J., Freund, P., (2001) Coal-bed Methane Enhancement with CO_2 Sequestration Worldwide Potential, *Environmental Geosciences*, Vol. 8, No. 3, pp. 210 - 217.

Gamson, P.D., Beamish, B.B., Johnson, D.P., (1993) Coal Micro-Structure and Micropermeability and Their Effects on Natural Gas Recovery, *Fuel*, Vol. 72, pp. 87 - 99.

Gentzis, T., (2000) Subsurface Sequestration of Carbon Dioxide - An Overview from an Alberta (Canada) Perspective, *International Journal of Coal Geology*, Vol. 43, pp. 287 - 305.

Gentzis, T., Deisman, N., Chalaturnyk, R.J., (2007) Geomechanical Properties and Permeability of Coals from the Foothills and Mountain Regions of Western Canada, *International Journal of Coal Geology*, Vol. 69, pp. 153 - 164.

Gray, I., (1987) Reservoir Engineering in Coalseams: Part 1 - The Physical Process of Gas Storage and Movement in Coal Seams, SPE Paper No. 12514, *Society of Petroleum Engineers Reservoir Engineering*.

GRI, (1996) A Guide to Coalbed Methane Reservoir Engineering, GRI Reference No. 94/ 0397, *Gas Research Institute*, Chicago, Illinois, U.S.A..

Grimston, M.C., Karakoussis, V., Fouquet, R., (2001) The European and Global Potential of Carbon Dioxide Sequestration in Tackling Climate Change, *Climate Policy*, Vol. 1, pp. 155 - 171.

Gunter, W.D., Wong, S., Cheel, D.B., Sjostrom, G., (1998) Large CO_2 Sinks: Their Role in the Migitation of Greenhouse Gases from an International, National (Canadian) and Provincial (Alberta) Perspective, *Applied Energy*, Vol. 61, pp. 209 – 227.

Harpalani, S., Schraufnagel, R.A., (1990) Influence of Matrix Shrinkage and Compressibility on Gas Production from Coalbed Methane Reservoirs, SPE Paper No. 20729, *Society of Petroleum Engineers Annual Technical Conference and Exhibition*, New Orleans, LA., 23 – 26 September.

Harpalani, S., Chen, G., (1997) Influence of Gas Production Induced Volumetric Strain on Permeability of Coal. *Geotechnical and Geological Engineering*, Vol. 15, pp. 303 - 325.

Hoch, O., (2005) The Dry Coal Anomaly - The Horseshoe Canyon Formation of Alberta, Canada, SPE Paper No. 95872, *Society of Petroleum Engineers Annual Technical Conference and Exhibition*, Dallas, Texas, U.S.A., 9 - 12 October.

IPCC, (1997) The Regional Impacts of Climate Change: An Assessment of Vulnerability, *Intergovernmental Panel on Climate Change.*

IPCC, (2000) Emissions Scenarios, *Intergovernmental Panel on Climate Change.*

IPCC, (2001) Climate Change 2001: The Scientific Basis, Intergovernmental Panel on Climate Change, *Cambridge University Press.*

IPCC, (2005) Carbon Dioxide Capture and Storage, Intergovernmental Panel on Climate Change, *Cambridge University Press.*

Karacan, C.Ö., Okandan, E., (2000) Fracture/Cleat Analysis of Coals from Zonguldak Basin/ Northwestern Turkey Relative to the Potential of Coalbed Methane Production, *International Journal of Coal Geology*, Vol. 44, pp. 109 - 125.

Katyal, S., Valix, M., Thambimuthu, K., (2007) Study of Parameters Affecting Enhanced Coalbed Methane Recovery, *Energy Sources Part A*, Vol. 29, pp. 193 - 205.

Kheshgi, H., Cappelen, F., Lee, A., (2006) Carbon Dioxide Capture and Geological Storage: Contributing to Climate Change Solutions, SPE Paper No. 98583, *Society of Petroleum Engineers International Conference on Health, Safety and Environment in Oil and Gas Exploration and Production,* Abu Dhabi, U.A.E., 2 - 4 April.

Klara, S.M., Srivastava, R.D., Mcllvierd, H.G., (2003) Integrated Collaborative Technology Development Program for CO_2 Sequestration in Geologic Formations, United States Department of Energy R&D, *Energy Conversion and Management,* Vol. 44, pp. 2699 - 2712.

Kural, O., (1994) Coal: Resources, Properties, Utilization, Pollution, *Istanbul Technical University Press,* Turkey.

Laubach, S.E., Marrett, R.A., Olson, J.E., Scott, A.R., (1998) Characteristics and Origins of Coal Cleat: A Review, *International Journal of Coal Geology,* Vol. 35, pp. 175 - 207.

Laxminarayana, C., Crosdale, P.J., (1999) Role of Coal Type and Rank on Methane Sorption Characteristics of Bowen Basin, Australia coals, *International Journal of Coal Geology,* Vol. 40, pp. 309 - 325.

Laxminarayana, C., Cui, X., Bustin, R.M., (2004) Implications of Volumetric Swelling/Shrinkage of Coal in Sequestration of Acid Gases, Paper No. 0435, *International Coalbed Methane Symposium,* Tuscaloosa, Alabama, May.

Lucia, F.J., (1983) Petrophysical Parameters Estimated from Visual Descriptions of Carbonate Rocks: A Field Classification of Carbonate Pore Space, SPE Paper No. 10073, *Society of Petroleum Engineers Journal of Petroleum Technology.*

Maricic, N., Mohaghegh, S.D., Artun, E., (2005) A Parametric Study on the Benefits of Drilling Horizontal and Multilateral Wells in Coalbed Methane Reservoirs, SPE Paper No. 96018, *Society of Petroleum Engineers Annual Technical Conference and Exhibition,* Dallas, Texas, U.S.A., 9 - 12 October.

Mavor, M.J., Vaughn, J.E., (1998) Increasing Coal Absolute Permeability in the San Juan Basin Fruitland Formation, SPE Paper No. 39105, *Society of Petroleum Engineers Reservoir Evaluations & Engineering.*

Mavor, M.J., Russell, B., Pratt, T.J., (2003) Powder River Basin Ft. Union Coal Reservoir Properties and Production Decline Analysis, SPE Paper No. 84427, *Society of Petroleum Engineers Annual Technical Conference and Exhibition*, Denver, Colorado, U.S.A., 5 - 8 October.

Mavor, M.J., Gunter, W.D., (2004) Secondary Porosity and Permeability of Coal vs. Gas Composition and Pressure, SPE Paper No. 90255, *Society of Petroleum Engineers Annual Technical Conference and Exhibition*, Houston, Texas, U.S.A., 26 - 29 September.

Mavor, M.J., Gunter, W.D., Robinson, J.R., (2004) Alberta Multiwell Micro-pilot Testing for Coalbed Methane Properties, Enhanced Methane Recovery and CO_2 Storage Potential, SPE Paper No. 90256, *Society of Petroleum Engineers Annual Technical Conference and Exhibition*, Houston, Texas, U.S.A., 26 - 29 September.

Mazumder, S., Karnik, A., Wolf, K.H., (2006) Swelling of Coal in Response to CO_2 Sequestration for ECBM and Its Effect on Fracture Permeability, SPE Paper No. 97754, *Society of Petroleum Engineers Journal.*

Mckee, C.R., Bumb, A.C., Koenlg, R.A., (1988) Stress-Dependent Permeability and Porosity of Coal and Other Geologic Formations, SPE Paper No. 12858, *Society of Petroleum Engineers Formation Evaluation.*

Mckee, C.R., Bumb, A.C., Horner, D.M., (1990) Use of Barometric Response to Obtain In-Situ Compressibility of a Coalbed Methane Reservoir, SPE Paper No. 17725, *Society of Petroleum Engineers Formation Evaluation.*

Nelson, C.R., (2000) Effects of Geologic Variables on Cleat Porosity Trends in Coalbed Gas Reservoirs, SPE Paper No. 59787, *SPE/CERI Gas Technology Symposium*, Calgary, Canada, 3 - 5 April.

Nguyen, D.N., (2003) Carbon Dioxide Geological Sequestration: Technical and Economic Reviews, SPE Paper No. 81199, *SPE/EPA/DOE Exploration and Production Environmental Conference*, San Antonio, Texas, U.S.A., 10 – 12 March.

OGS, Project Report: Acid Gas Sorption by British Columbia Coals: Implications for Permanent Disposal of Acid Gas in Deep Coal Seams and Possible Co-Production of Methane, *Oil and Gas Commission* (last accessed 5 June, 2007) https://www.ogc.gov.bc.ca/documents/scek/Final_Reports/d-ET-Com-UBC-2000-16-Rep.pdf.

Palmer, I., Mansoori, J., (1998) How Permeability Depends on Stress and Pore Pressure in Coalbeds: A New Model, SPE Paper No. 52607, *Society of Petroleum Engineers Reservoir Evaluation and Engineering.*

Pashin, J.C., Mcintyre, M.R., (2003) Temperature - Pressure Conditions in Coalbed Methane Reservoirs of the Black Warrior Basin: Implications for Carbon Sequestration and Enhanced Coalbed Methane Recovery, *International Journal of Coal Geology*, Vol. 54, pp. 167 - 183.

Reeves, S., Gonzales, R., (2005) Measurement and Prediction of Single and Multicomponent, Methane, Carbon Dioxide, Nitrogen Isotherms for U.S. Coals, *International Coalbed Methane Symposium*, Tuscaloosa, AL., 16 – 20 May.

Robertson, E.P., Christiansen, R.L., (2005) Modeling Permeability in Coal Using Sorption-Induced Strain Data, SPE Paper No. 97068, *Society of Petroleum Engineers Annual Technical Conference and Exhibition*, Dallas, Texas, U.S.A., 9 - 12 October.

Robertson, E.P., Christiansen, R.L., (2006) A Permeability Model for Coal and Other Fractured, Sorptive-Elastic Media, SPE Paper No. 104380, *Society of Petroleum Engineers Eastern Regional Meeting,* Canton, Ohio, U.S.A., 11 – 13 October.

Rodrigues, C.F., Lemos de Sousa, M.J., (2002) The Measurement of Coal Porosity with Different Gases, *International Journal of Coal Geology*, Vol. 48, pp. 245 - 251.

Scott, A.R., (2002) Hydrogeologic Factors Affecting Gas Content Distribution in Coal Beds, *International Journal of Coal Geology*, Vol. 50, pp. 363 - 387.

Seidle, J.P., (1992) Application of Matchstick Geometry to Stress Dependent Permeability in Coals, SPE Paper No. 24361, *Society of Petroleum Engineers Rocky Mountain Regional Meeting*, Casper, Wyoming, 18 - 21 May.

Seidle, J.P., Huitt, L.G., (1995) Experimental Measurement of Coal Matrix Shrinkage due to Gas Desorption and Implications for Cleat Permeability Increases, SPE Paper No. 30010, *International Meeting of Petroleum Engineering*, Beijing, China, 14 - 17 November.

Seidle, J.P., O'connor, L.S., (2007) The Impact of Undersaturation on Coal Gas Economics, SPE Paper No. 107731, *Society of Petroleum Engineers Rocky Mountain Oil and Gas Technology Symposium*, Denver, Colorado, U.S.A., 16 - 19 April.

Sengul, M., (2006) CO_2 Sequestration - A Safe Transition Technology, SPE Paper No. 98617, *Society of Petroleum Engineers International Conference on Health, Safety and Environment in Oil and Gas Exploration and Production*, Abu Dhabi, U.A.E., 2 - 4 April.

Shi, J.Q., Durucan, S., Syahrial, E., (2004) Reservoir Depletion Induced Changes in Coal Bed Permeability and Implications for Enhanced CBM Recovery Using CO_2 Injection, *Geologica Belgica*, Vol. 7, No. 3 - 4, pp. 123 - 127.

Shi, J.Q., Durucan, S., (2005) A Model for Changes in Coalbed Permeability during Primary and Enhanced Coalbed Methane Recovery, SPE Paper No. 87230, *Society of Petroleum Engineers Reservoir Evaluation & Engineering.*

Sinayuc, C., (2007) Modeling of Enhanced Coalbed Methane Recovery from Amasra Coalbed in Zonguldak Coal Basin, Ph.D. Thesis, Middle East Technical University.

Sinha, R.P., (2000) Energy and Environment: The Dilemma of Global Warming, SPE Paper No. 61269, *Society of Petroleum Engineers International Conference on Health, Safety and Environment in Oil and Gas Exploration and Production*, Stavanger, Norway, 26 - 27 June.

Smith, D.H., Sams, W.N., Bromhal, G., Jikich, S., Ertekin, T., (2003) Simulating Carbon Dioxide Sequestration/ECBM Production in Coal Seams: Effects of Permeability Anisotropies and Other Coal Properties, SPE Paper No. 84423, *Society of Petroleum Engineers Annual Technical Conference and Exhibition*, Denver, Colorado, U.S.A., 5 - 8 October.

Solano-Acosta, W., Mastalerz, M., Schimmelmann, A., (2007) Cleats and Their Relation to Geologic Lineaments and Coalbed Methane Potential in Pennsylvanian Coals in Indiana, *International Journal of Coal Geology,* Vol. 72, pp. 187 - 208, November.

Stevens, S.H., Kuuskraa, V.A., Gale, J., Beecy, D., (2001) CO_2 Injection and Sequestration in Depleted Oil and Gas Fields and Deep Coal Seams: World Wide Potential and Costs, *Environmental Geosciences*, Vol. 8, No. 3, pp. 200 - 209.

Su, X., Feng, Y., Chen, J., Pan, J., (2001) The Characteristics and Origins of Cleat in Coal from Western North China, *International Journal of Coal Geology*, Vol. 47, pp. 51 - 62.

Vaziri, H.H., Wang, X., Palmer, I.D., (1997) Back Analysis of Coalbed Strength Properties from Field Measurements of Wellbore Cavitation and Methane Production, *International Journal of Rock Mechanics and Mining Sciences*, Vol. 34, No. 6, pp. 963 - 978.

White, C.M., Smith, D.H., Jones, K.L., Goodman, A.L., Jikich, S.A., LaCount, R.B., DuBose, S.B., Ozdemir, E., Morsi, B.I., Schroeder, K.T., (2005) Sequestration of Carbon Dioxide in Coal with Enhanced Coalbed Methane Recovery - A Review, *Energy&Fuels*, Vol. 19, No. 3.

Williamson, I.A, (1967) Coal Mining Geology, *Oxford University Press*, London.

Wong, S., Law, D., Deng, X., (2007) Enhanced Coalbed Methane and CO_2 Storage in Anthracitic Coals, Micro-pilot Test at South Qinshui, Shanxi, China., *International Journal of Greenhouse Gas Control*, Vol. 1, pp. 215 - 222.

WCI, What is Coal?, *World Coal Institute* (last accessed 10 January, 2007) http://www.worldcoal.org/assets_cm/files/PDF/whatiscoal.pdf.

APPENDIX A

RAW INPUT DATA OF COAL PROPERTIES

Table A.1 Vitrinite Reflectance vs. Cleat Frequency Data Set (Su et al., 2001)

Vitrinite Reflectance	Cleat Frequency	Cleat Spacing
%	numbers/5cm	cm
0.5	10	0.50
0.8	25	0.20
0.97	26	0.19
1.08	35	0.14
1.16	49	0.10
1.32	51	0.10
1.89	33	0.15
3.51	20	0.25
4.22	12	0.42
5.5	4	1.25

Table A.2 Elastic Modulus and Poisson's Ratio Data Set.

Cr [1]	Elastic Modulus	Poisson's ratio	References
-	10^5 psi	-	
Sb[2]	4.69	-	
Sb	5.88	-	
Sb	3.9	-	(Evans and Pomeroy, 1966)
Sb	4.55	-	
Sb	3.78	-	
Sb	4.93	0.35	(Berkowitz, 1979)
Hvb[3]	5.21	0.21	(Mavor and Vaughn, 1998)
Mvb[4]	6.41	0.27	(Vaziri et al., 1997)
Mvb	6.00	0.32	
Mvb	4.62	0.34	
Mvb	4.56	0.35	
Mvb	6.6	0.35	(Gentzis et al., 2007)
Mvb	6.53	0.36	
Mvb	7.35	0.33	
Mvb	5.94	0.34	

[1] Coal Rank, [2] Sub-bituminous, [3] High-volatile Bituminous, [4] Medium-volatile Bituminous

Table A.3 Descriptive Statistics of Elastic Modulus.

	Mean	Standard Deviation	Sample Variance
	10^5 psi	-	-
Mvb	6.00	0.97	0.94
Hvb	5.21	-	-
Sb	4.62	0.76	0.58

Table A.4 Descriptive Statistics of Poisson's Ratio.

Mean	Standard Deviation	Sample Variance
0.3425	0.06566	0.00431

Table A.5 Matrix and Fracture Compressibilities Data Set.

Matrix Compressibility	Fracture Compressibility	References
(10^{-6}) 1/psi	(10^{-4}) 1/psi	
-	18.7	(Mckee et al.,1988)
-	13.4	
-	7.76	
6.20	0.45	(Harpalani and Schraufnagel, 1990)
-	9.60	(Shi and Durucan, 2005)
-	6.30	
7.00	-	(Mckee et al., 1990)
1.43	-	(Berkowitz, 1979)
1.21	-	
1.43	-	
1.35	-	
1.27	-	

Table A.6 Descriptive Statistics of Matrix and Fracture Compressibilities.

	Mean	Standard Deviation	Sample Variance
	1/psi	-	-
Matrix	$2.84*10^{-6}$	$2.58*10^{-6}$	$6.66*10^{-12}$
Fracture	$5.78*10^{-4}$	$5.67*10^{-4}$	$3.21*10^{-7}$

Seam Name	Cr[1]	R_{or}[2]	T[3]	N_2		CH_4		CO_2		References
				ε_{inf}	P_{inf}	ε_{inf}	P_{inf}	ε_{inf}	P_{inf}	
-	-	%	°F	10^{-3}	psia	10^{-3}	psia	10^{-3}	psia	
Anderson	Sb	0.24	80	3.05	1120	9.31	886	35.27	555	(Robertson and Christiansen, 2005)
Gilson	Hvb	0.53	80	1.96	1120	7.65	886	15.59	555	
Upper Medicine Mannville	Hvb	0.51	117	7.74	750	13	600	15.93	550	(Mavor and Gunter, 2004)
Valencia Canyon Fruitland	Mvb	1.33	100	-	-	10.1	705	23.40	386	(Mavor and Vaughn, 1998)
San Juan	Mvb	1.33	130	-	-	11.6	-	18.20	-	(Shi et al., 2004)
Warndt Luisal	Hvb	0.71	113	-	-	-	-	16.00	-	(Mazumder et al., 2006)
WolfMountain	Hvb	0.62	77	4.20	1308	8.70	168	67.40	1166	
Quinsam	Hvb	0.62	77	2.10	1491	7.40	436	59.00	696	(Cui et al., 2007)
Illinois	Hvb	0.5	77	0.90	993	6.40	470	42.70	825	
Ardley	Sb	0.46	77	1.20	2636	3.5	247	48.50	1527	

[1] Coal Rank, [2] Vitrinite Reflectance, [3] Temperature
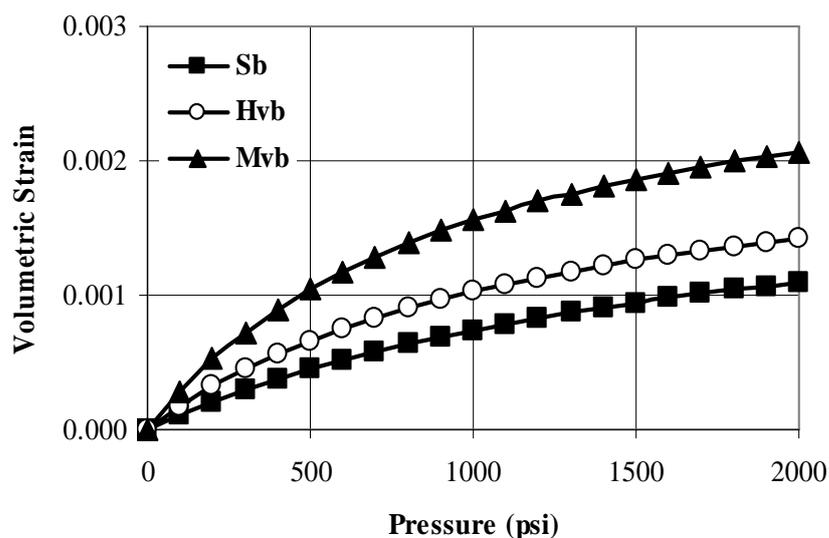
Figure A.1 Volumetric Strain vs. Pressure of N_2 with respect to Rank of Coal.
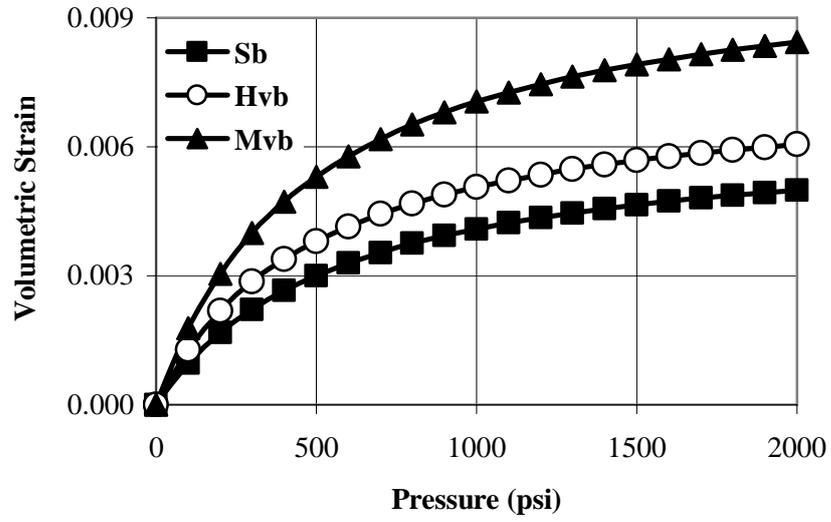
Figure A.2 Volumetric Strain vs. Pressure of CH_4 with respect to Rank of Coal.
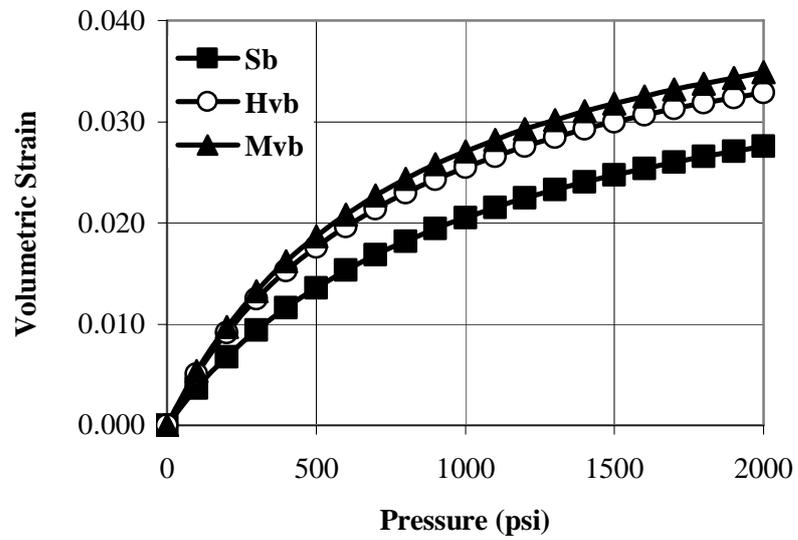
Figure A.3 Volumetric Strain vs. Pressure of CO_2 with respect to Rank of Coal.

Table A.8 Langmuir Volume and Pressure Data Set (1).

#	Basin	Seam Name	Dp [1]	R$_{or}$ [2]	Cr [3]	References
			ft	%	-	
1	Powder River	Big George	1225	0.36	Sb	(Reeves and Gonzales, 2005)
2	Gulf Coast	Wilcox	4898	0.41	Sb	
3	Forest City	Mineral	780	0.54	Hvb	
4	Illinois	Herrin	604	0.59	Hvb	
5	N. Appalachian	Pittsburgh	714	0.62	Hvb	
6	Cherokee	Mineral	772	0.69	Hvb	
7	N. Appalachian	Lower Freeport	1361	0.76	Hvb	
8	Piceance	Cameo	6700	0.8	Hvb	
9	Warrior	Mary Lee	0	0.9	Hvb	
10	San Juan	Fruitland	3100	1.33	Mvb	
11	Warrior	Newcastle	1948	1.4	Mvb	
12	Powder River	Ft Union Canyon	557	0.42	Sb	(Mavor et al., 2003)
13	-	Upper Medicine River	4215	0.51	Hvb	(Mavor et al., 2004)
14	British Columbia	Wolf Mtn	-	0.62	Hvb	(OGS, 2007)
15	British Columbia	Quinsam	-	0.62	Hvb	
16	British Columbia	Telkwa	-	0.8	Hvb	
17	British Columbia	Sable River	-	0.84	Hvb	
18	British Columbia	Mist Mtn-NE	-	0.95	Hvb	
19	British Columbia	Mist Mtn-SE	-	0.88	Hvb	
20	British Columbia	Sheriff	-	1.27	Mvb	
21	British Columbia	Bennet Dam	-	1.31	Mvb	

[1] Depth, [2] Vitrinite Reflectance, [3] Coal Rank

Table A.9 Langmuir Volume and Pressure Data Set (2).

				In Situ					
	T^1	m^2	a^3	N_2		CH_4		CO_2	
				V_L	P_L	V_L	P_L	V_L	P_L
#	°F	%	%	Scf/ton	psi	Scf/ton	psi	Scf/ton	psi
1	75	23.9	2.9	59	1344	159	820	1706	1172
2	140	12.0	9.2	121	2315	299	1010	874	885
3	70	2.6	14.0	182	744	388	406	735	185
4	65	13.2	11.3	157	1125	326	458	942	303
5	64	2.3	7.7	384	2919	512	537	888	240
6	75	2.1	13.1	211	819	404	357	723	171
7	69	1.6	11.2	343	2478	477	560	783	261
8	155	1.8	4.7	384	2101	576	871	852	340
9	86	4.7	14.0	208	1023	498	845	863	292
10	130	2.2	20.0	405	1587	660	663	897	223
11	86	2.3	18.6	609	1245	855	559	1035	218
12	65	27.0	4.4	-	-	80	394	1181	791
13	117	6.7	15.6	374	3951	377	680	771	276
14	-	4.56	5.05	365	1314	488	345	981	264
15	-	6.69	9.3	227	1415	158	296	943	91
16	-	8.88	10.12	138	1173	277	600	1035	305
17	-	2.12	14.28	244	1041	400	407	817	215
18	-	2.27	8.47	424	706	374	235	900	80
19	-	2.16	8.49	320	1224	465	247	869	142
20	-	2.23	8.17	376	821	485	318	913	132
21	-	4.84	2.01	245	1111	427	421	1140	242

[1] Temperature, [2] Moisture Content, [3] Ash Content
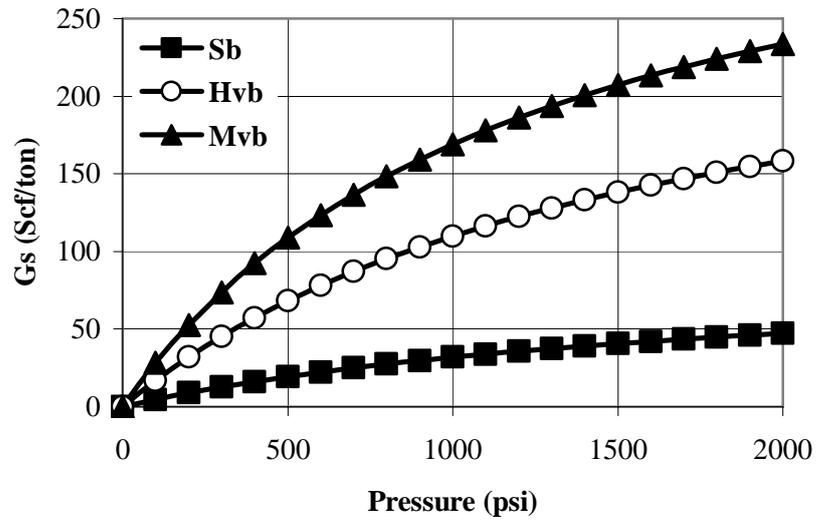
Figure A.4 N$_2$ Storage Capacity vs. Pressure with respect to Rank of Coal.
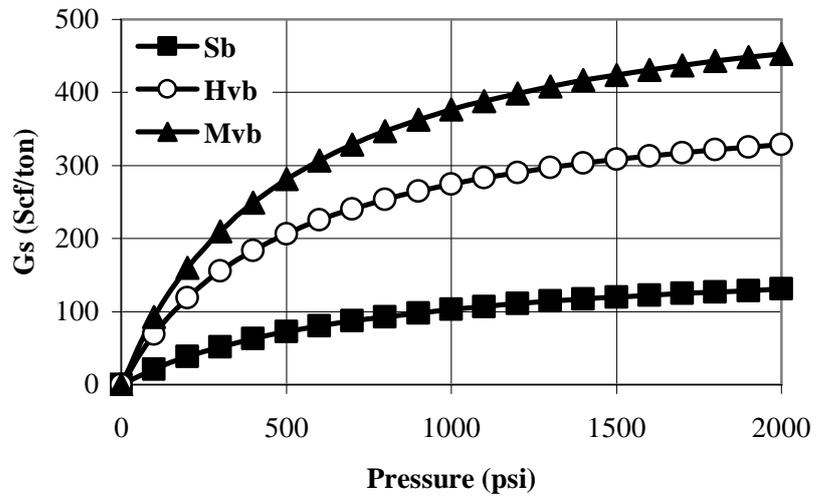
Figure A.5 CH$_4$ Storage Capacity vs. Pressure with respect to Rank of Coal.

121
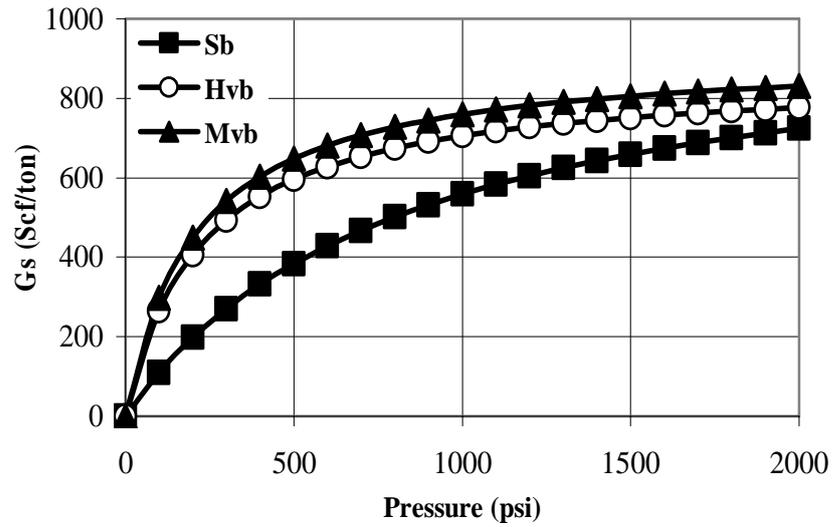
Figure A.6 CO₂ Storage Capacity vs. Pressure with respect to Rank of Coal.

Table A.10 Relative Permeability Data Set (Mavor and Vaughn, 1998).

S_w	k_{rw}	k_{rg}
fraction	-	-
1.000	1.000	0.000
0.975	0.814	0.000
0.950	0.731	0.007
0.900	0.601	0.018
0.850	0.490	0.033
0.800	0.392	0.051
0.750	0.312	0.070
0.700	0.251	0.090
0.650	0.200	0.118
0.600	0.154	0.147
0.550	0.116	0.180
0.500	0.088	0.216
0.450	0.067	0.253
0.400	0.049	0.295
0.350	0.035	0.342
0.300	0.024	0.401
0.250	0.015	0.465
0.200	0.007	0.537
0.150	0.002	0.627
0.100	0.000	0.720
0.050	0.000	0.835
0.000	0.000	1.000

APPENDIX B

SIMULATION INPUT DATA

Table B.1 Vitrinite Reflectance and Carbon Content with respect to Rank of Coal.

			Rank of Coal		
References	*Property Name*	*Units*	*Sb*	*Hvb*	*Mvb*
(GRI, 1996)	Vitrinite Reflectance	*%*	0.4 - 0.5	0.5 - 1.1	1.1 - 1.5
	Carbon Content	*%*	69 - 74	74 - 85	85 - 88

Table B.2 Simulation Inputs #1 with respect to Rank of Coal.

				Rank of Coal			k (md)	
References		*Property Name*	*Units*	*Sb*	*Hvb*	*Mvb*		
(Su et al., 2001)	CLEAT PROPERTIES	Spacing	*10^{-2} ft*	1.65	0.62	0.36	*F^1*	*Ma^2*
(Laubach et al., 1998) (Lucia, 1983) (Scott, 2002)		Aperture	*μm*	6	4	4	4	$1*10^{-3}$
				8	**6**	**5**	**10**	
				11	8	7	25	
				14	10	9	50	
				18	13	11	100	

[1] Fracture (Cleat), [2] Matrix

Table B.3 Simulation Inputs #2 with respect to Rank of Coal.

References	Property Name			Units	Sb	Hvb	Mvb
					Rank of Coal		
(Berkowitz, 1979)	PHYSICAL COAL PROPERTIES	Porosity	Total	%	**9**	**5**	**3**
-			Ma^2	%	8.66	4.32	1.99
					8.54	**4.08**	**1.63**
					8.38	3.74	1.13
					8.21	3.41	0.63
					8.00	2.99	0.00
(Robertson and Christiansen, 2006)			F^1	%	0.37	0.71	1.03
					0.50	**0.96**	**1.39**
					0.68	1.31	1.89
					0.86	1.65	2.38
					1.08	2.08	3.00
(Williamson, 1967)			Coal Density	lb/ft^3	94	92	86

[1] Fracture (Cleat), [2] Matrix

Table B.4 Simulation Inputs #3 with respect to Rank of Coal.

References	Property Name			Unit	Sb	Hvb	Mvb
					Rank of Coal		
(Berkowitz, 1979) (Harpalani and Schraufnagel, 1990) (Mckee et al., 1990)	STRENGTH PARAMETERS	Compressibility	Ma^2	10^{-6} 1/psi	2.84		
(Mavor and Gunter, 2004)			F^1	10^{-4} 1/psi	4.3	2.0	1.2
					3.2	**1.5**	**0.89**
					2.4	1.1	0.66
					1.9	0.87	0.52
					1.5	0.69	0.41
(Berkowitz, 1979) (Evans and Pomeroy, 1966) (Gentzis, 2000) (Mavor and Vaughn, 1998) (Vaziri et al., 1997)		Elastic Modulus		10^5 psi	4.62	5.21	6
		Poisson Ratio		-	0.35		

[1] Fracture (Cleat), [2] Matrix, [3] Component Name

Table B.5 Simulation Inputs #4 with respect to Rank of Coal.

References	Property Name		Unit	Sb	Hvb	Mvb	C[3]
(Cui et al., 2007) (Laxminarayana et al., 2004) (Mavor and Vaughn, 1998) (Mavor and Gunter, 2004) (Mazumder et al.,2006) (Robertson and Christiansen, 2005) (Shi et al., 2004)	SHRINKAGE & SWELLING	Strain Data	ε_{inf}	10^{-2}	0.21	0.23	0.31	N_2
			P_{inf}	psi	1878	1228	966	
			ε_{inf}	10^{-2}	0.64	0.75	1.1	CH_4
			P_{inf}	psi	566	490	490	
			ε_{inf}	10^{-2}	4.2	4.6	4.9	CO_2
			P_{inf}	psi	1041	810	810	
(Mavor et al., 2003, 2004) (OGS, 2007) (Reeves and Gonzales, 2005)	SORPTION PARAMETERS	Langmuir Parameters	P_L	psi	1830	1574	1238	N_2
			V_L	scf/ton	90	283	378	
			P_L	psi	741	489	513	CH_4
			V_L	scf/ton	179	409	570	
			P_L	psi	838	226	208	CO_2
			V_L	scf/ton	1028	865	917	
(Clarkson and Bustin, 1999) (Cui et al, 2004) (Laxminarayana and Crosdale, 1999)		Diffusion Coefficient	D	$10^{-4}\,cm^2/s$	6.6	0.66	0.15	N_2
			D_e	$10^{-4}\,1/s$	5.2	3.7	2.6	CH_4
			D	$10^{-4}\,cm^2/s$	1.3	0.13	0.03	
			D	$10^{-4}\,cm^2/s$	130	13	3.0	CO_2

[1] Fracture (Cleat), [2] Matrix, [3] Component Name

Table B.6 Initial Reservoir Pressures with respect to Coal Reservoir Types.

Initial Reservoir Pressure (psia)							
References	Reservoir Type		Dual Media	Undersaturation (%)			
	Methane Saturation	Type		0	10	20	40
(Hoch, 2005) (Pashin and Mcintyre, 2003)	Undersaturated	Wet	Fracture	1170	1170	1170	1170
			Matrix	1170	850	633	359
	Saturated	Wet	Fracture	1170			
			Matrix	1170			
	Saturated	Dry	Fracture	387			
			Matrix	387			

APPENDIX C

GEM/CMG SIMULATOR CODE

One of codes written for high-volatile bituminous coal rank case with CMG/GEM compositional simulator is provided in this section with the explanations in bold letters.

** 2007-11-16, 10:47:26, onur
RESULTS SIMULATOR GEM 2007

** Memory Dimensioning

DIM MDALP 150000
DIM MDLU 50000
INTERRUPT INTERACTIVE

**TITLE1 'Inverse 5-Spot Pattern ECBM Project'
**TITLE2 'Saturated Wet Coal, S w 100%,Hvb '
**TITLE3 '100 Acre, 10md, Isotropic'

CASEID 'CASE 3'

DIARY CHANGES
INUNIT FIELD
RANGECHECK ON

** Output Printing Frequency

WPRN WELL TIME
WPRN GRID TIME
WPRN ITER BRIEF

** Simulation Results Writing Frequency

WSRF WELL TIME
WSRF GRID TIME

** Items in the Output Print File

OUTPRN WELL BRIEF
OUTPRN GRID Y 'N2'
       Y 'CH4'
       Y 'CO2'
       PRES
       POROS
       PERM
OUTPRN RES ALL

WRST 1000

**** Items in Simulation Results File**

****

** Mole Fraction of Component in Total Well Stream

** Average Reservoir Pressure

** Gas in Place in Fracture

** Water in Place in Fracture

** Gas in Place in Matrix

** Water in Place in Matrix

** Total Gas in Place in Reservoir

** Total Water in Place in Reservoir

** Total Gas Recovery

OUTSRF WELL zWEL 'CO2' 'Producer 1'
          zWEL 'N2' 'Producer 1'
          zWEL 'CH4' 'Producer 1'
          PAVG
          FGIP
          FWIP

MGIP

MWIP

TGIP

TWIP

RECG

** Adsorbed Mass Fraction of Component X

** Global Mol Fraction of Component X

** Mol Fraction of Component X in Gas Phase

** Reservoir Pressure

** Gas and Water Relative Permeability

** Gas and Water Saturation

OUTSRF GRID ADS 'N2' ADS 'CH4' ADS 'CO2' Z 'N2' Z 'CH4' Z 'CO2' Y 'N2' Y 'CH4' Y 'CO2'

PRES KRG KRW SG SW

OUTSRF RES ALL

**Distance Units [ft]

RESULTS XOFFSET   0.0000

RESULTS YOFFSET   0.0000

RESULTS ROTATION   0.0000 **$ (DEGREES)

RESULTS AXES-DIRECTIONS 1.0 -1.0 1.0

**Definition of Fundamental Cartesian Grid

GRID VARI 29 29 1

KDIR DOWN

** Grid Dimensions [ft]

DI IVAR 29*74.5357

DJ JVAR 29*74.5357

DK ALL 841*20

** Top Grid Depth [ft]

DTOP 841*3000

** Dual Porosity

** Gilman-Kazemi Shape Factor

** Pseudo-Capillary Pressure Model with Corrections to Contact Areas

** Between Phases

DUALPOR
SHAPE GK
TRANSFER 3

** Fracture Spacing [ft]

DIFRAC CON 0.0062
DJFRAC CON 0.0062
DKFRAC CON 0.0062

** All Grids are Active

NULL MATRIX CON   1
NULL FRACTURE CON 1

** Matrix and Fracture Porosity [Fraction]

POR MATRIX CON 0.0408
POR FRACTURE CON 0.0096

** Matrix and Fracture Compressibility of Rock @ Reservoir Pressure

PRPOR MATRIX 1170
PRPOR FRACTURE 1170
CPOR MATRIX 0.00000284
CPOR FRACTURE 0.000148

** Pore Volume Modifiers

VOLMOD MATRIX ALL
 0.25 27*0.5 0.25 0.5 27*1 2*0.5 27*1 2*0.5 27*1 2*0.5 27*1 2*0.5 27*1

2*0.5 27*1 2*0.5 27*1 2*0.5 27*1 2*0.5 27*1 2*0.5 27*1 2*0.5 27*1
2*0.5 27*1 2*0.5 27*1 2*0.5 27*1 2*0.5 27*1 2*0.5 27*1 2*0.5 27*1
2*0.5 27*1 2*0.5 27*1 2*0.5 27*1 2*0.5 27*1 2*0.5 27*1 2*0.5 27*1
2*0.5 27*1 2*0.5 27*1 2*0.5 27*1 2*0.5 27*1 0.5 0.25 27*0.5 0.25

VOLMOD FRACTURE ALL
 0.25 27*0.5 0.25 0.5 27*1 2*0.5 27*1 2*0.5 27*1 2*0.5 27*1 2*0.5 27*1
2*0.5 27*1 2*0.5 27*1 2*0.5 27*1 2*0.5 27*1 2*0.5 27*1 2*0.5 27*1
2*0.5 27*1 2*0.5 27*1 2*0.5 27*1 2*0.5 27*1 2*0.5 27*1 2*0.5 27*1
2*0.5 27*1 2*0.5 27*1 2*0.5 27*1 2*0.5 27*1 2*0.5 27*1 2*0.5 27*1
2*0.5 27*1 2*0.5 27*1 2*0.5 27*1 2*0.5 27*1 0.5 0.25 27*0.5 0.25

** Matrix and Fracture Permeability

PERMI MATRIX CON 0.001
PERMI FRACTURE CON 10
PERMJ MATRIX CON 0.001
PERMJ FRACTURE CON 10
PERMK MATRIX CON 0.001
PERMK FRACTURE CON 1

** Matrix and Fracture Transmissibility Multipliers

TRANSI MATRIX ALL
 29*0.5 783*1 29*0.5

TRANSI FRACTURE ALL
 29*0.5 783*1 29*0.5

TRANSJ MATRIX ALL
 0.5 27*1 2*0.5 27*1 2*0.5 27*1 2*0.5 27*1 2*0.5 27*1 2*0.5 27*1 2*0.5
27*1 2*0.5 27*1 2*0.5 27*1 2*0.5 27*1 2*0.5 27*1 2*0.5 27*1 2*0.5
27*1 2*0.5 27*1 2*0.5 27*1 2*0.5 27*1 2*0.5 27*1 2*0.5 27*1 2*0.5
27*1 2*0.5 27*1 2*0.5 27*1 2*0.5 27*1 2*0.5 27*1 2*0.5 27*1 2*0.5
27*1 2*0.5 27*1 2*0.5 27*1 2*0.5 27*1 2*0.5 27*1 0.5

TRANSJ FRACTURE ALL

 0.5 27*1 2*0.5 27*1 2*0.5 27*1 2*0.5 27*1 2*0.5 27*1 2*0.5 27*1 2*0.5
 27*1 2*0.5 27*1 2*0.5 27*1 2*0.5 27*1 2*0.5 27*1 2*0.5 27*1 2*0.5
 27*1 2*0.5 27*1 2*0.5 27*1 2*0.5 27*1 2*0.5 27*1 2*0.5 27*1 2*0.5
 27*1 2*0.5 27*1 2*0.5 27*1 2*0.5 27*1 2*0.5 27*1 2*0.5 27*1 2*0.5
 27*1 2*0.5 27*1 2*0.5 27*1 2*0.5 27*1 2*0.5 27*1 0.5

TRANSK MATRIX ALL

 0.25 27*0.5 0.25 0.5 27*1 2*0.5 27*1 2*0.5 27*1 2*0.5 27*1 2*0.5 27*1
 2*0.5 27*1 2*0.5 27*1 2*0.5 27*1 2*0.5 27*1 2*0.5 27*1 2*0.5 27*1
 2*0.5 27*1 2*0.5 27*1 2*0.5 27*1 2*0.5 27*1 2*0.5 27*1 2*0.5 27*1
 2*0.5 27*1 2*0.5 27*1 2*0.5 27*1 2*0.5 27*1 2*0.5 27*1 2*0.5 27*1
 2*0.5 27*1 2*0.5 27*1 2*0.5 27*1 2*0.5 27*1 0.5 0.25 27*0.5 0.25

TRANSK FRACTURE ALL

 0.25 27*0.5 0.25 0.5 27*1 2*0.5 27*1 2*0.5 27*1 2*0.5 27*1 2*0.5 27*1
 2*0.5 27*1 2*0.5 27*1 2*0.5 27*1 2*0.5 27*1 2*0.5 27*1 2*0.5 27*1
 2*0.5 27*1 2*0.5 27*1 2*0.5 27*1 2*0.5 27*1 2*0.5 27*1 2*0.5 27*1
 2*0.5 27*1 2*0.5 27*1 2*0.5 27*1 2*0.5 27*1 2*0.5 27*1 2*0.5 27*1
 2*0.5 27*1 2*0.5 27*1 2*0.5 27*1 2*0.5 27*1 0.5 0.25 27*0.5 0.25

** Pinch Out Array

PINCHOUTARRAY CON   1
** Palmer Mansoori Swelling Model Parameters

CROCKTYPE 1

CPRPOR MATRIX 1170
CPRPOR FRACTURE 1170
CCPOR MATRIX 0.00000284
CCPOR FRACTURE 0.000148

** Poisson ratio
POISSR 0.3

** Young Modulus [psi]
YOUNGM 521000

** Strain @ Infinite Pressure

STRINF 0.00229 0.00754 0.0462

** Infinite Pressure [psi]

PRESLN 1228 490 810

** Exponent Relating Fracture Porosity to Permeability

EXPPM 3.0

** Fluid Model : Peng-Robinson EOS

MODEL PR

** Number of Components

NC 3 0

** Component Names

COMPNAME 'N2' 'CH4' 'CO2'

** Reservoir Temperature [F]

TRES 113

ROCKFLUID
RPT 1 DRAINAGE SCALING-NEW

**Relative permeability of oil and water

SWT

0.000000 0.000000 0.00010 0.000000
0.050000 0.000000 0.000095 0.000000
0.100000 0.000000 0.00009 0.000000
0.150000 0.002000 0.000085 0.000000
0.200000 0.007000 0.00008 0.000000
0.250000 0.015000 0.000075 0.000000
0.300000 0.024000 0.00007 0.000000
0.350000 0.035000 0.000065 0.000000

0.400000 0.049000 0.00006 0.000000

0.450000 0.067000 0.000055 0.000000

0.500000 0.088000 0.00005 0.000000

0.550000 0.116000 0.000045 0.000000

0.600000 0.154000 0.00004 0.000000

0.650000 0.200000 0.000035 0.000000

0.700000 0.251000 0.00003 0.000000

0.750000 0.312000 0.000025 0.000000

0.800000 0.392000 0.00002 0.000000

0.850000 0.490000 0.000015 0.000000

0.900000 0.601000 0.00001 0.000000

0.950000 0.731000 0.000005 0.000000

0.975000 0.814000 0.000002 0.000000

1.000000 1.000000 0.00000 0.000000

Relative permeability of oil and gas

SLT

0.000000 1.000000 0.00000 0.000000

0.050000 0.835000 0.000005 0.000000

0.100000 0.720000 0.00001 0.000000

0.150000 0.627000 0.000015 0.000000

0.200000 0.537000 0.00002 0.000000

0.250000 0.465000 0.000025 0.000000

0.300000 0.401000 0.00003 0.000000

0.350000 0.342000 0.000035 0.000000

0.400000 0.295000 0.00004 0.000000

0.450000 0.253000 0.000045 0.000000

0.500000 0.216000 0.00005 0.000000

0.550000 0.180000 0.000055 0.000000

0.600000 0.147000 0.00006 0.000000

0.650000 0.118000 0.000065 0.000000

0.700000 0.090000 0.00007 0.000000

0.750000 0.070000 0.000075 0.000000

0.800000 0.051000 0.00008 0.000000

0.850000 0.033000 0.000085 0.000000

0.900000 0.018000 0.00009 0.000000

0.950000 0.007000 0.000095 0.000000

0.975000 0.000000 0.000097 0.000000

1.000000 0.000000 0.00010 0.000000

*KROIL *STONE2 *SWSG

** Langmuir Sorption Parameters

** ADGMAXC [gmol/lbm]

** ADGCSTC [1/psi]

 ADGMAXC 'N2' MATRIX CON 0.151021
 ADGMAXC 'CH4' MATRIX CON 0.218212
 ADGMAXC 'CO2' MATRIX CON 0.461628
 ADGCSTC 'N2' MATRIX CON 0.000635411
 ADGCSTC 'CH4' MATRIX CON 0.002045572
 ADGCSTC 'CO2' MATRIX CON 0.004424499

 ADGMAXC 'N2' FRACTURE CON 0
 ADGMAXC 'CH4' FRACTURE CON 0
 ADGMAXC 'CO2' FRACTURE CON 0
 ADGCSTC 'N2' FRACTURE CON 0
 ADGCSTC 'CH4' FRACTURE CON 0
 ADGCSTC 'CO2' FRACTURE CON 0

** Rock Density [lb/ft3]
 ROCKDEN CON 92

** Multicomponent Diffusion [cm2/sec]
 COAL-DIF-COMP 'N2' MATRIX CON 0.0103541
 COAL-DIF-COMP 'CH4' MATRIX CON 0.0103541
 COAL-DIF-COMP 'CO2' MATRIX CON 0.000103541

** Initialization of Simulation Parameters
INITIAL

USER_INPUT

** Initial Reservoir Pressure
 PRES FRACTURE KVAR 1*1170
 PRES MATRIX KVAR 1*1170

** Initial Water Saturation
 SW MATRIX CON 0.001
 SW FRACTURE CON 0.99

** Initial Composition in the Reservoir
 ZGLOBALC 'N2' MATRIX CON 0.0
 ZGLOBALC 'N2' FRACTURE CON 0.0

 ZGLOBALC 'CH4' MATRIX CON 1.0
 ZGLOBALC 'CH4' FRACTURE CON 1.0

 ZGLOBALC 'CO2' MATRIX CON 0.0
 ZGLOBALC 'CO2' FRACTURE CON 0.0

** Numerical Controls

NUMERICAL
DTMAX 0.5
DTMIN 0.01
MAXCHANGE GMOLAR 1

** Numerical Dispersion Control
TWOPTFLUX

** Well and Recurrent Data

RUN
DATE 2008 1 1
 DTWELL 1.E-06
 AIMSET MATRIX CON 3
 AIMSET FRACTURE CON 3
**$
WELL 'Producer 1'

PRODUCER 'Producer 1'

OPERATE MIN BHP 50. CONT

\$ rad geofac wfrac skin

GEOMETRY K 0.25 0.37 1. 0.

PERF GEO 'Producer 1'

\$ UBA   ff Status Connection

　1 1 1 1. OPEN   FLOW-TO 'SURFACE'

OPEN 'Producer 1'

\$

WELL 'Producer 2'

PRODUCER 'Producer 2'

OPERATE MIN BHP 50. CONT

\$ rad geofac wfrac skin

GEOMETRY K 0.25 0.37 1. 0.

PERF GEO 'Producer 2'

\$ UBA   ff Status Connection

　29 29 1 1. OPEN   FLOW-TO 'SURFACE'

OPEN 'Producer 2'

\$

WELL 'Producer 3'

PRODUCER 'Producer 3'

OPERATE MIN BHP 50. CONT

\$ rad geofac wfrac skin

GEOMETRY K 0.25 0.37 1. 0.

PERF GEO 'Producer 3'

\$ UBA   ff Status Connection

　1 29 1 1. OPEN   FLOW-TO 'SURFACE'

OPEN 'Producer 3'

\$

WELL 'Producer 4'

PRODUCER 'Producer 4'

OPERATE MIN BHP 50. CONT

\$ rad geofac wfrac skin

GEOMETRY K 0.25 0.37 1. 0.

PERF GEO 'Producer 4'

**$ UBA   ff Status Connection

   29 1 1 1. OPEN   FLOW-TO 'SURFACE'

OPEN 'Producer 4'

**$

WELL 'Injector 1'

INJECTOR 'Injector 1'

INCOMP SOLVENT 0. 0. 1.0

OPERATE MAX BHP 1170 CONT

**$ rad geofac wfrac skin

GEOMETRY K 0.25 0.37 1. 0.

PERF GEO 'Injector 1'

**$ UBA   ff Status Connection

   15 15 1 1. OPEN   FLOW-FROM 'SURFACE'

SHUTIN 'Injector 1'

DATE 2008 01 02

DATE 2008 01 15

DATE 2008 02 01

DATE 2008 02 15

DATE 2008 03 01

DATE 2008 04 01

DATE 2008 05 01

DATE 2008 06 01

DATE 2008 07 01

DATE 2008 08 01

DATE 2008 09 01

DATE 2008 10 01

DATE 2008 11 01

DATE 2008 12 01

DATE 2009 03 01

DATE 2009 06 01

DATE 2009 09 01

DATE 2009 12 01

……

DATE 2017 03 01

DATE 2017 06 01

DATE 2017 09 01

DATE 2017 12 01

OPEN 'Injector 1'

** CO$_2$ Breakthrough Condition

TRIGGER 'trig1' ON_WELL 'Producer 1' 'Producer 2' 'Producer 3' 'Producer 4' MPVS M2 < 90

SHUTIN 'Producer 1' 'Producer 2' 'Producer 3' 'Producer 4' 'Injector 1'

END_TRIGGER

DATE 2018 01 15

DATE 2018 02 01

DATE 2018 02 15

DATE 2018 03 01

DATE 2018 04 01

DATE 2018 05 01

DATE 2018 06 01

DATE 2018 07 01

DATE 2018 08 01

DATE 2018 09 01

DATE 2018 10 01

DATE 2018 11 01

DATE 2018 12 01

DATE 2019 03 01

DATE 2019 06 01

DATE 2019 09 01

DATE 2019 12 01

……

DATE 2057 03 01

DATE 2057 06 01

DATE 2057 09 01

DATE 2057 12 01

DATE 2058 01 01

STOP

APPENDIX D

SIMULATION RESULTS

Table D.1 Case #1 (Coal Rank) Coal Properties and Operational Parameters.

#	Coal Rank	CO$_2$ Storage		CO$_2$ Storage
		Breakthrough		Mass
	-	Days	Date	10^4 Ton
1	Mvb	9556	01.03.2034	9.16
2	Hvb	15949	01.09.2051	6.80
3	Sb	21063	01.09.2065	2.16

#	Initial CH$_4$ in Place	CH$_4$ Recovery			
		CBM	TMRB	TMRB - CBM	Displacement Ratio
	10^8 Scf	%	%	%	-
1	14	76.0	95.8	19.8	3.34
2	12.6	84.6	98.1	13.6	2.99
3	9.67	93.4	99.0	5.6	2.21

Table D.2 Case #2 (Reservoir Type) Coal Properties and Operational Parameters.

#	Reservoir Types			CO$_2$ Storage		
	Coal Type	Initial CH$_4$ Saturation	Initial Water Saturation	Breakthrough		Mass
	-	-	%	Days	Date	10^4 Ton
1	Dry	S	0	5722	01.09.2023	6.41
2	Wet	S	30	15127	01.06.2049	6.76
3	Wet	S	60	15857	01.06.2051	6.80
4	Wet	S	100	16040	01.12.2051	6.81
5	Wet	10 % US	100	17136	01.12.2054	6.72
6	Wet	20 % US	100	18506	01.09.2058	6.62
7	Wet	40 % US	100	21975	01.03.2068	6.41

		CH$_4$ Recovery			
	Initial CH$_4$ in Place	CBM	TMRB	TMRB - CBM	Displacement Ratio
#	10^8 Scf	%	%	%	-
1	7.20	74.2	99.4	25.2	11.89
2	13.1	86.7	98.9	12.1	3.80
3	12.9	85.2	98.3	13.1	3.20
4	12.6	84.4	97.5	13.2	3.04
5	11.2	82.5	97.5	15.0	2.87
6	9.89	80.4	97.6	17.3	2.71
7	7.48	74.2	96.9	22.7	2.53

Table D.3 Case #3 (Well-Pattern) Coal Properties and Operational Parameters.

		CO$_2$ Storage		
	Well Pattern	Breakthrough		Mass
#	-	Days	Date	10^4 Ton
1	Direct Line Drive	26723	01.03.2081	6.19
2	Staggered Line Drive	31655	01.09.2094	7.25
3	Inverse 5-spot	16040	01.12.2051	6.81
4	Inverse 9-spot	8918	01.06.2032	3.55
5	Normal 9-spot	10836	01.09.2037	9.27
6	Inverse Hexagonal 7-spot	11657	01.12.2039	5.33
7	Normal Hexagonal 7-spot	13393	01.09.2044	9.54

		CH$_4$ Recovery			
	Initial CH$_4$ in Place	CBM	TMRB	TMRB - CBM	Displacement Ratio
#	10^8 Scf	%	%	%	-
1		81.9	93.9	12.0	1.92
2		83.5	98.1	14.6	2.07
3		84.6	98.1	13.5	2.99
4	12.6	87.3	92.9	5.6	4.28
5		74.4	95.0	20.5	3.34
6		87.2	96.9	9.7	3.89
7		77.9	99.2	21.3	3.15

Table D.4 Case #4 (Drainage Area) Coal Properties and Operational Parameters.

#	Drainage Area	CO₂ Storage		
		Breakthrough		Mass
	Acre	Days	Date	10^4 Ton
1	50	9010	01.09.2032	3.38
2	100	16040	01.12.2051	6.81
3	150	23620	01.09.2072	10.2
4	200	31563	01.06.2094	13.8

#	Initial CH₄ in Place	CH₄ Recovery			
		CBM	TMRB	TMRB - CBM	Displacement Ratio
	10^8 Scf	%	%	%	-
1	6.32	86.0	98.2	12.1	4.80
2	12.6	84.6	98.1	13.5	2.99
3	19	84.1	98.1	14.1	2.34
4	25.3	83.7	98.1	14.4	2.00

Table D.5 Case #5 (Cleat Permeability) Coal Properties and Operational Parameters.

#	Cleat Permeability	CO₂ Storage		
		Breakthrough		Mass
	md	Days	Date	10^4 Ton
1	4	60690	01.03.2174	5.39
2	10	16040	01.12.2051	6.81
3	25	6453	01.09.2025	8.45
4	50	4627	01.09.2020	9.42
5	100	4077	01.03.2019	10.1

#	Initial CH₄ in Place	CH₄ Recovery			
		CBM	TMRB	TMRB - CBM	Displacement Ratio
	10^8 Scf	%	%	%	-
1	12.8	87.6	99.1	11.5	1.49
2	12.6	84.6	98.1	13.5	2.95
3	12.4	83.6	97.1	13.5	5.69
4	12.1	85.5	96.6	11.1	6.86
5	11.8	87.5	96.2	8.7	5.11

Table D.6 Case #6 (Anisotropy) Coal Properties and Operational Parameters.

	Anisotropy	CO₂ Storage		
		Breakthrough		Mass
#	-	Days	Date	10^4 Ton
1	1 : 1	36128	01.12.2106	6.86
2	1 : 2	26723	01.03.2081	6.89
3	1 : 4	20148	01.03.2063	6.94
4	1 : 9	15219	01.09.2049	7.12
5	1: 16	13027	01.09.2043	7.34
6	1: 25	11748	01.03.2040	7.49

	Initial CH₄ in Place	CH₄ Recovery			Displacement Ratio
		CBM	TMRB	TMRB - CBM	
#	10^8 Scf	%	%	%	-
1		83.7	98.1	14.3	1.88
2		84.1	98.1	14.1	2.21
3	12.6	84.4	97.9	13.5	2.66
4		86.1	97.9	11.7	3.35
5		87.2	98.1	10.9	3.91
6		87.8	98.2	10.4	4.37

Table D.7 Case #7 (Molar Composition of Injected Fluid) Coal Properties and Operational Parameters.

	Injected Molar Composition	CO₂ Storage		
		Breakthrough		Mass
#	-	Days	Date	10^4 Ton
1	25 % CO_2 - 75 % N_2	8735	01.12.2031	4.44
2	50 % CO_2 - 50 % N_2	10196	01.12.2035	6.22
3	75 % CO_2 - 25 % N_2	12935	01.06.2043	6.85
4	100 % CO_2	16040	01.12.2051	6.81

	Initial CH₄ in Place	CH₄ Recovery			Displacement Ratio
		CBM	TMRB	TMRB - CBM	
#	10^8 Scf		%	%	-
1		78.5	100.0	21.5	1.85
2	12.6	80.3	99.7	19.4	2.61
3		82.8	99.2	16.4	2.92
4		84.6	98.1	13.6	2.99

Table D.8 Case #1 (Coal Rank) Shrinkage and Swelling Effect.

#	Coal Rank	Shrinkage/Swelling	CO₂ Storage Breakthrough Days	Date	Mass 10^4 Ton
	-	-	*Days*	*Date*	10^4 *Ton*
1	Sb	Yes	21154	01.12.2065	2.16
2	Hvb	Yes	16040	01.12.2051	6.81
3	Mbv	Yes	9648	01.06.2034	9.22
4	Sb	No	4535	01.06.2020	7.49
5	Hvb	No	4992	01.09.2021	1.08
6	Mvb	No	5173	01.03.2022	1.12

#	Initial CH₄ in Place 10^8 Scf	CBM %	TMRB %	Displacement Ratio
	10^8 *Scf*	*%*	*%*	-
1	9.67	79.9	99.5	2.17
2	12.6	63.9	98.1	2.99
3	14.0	58.4	96.0	3.34
4	9.67	83.7	95.3	12.69
5	12.6	64.5	90.2	6.33
6	14.0	56.2	89.4	4.57

Table D.9 Case #2 (Reservoir Type) Shrinkage and Swelling Effect.

#	Reservoir Types Coal Type	Initial CH₄ Saturation	Initial Water Saturation	Shrinkage/ Swelling	CO₂ Storage Breakthrough Days	Date	Mass
	-	*%*	*%*	-	*Days*	*Date*	10^4 *Ton*
1	Dry	S	0	Yes	5630	01.06.2023	6.38
2	Wet	S	30	Yes	15035	01.03.2049	6.74
3	Wet	S	60	Yes	15765	01.03.2051	6.79
4	Wet	S	100	Yes	15949	01.09.2051	6.80
5	Wet	10 % US	100	Yes	17045	01.09.2054	6.69
6	Wet	20 % US	100	Yes	18414	01.06.2058	6.61
7	Wet	40 % US	100	Yes	21884	01.12.2067	6.41
8	Dry	S	0	No	882	01.06.2010	10.4
9	Wet	S	30	No	4992	01.09.2021	11.1
10	Wet	S	60	No	4992	01.09.2021	10.9
11	Wet	S	100	No	4992	01.09.2021	10.8
12	Wet	10 % US	100	No	4992	01.09.2021	10.8
13	Wet	20 % US	100	No	4992	01.09.2021	10.8
14	Wet	40 % US	100	No	5083	01.12.2021	10.8

#	Initial CH₄ in Place	CH₄ Recovery		
		CBM	TMRB	Displacement Ratio
#	10^8 Scf	%	%	-
1	7.22	85	99	11.9
2	13.1	73	99	3.8
3	12.9	67	98	3.2
4	12.6	64	98	3.0
5	11.2	58	98	2.8
6	9.89	51	98	2.7
7	7.48	32	97	2.5
8	7.22	0	92	3.0
9	13.1	73	94	7.5
10	12.9	67	91	6.7
11	12.6	64	90	6.3
12	11.2	60	89	6.3
13	9.89	54	87	6.3
14	7.48	40	82	6.5

Table D.10 Case #3 (Molar Composition of Injected Fluid) Shrinkage and Swelling Effect.

#	Injected Molar Composition	Shrinkage/ Swelling	CO₂ Storage		Mass
			Breakthrough		
#	-	-	Days	Date	10^4 Ton
1	25 % CO_2 - 75 % N_2	Yes	8735	01.12.2031	4.44
2	50 % CO_2 - 50 % N_2	Yes	10196	01.12.2035	6.22
3	75 % CO_2 - 25 % N_2	Yes	12935	01.06.2043	6.85
4	100 % CO_2	Yes	16040	01.12.2051	6.81
5	25 % CO_2 - 75 % N_2	No	7549	01.09.2028	4.46
6	50 % CO_2 - 50 % N_2	No	6361	01.06.2025	7.09
7	75 % CO_2 - 25 % N_2	No	5538	01.03.2023	9.15
8	100 % CO_2	No	4992	01.09.2021	1.08

#	Initial CH₄ in Place	CH₄ Recovery		
		CBM	TMRB	Displacement Ratio
#	10^8 Scf	%	%	-
1		63.9	100.0	1.85
2		63.9	99.7	2.61
3		63.9	99.2	2.92
4	12.6	63.9	98.1	2.99
5		64.5	99.5	1.91
6		64.5	97.8	3.19
7		64.5	94.8	4.53
8		64.5	90.2	6.33